The copyright of this thesis vests in the author. No quotation from it or information derived from it is to be published without full acknowledgement of the source. The thesis is to be used for private study or non-commercial research purposes only.

Published by the University of Cape Town (UCT) in terms of the non-exclusive license granted to UCT by the author.

University of Cape Town

APPLICATION OF CEPSTRAL TECHNIQUES TO THE AUTOMATED DETERMINATION OF THE SOUND POWER ABSORPTION COEFFICIENT

LANCE JENKIN

University of Cape Town

Central Acoustics Laboratory
Department of Electrical Engineering
University of Cape Town
November 2012

Thesis submitted in fulfillment of the requirements for the degree of
Master of Science in Electrical Engineering

DECLARATION

I declare that this dissertation is my own, unaided work. It is being submitted for the degree of Master of Science in Engineering at the University of Cape Town. It has not been submitted before for any degree or examination in any other university.

November 2012

Lance Jenkin

University of Cape Town

Gone Surfing.

University of Cape Town

ABSTRACT

This thesis builds on research by Bolton and Gold, who developed the theory of using cepstral analysis to determine the absorption coefficient of elastic porous materials. Jongens, in his Masters thesis, applied this technique to determine the absorption coefficient of asphalt samples mounted in a sample holder at the end of a tube. Jongens and others identified numerous factors that introduced uncertainties into the measurement. These uncertainties fall into two main categories. The first deals with the influences that the links of the measurement chain have on the ability to separate the incident and reflected signal. The second deals with the influence of the air leakage between the tube and the surface under measurement *in-situ*. This thesis deals with the first category.

The objectives of this project are to continue the work of Jongens [27], to produce an apparatus that can rapidly determine the sound power absorption coefficient by a non-skilled operator in a noisy environment. The results should correlate closely with the standardised impedance tube method, within 0.05 over the range 200 Hz to 2000 Hz. The constraint that the apparatus be usable by a non-skilled operator means that little or no calibration should be required, nor should the microphone need to be handled.

This thesis presents a survey of related methods used to determine the sound power absorption coefficient. Theory of the cepstral technique is discussed, along with methods that could be used to improve the accuracy of the technique. Excitation signals that could be used with the cepstral method are put forward. The Inverse Repeat Sequence (IRS) was used to excite the system. It was chosen for its high noise immunity, as well as its complete odd-order non-linearity immunity. Sources of uncertainties from the links of the measurement chain are considered and methods to overcome them are presented. Issues that arise from *liftering* - cepstral equivalent of windowing - are then highlighted. The apparatus for the cepstral technique and method of standing wave ratios used to determine the absorption coefficient is given. The results obtained using the cepstral technique are correlated with the impedance tube results.

It was found that the cepstral method correlates closely with the impedance tube over the range of 200 Hz to 2000 Hz for a wide variety of samples.

The apparatus was developed to be used by a non-skilled operator, only requiring the press of a button to perform the measurement. With the high noise immunity of the IRS signal, the measurement could be carried out in a noisy environment.

University of Cape Town

ACKNOWLEDGMENTS

Firstly, I'd like to express my extreme gratitude to my supervisor, Adrian Jongens, for piquing my interesting in the field of Acoustics, advising and motivating me to complete my thesis.

Tony Welbourne and the staff at Global Acoustics are thanked for the keeping me gainfully employed during my period of studies.

I would also like to thank Stephen Schrire for loaning me equipment from the electronics lab, and offering advise on fixing faults in the equipment.

Kenneth Anderson from DB Audio is sincerely thanked for donating the loudspeaker driver.

I wish to acknowledge Gareth Cairncross, Bruce Davidson and Bernd Jendrissek for helping me with the construction of the apparatus.

My appreciation is given to David Jenkin, Michael Godfrey and Kady-Rose Hull for the help with spelling and grammar.

Finally, this thesis would not have been possible without the support and entertainment offered by Kady-Rose, my parents, friends and family.

University of Cape Town

CONTENTS

University of Cape Town

University of Cape Town

University of Cape Town

University of Cape Town

LIST OF FIGURES

University of Cape Town

University of Cape Town

University of Cape Town

University of Cape Town

University of Cape Town

LIST OF TABLES

University of Cape Town

α	Sound Power Absorption Coefficient
$\alpha(f)$	Frequency dependent absorption coefficient
β	The scaling coefficient of the spectral resolution
$\mathbf{z}$	The specific acoustic impedance of a material
Δf	The spectral resolution
$\delta'[n]$	Periodic unit sample function
$\hat{p}(t)$	The cepstrum of the signal captured by the microphone
$\hat{s}(t)$	The cepstrum of the signal emitted by the loudspeaker
$\mathcal{V}$	The wave velocity
$\Omega_{ss}[n]$	The autocorrelation of the MLS signal
$\Omega_{sy}[n]$	The cross correlation of functions $s[n]$ and $y[n]$
$\phi_{mp}[k]$	The minimum phase function
ρ	The percentage of taper of the Tukey window.
ρ_0	The density of air
σ_α^2	The variance of the absorption coefficient
σ_H^2	The variance of the measured frequency response of the material sample
τ	The delay between the arrival of the signal to the arrival of the first reflection
θ_{LS}	The angle that the cone makes with the axial-axis
$\tilde{H}(f)$	The windowed frequency response
$\tilde{h}[n]$	The windowed impulse response
ε	The DC offset in the cepstrum
a	The radius of the pipe
B	The radial induction in the air-gap of a loudspeaker

University of Cape Town

$C(f)$ The logarithm of the squared magnitude spectrum of the signal emitted by the loudspeaker

d Distance from sound source

d_m Distance from microphone to material under test

d_s Distance from loudspeaker to material under test

f Frequency of the wave

f_0 The frequency of a sinusoidal signal

$f_{1,0}$ The cutoff frequency for the (1,0)-mode

f_1 The lower frequency in the swept sine signal

f_2 The upper frequency in the swept sine signal

f_{low} The low frequency limit for the impedance tube

f_c The cut off frequency of the filter

f_{mn} The cut-off frequency for the (m,n)-mode

f_n Frequency of the cut-off mode

f_{ra} The ring anti-resonant frequency of a loudspeaker cone

f_s The sampling frequency of the ADC

$h'[n]$ The liftered impulse response, including the DC offset

$h(t)$ The impulse response of the material being tested

H_{12} The transfer function between microphone 1 and microphone 2

$H_1(x)$ Struve function of the first order

$h_{ADC}(t)$ The impulse response of the analog-to-digital converter

$H_{DAC}(f)$ The frequency response of the digital-to-analog converter

$h_{DAC}(t)$ The impulse response of the digital-to-analog converter

$H_{LS}(f)$ The frequency response of the loudspeaker

$h_{LS}(t)$ The impulse response of the loud speaker

$H_{MIC}(f)$ The frequency response of the microphone

$h_{MIC}(t)$ The impulse response of the microphone

$H_{PA}(f)$ The frequency response of the power amplifier

University of Cape Town

$h_{PA}(t)$ The impulse response of the power amplifier

$h_s[n]$ The impulse response of the total system

I_a Sound intensity absorbed

I_r Sound intensity reflected

j The unit imaginary number. $j^2 = -1$

$J_1(x)$ Bessel function of the first order

k_n Wave number of the cut-off frequency

K_r Scaling factor due to geometric spreading

L The length of the window

N The number of samples in the signal

N The number of taps used to generate the MLS signal

P The periodicity of the MLS signal

$P(f)$ The spectrum of the signal captured by the microphone

$p(t)$ The signal captured by the microphone

R Acoustic resistance

$R(f)$ The frequency dependent reflection coefficient

R_1 Radiation resistance function

R_b The outer edge radius of the loudspeaker cone

R_r Radiation resistance of a piston

S Cross section area of the tube

$S(f)$ The spectrum of the signal emitted by the loudspeaker

$s(t)$ The signal emitted by the loudspeaker

$S[k]$ The discrete spectrum of a signal

$s_{\{0,1\}}[n]$ The MLS signal made up of digits 0 and 1

$s_{\{1,-1\}}[n]$ The MLS signal made up of digits 1 and -1

U_0 The velocity amplitude of a piston

W Sound power

University of Cape Town

$W(f)$ The frequency response of the window

$w[n]$ The window function, or band pass liftered, used to extract the impulse response from the cepstrum

X_1 Radiation reactance function

$x_m[n]$ Minimum phase signal

X_r Radiation reactance of a piston

Z_m The mechanical impedance of the loudspeaker

Z_r Radiation impedance of a pistion

c The speed of sound

D The diamater of the pipe

DFT Discrete Fourier Transform

ENBW Equivalent Noise Bandwidth

j Imaginary number unit

k The wave number

L Distance between sample and reference microphone

L The length of the tube

s Distance between the two microphones

SWR Standing Wave Ratio

University of Cape Town

1 INTRODUCTION

The focus of this project is to continue the work of Jongens [27], to produce an apparatus that can rapidly determine the sound power absorption coefficient by a non-skilled operator in a noisy environment. The results must correlate closely with the standardised impedance tube method, within 0.05 over the range 200 Hz to 2000 Hz. The constraint that the apparatus be usable by a non-skilled operator means that little or no calibration should be required, nor should the microphone need to be handled.

The work described in this thesis focuses on highlighting major sources of uncertainties in the measurements, and developing software that can determine the absorption coefficient with minimal interaction.

1.1 BACKGROUND

The noise arising from the interaction of the tyre with the road surface is a significant source of noise pollution [51]. Road surfaces can be designed to reduce this road/tyre noise. To effectively develop these road surfaces, a method to measure the normal incident sound power absorption coefficient, *in-situ*, was needed. This need led to the *International Organisation for Standardisation (ISO)* forming a Working Group, SO/TC 43/SC WG 38, to produce an International Standard titled "Procedure for measuring sound absorption properties of road surfaces - *In- situ* method.". Subsequently the group produced two international standards; the Extended Surface Method - ISO 13472-1 and the Spot Method - ISO 13472-2.

The Extended Surface Method, discussed in Section 2.6, uses a single microphone located under a loudspeaker and determines the average sound power absorption coefficient over a 3 m^2 area. The Spot Method, discussed in Section 2.5, uses a short tube with a loudspeaker on one end and two microphones attached to the wall of the tube. The method is able to determine the sound power absorption coefficient over a small 0.08 m^2 area. Since two microphones are used, careful calibration of the phase differences in the microphones are required - this means that a skilled operator is required to make accurate measurements.

Bolton [6] presented a free-field method to measure the acoustic reflection coefficient of materials. The focus of his work was determining the acoustic properties of elastic porous material. Using cepstral signal

University of Cape Town

processing techniques, he was able to extract the impulse response of the material and hence determine the reflection coefficient.

Jongens [27] applied this cepstral signal processing technique to measure the normal incidence sound power absorption coefficient of material samples. The apparatus was similar to that of the standing wave ratio method. It consisted of a loudspeaker mounted on one end of a 2 meter tube, with a microphone situated halfway between the loudspeaker and the material sample, which was mounted at the other end of the tube. The results obtained were correlated with the measurements performed using the standing wave ratio method, and a close correlation was achieved.

Previous work identified numerous factors that influenced the accuracy of the results. An overview of the measurement chain showing the links that influence the results are shown in Figure 1. The work in this thesis discusses the inf
presents methods that

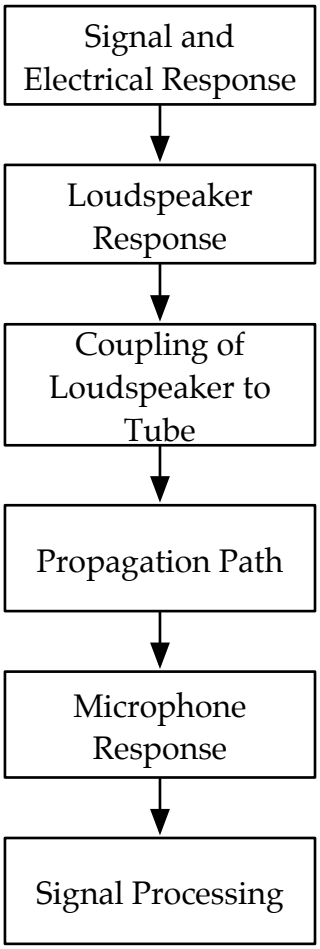

Figure 1: Measurement chain used to determine the normal incidence sound power absorption coefficient.

1.2 OBJECTIVES AND SCOPE

The development of an apparatus to rapidly determine the sound power absorption coefficient begins with the development of the theory in a laboratory. The theory developed is then incorporated into the apparatus to rapidly determine the absorption coefficient in a laboratory, understanding all factors that influence the accuracy of the measurement. Finally, an *in-situ* device can be developed and tested in real world applications.

The objectives for the project are:

1. Determine the factors that influence the accuracy of the cepstral measurements.
2. Measure the absorption coefficient of materials. These measurements must be within 0.05 of the measurements measured by the standardised impedance tube method in the frequency range 200 Hz to 2000 Hz.
3. The measurements should be able to be performed by a non-skilled operator. This constraint means that the operation is simple, there should be no manual adjustments, the measurement is performed automatically, and the construction is of a robust nature.
4. The measurement will be carried out in a noisy environment, and therefore should offer high noise immunity.

1.3 PLAN OF DEVELOPMENT

This thesis is organised in the following manner:

Chapter 2 gives an overview of the relevant related techniques used to determine the absorption coefficient of a material. It also discusses the measurement of the absorption coefficient using the Standing Wave tube apparatus, which is used to correlate the results obtained by the cepstral technique. The other measurement techniques discussed are:

- ISO 10534-2 - The two microphone technique,
- ISO 13472-2 - The spot method, and
- ISO 13472-1 - The extended surface method.

Chapter 3 gives a brief background of using the cepstral technique to determine acoustic properties of materials. The mathematical theory of extracting the impulse response from the cepstrum is discussed. Five methods to improve the accuracy of the results are given.

Chapters 4 to 7 discuss the influences that each of the links in the measurement chain have on the results. Some techniques that can be

University of Cape Town

employed to reduce the significance of these factors are presented in these chapters.

The measurement starts with the generation of the excitation signal. **Chapter 4** introduces various signals that can be used to excite the system. Four signals are discussed. These are the swept sine, the low pass swept sine, the Maximum Length Sequence and the Inverse Repeat Sequence.

The electrical signal is then passed through the power amplifier to the loudspeaker. The loudspeaker is the weakest link in the measurement chain and is discussed in **Chapter 5**.

The electrical signal is transformed into an acoustic signal by the loudspeaker, which then propagates in the waveguide. The influences that the tube has on the acoustic signal are presented in **Chapter 6.** Techniques used to reduce the influence of the waveguide are also presented.

The acoustic signal is captured by the microphone and converted back to an electrical signal. This signal is then analysed and the impulse response is *liftered* from the cepstrum. The effect that the *bandpass lifterer* has on the impulse response of the material is discussed.

Chapter 8 presents the apparatus to measure the sound power absorption coefficient using the cepstral technique as well as the impedance tube. The effects that the apparatus and the sample being measured, have on the absorption coefficient are discussed. A method to calibrate the signal level is given. The software developed for this thesis is also presented.

Chapter 9 gives the measurement settings that were used for all the measurements, the sound power absorption coefficient obtained for the various samples using the cepstral technique and the impedance tube are correlated. The captured cepstrum showing the impulse response of the material are also given.

Finally, **Chapter 10** draws the conclusions from the results and presents ideas for future work.

University of Cape Town

2

SURVEY OF RELEVANT RELATED MEASUREMENT TECHNIQUES

2.1 INTRODUCTION

As a sound wave travels through a material, some of the energy is absorbed by the material - usually through a process of converting the sound energy into heat energy. The ratio of the absorbed sound power to the incident sound power is always between 0 and 1, and this property of the material is known as the sound power absorption coefficient.

There are a wide variety of methods available to measure the absorption coefficient of material samples. This chapter is going to explain the acoustic properties of materials, and standardised techniques to measure the properties, that are relevant to this thesis. An overview of the four standardised techniques are going to be discussed, as well as the advantages and disadvantages of the method with reference to the objectives of this thesis.

The measurements achieved using the cepstral technique were correlated with the results from the method using standing wave ratios, ISO 10534-1, and therefore it will be discussed in more detail than the other standardised methods.

University of Cape Town

2.2 ACOUSTIC PROPERTIES OF MATERIALS

An acoustic wave that impinges on a material surface will be modified in some way by the material. A portion of the acoustic energy will be reflected off the surface, a portion will be absorbed by the material, and the remainder will be transmitted through the material.

The acoustic property that determines how much of the energy is reflected and how much is absorbed is the acoustic impedance of the material. The acoustic impedance, $\mathbf{z}$, is defined as the ratio of pressure, $\mathbf{p}$, to particle velocity, $\mathbf{u}$, or

$$\mathbf{z} = \frac{\mathbf{p}}{\mathbf{u}}. \tag{1}$$

In general, $\mathbf{z}$ will be a complex quantity and frequency dependent. The real component, or *acoustic resistance*, represents the energy transfer of the acoustic wave. The *acoustic reactance*, the imaginary component, represents the particle motion that is out of phase with the acoustic pressure. This out of phase motion causes no average energy transfer.

It is often easier to measure the ratio of sound energy absorbed by a surface of a material exposed to a sound field to the sound energy incident on the surface. The ratio is known as the *absorption coefficient* of the material. Formally, the sound power absorption coefficient, α, is defined as

$$\alpha = \frac{I_a}{I_r}. \tag{2}$$

Here I_a is the sound intensity absorbed by the material and I_r is the sound intensity absorbed.

The measurement of the sound power absorption coefficient is the focus of this thesis. The rest of this chapter will describe current standardised methods used to measure the coefficient.

2.3 METHOD USING STANDING WAVE RATIO - ISO 10534-1

2.3.1 *Introduction*

The method using standing wave ratios, also known as the impedance tube or Kundt Tube method, is a standardised laboratory method to determine the normal incident sound power absorption coefficient, and acoustic impedance of material samples. It is a simple, albeit tedious, method to measure the absorption coefficient, and therefore used as the control method which the cepstral technique results were correlated.

2.3.2 *Method Details*

The standing wave ratio method is a simple method to determine the sound power absorption coefficient. The apparatus used to measure the absorption coefficient using the standing wave ratio method is shown in Figure 2. It requires that the material sample be securely fitted to one end of a rigid tube, and a loudspeaker mounted on the other end. The basic idea is to generate a single frequency sinusoidal signal to propagate plane waves inside a rigid tube. The plane wave propagates down the tube, impinges on a material sample with some of the sound energy being reflected back towards the loudspeaker. The incident wave and the reflected wave produce a standing wave pattern inside the tube, shown in Figure 3, which the microphone can measure. The filter bank contains a collection of band pass filters, which is used to filter out the generated signal from the background noise including electrical noise and harmonics caused by non-linearities. The signal captured by the microphone is displayed on the oscilloscope, and the movable microphone train is transversed along the calibrated scale until the pressure maximum and minimum closest to the sample are found and recorded. This

University of Cape Town

process is repeated for all frequencies of interest, normally the preferred frequencies as specified by the standard ISO 266:1997 [23].

The first pressure minimum, which is approximately a quarter wave length of the generated signal from the sample, and a pressure maximum are recorded. The ratio of the pressure maximum to the pressure minimum is known as the *standing wave ratio.* The absorption coefficient, α,

w

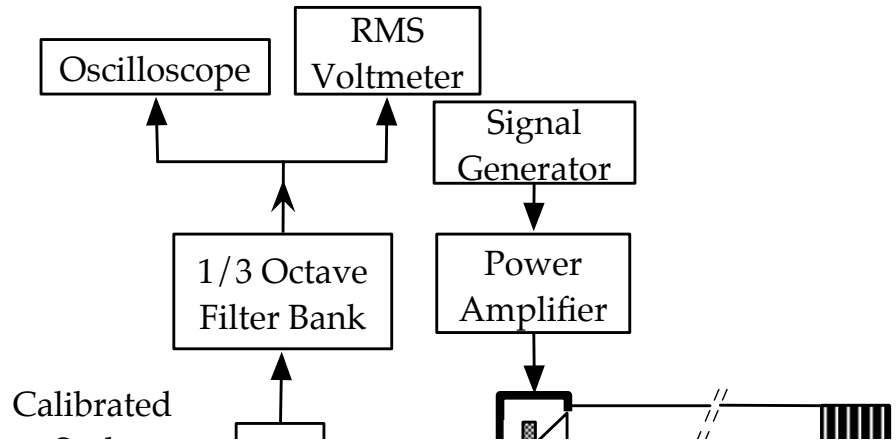

Fi

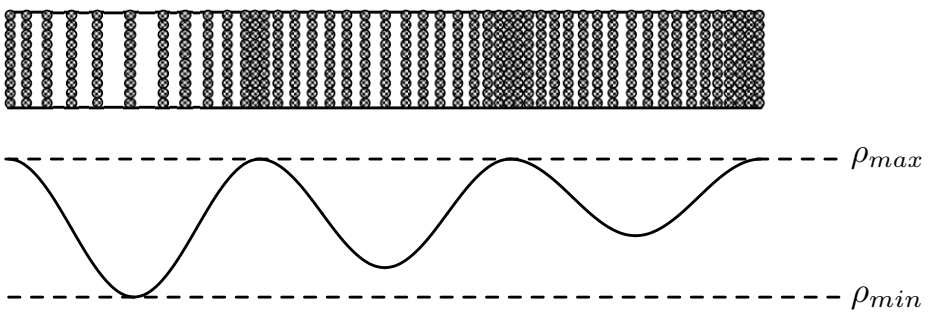

Figure 3: Pressure distribution of standing waves in the impedance tube.

The complex acoustic impedance can also be determined, with further measurements of the speed of sound, c, in the tube and the distances from the face of the material sample that the pressure maximum and minimum occur.

It is essential that only plane waves propagate in the tube, it is therefore important that the walls of the tube are rigid, so that tube resonances are not excited by the sound energy, and that the cross sectional diameter be constant (to within 0.2%). This condition also sets the maximum frequency that can be measured in a specific tube, the frequency is equal to the cutoff frequency of the first higher order mode. Higher order modes are discussed in more detail in Section 6.2.3. The cutoff frequency for the $(1,0)$-mode, $f_{1,0}$, is approximately,

$$f_{1,0} = \frac{c}{1.7D}. \tag{4}$$

Here c is the speed of sound and D is the diameter of the tube. Because of this cutoff frequency, The *Bruel and Kjaer Type 4002 Standing Wave Tube* makes use of two impedance tubes with different internal diameters. The larger tube has an internal diameter of 100 mm, and therefore the upper frequency is approximately 2000 Hz. The smaller tube has an internal diameter of 30 mm, and therefore has a upper frequency of approximately is 6600 Hz. The low frequency is related to the length and diameter of the tube, and is given by [8]

$$f_{low} = \frac{250}{L - 3D}. \tag{5}$$

Where L is the length of the tube, and D is the tube's diameter. For the larger tube, this lower frequency limit is 90 Hz and for the smaller tube, the lower frequency limit is 800 Hz.

More information on the method of standing wave ratios can be found in the relevant ISO standard [22].

University of Cape Town

2.3.3 *Remarks*

Provided that the sample under test is homogeneous the method of standing wave ratios is a reliable way to determine the sound power absorption coefficient. It is also a relatively low cost and simple method to implement, and therefore a popular approach to measure the absorption coefficient.

Since the method relies on the interference of the incident and reflected waves to produce a standing wave pattern inside the tube, it requires a continuous signal being generated while the pressure maximum and minimum are measured. This means that it takes a great deal of time, on the order of 10's of minutes, to measure the absorption coefficient for all the ISO preferred frequencies.

The method requires that the microphone be manually moved throughout the measurement. If the operator is not careful with the measurements, it could lead to damaging the equipment.

It is made for laboratory methods, and is not easily transportable, it is therefore not suitable for *in-situ* measurements.

2.4 2 MICROPHONE TRANSFER FUNCTION - ISO 10534-2

2.4.1 *Introduction*

With the advent of low-cost high-speed computing devices, new methods of determining the sound power absorption coefficient were developed. Seybert and Ross [42] introduced a method to determine the acoustic properties of materials using a Gaussian noise source, and two fixed microphones. It allows for the rapid evaluation of the acoustical properties of a material sample, only needing one continuous measurement. This method was later standardised and became known as the 2 Microphone Transfer Function Method - ISO 10534-2[24]. The next section gives a brief outline of the method, followed by some remarks on the method.

2.4.2 *Method Details*

Figure 4 shows the apparatus required to measure the acoustic properties of a material sample using the two microphone transfer function method. The noise generator need not be a separate noise generator and can be implemented in the laptop used to analyse the signals. The sample holder needs to be securely fitted with an air-tight connection to the end of the tube, and the loudspeaker connected to the other end of the tube. The two microphones should be connected with an airtight connection, to the wall of the tube. The faces of the microphones should be flush with the wall of the tube. The distance between the two microphones as well as the distances of the microphones from the face of the sample need to be accurately known.

University of Cape Town

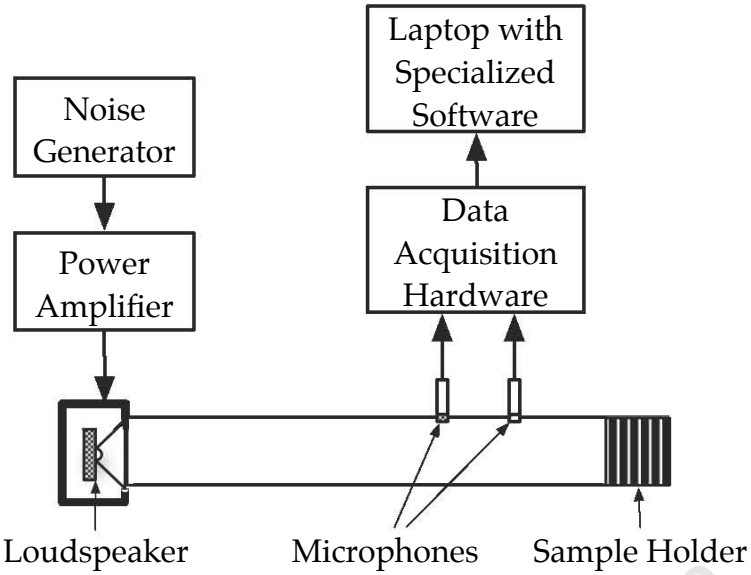

Figure 4: The apparatus used in the two microphone transfer function method. The noise generator may be integrated into the laptop.

A random noise signal is generated with the noise generator, which is then used to create a sound field in the tube with the loudspeaker driver. Using a multi-channel spectrum analyser the transfer function between the two microphones, H_{12}, can be measured. The microphone that is closest to the sample is the microphone 1, or reference microphone. The acoustic reflection coefficient, R, of the material is then determined from the relation,

$$R(f) = \frac{H_{12} - e^{-jks}}{e^{-jks} - H_{12}} e^{j2k(L+s)}, \tag{6}$$

where L is the distance between the face of sample and the reference microphone (the microphone closet to the sample), s is the distance between the two microphones. The wavenumber k is given as $k = 2\pi f/c$, with f the frequency, and c the speed of sound. The sound power absorption coefficient, α, is then given as

$$\alpha(f) = 1 - |R(f)|^2. \tag{7}$$

2.4.3 *Remarks*

The two microphone transfer function method offers advantages over the standing wave ratio method. The primary advantage is that it can be carried out in one rapid measurement, giving a better resolution than that achieved with the standing wave ratio method. The other advantage of this method is that it only requires a short tube, making it easy to transport.

University of Cape Town

There are several disadvantages with this technique, it suffers from bias errors which are a function of the microphone positions and the bandwidth used in the signal processing. These errors can be improved by locating the microphones close to the sample and using a small analysis bandwidth[43]. Random errors are also an issue that need high coherence between microphones in order to be minimised. This high coherence can be achieved by locating the two microphones close together, which introduces another problem of reduced accuracy at lower frequencies. A high coherence also requires careful phase calibration between the two microphones. Another issue that arises with the spacing of the microphone is at frequencies where the wavelength approaches a half wavelength.

It is to be noted that there is a single microphone transfer method [10], that is not a standardised method, which does not require careful calibration between two microphones. Instead of using two microphones, a single microphone is used and a measurement is performed, then the microphone is moved to a second location on the tube, and another measurement is performed. Instead of using a stationary random noise, a deterministic noise source is used, such as the Maximum Length Sequence (MLS). The signal process remains the same as the two microphone transfer function method.

University of Cape Town

2.5 SPOT METHOD - ISO 13472-1

2.5.1 *Introduction*

The Spot Method is an *in-situ* method to determine normal incident sound absorption coefficient of road surfaces[26]. It uses the same theory as the Two Microphone Transfer Function Method, ISO 10534-2, discussed in the previous subsection. Because it is used to measure road surfaces, the frequency range is 250 Hz to 1600 Hz, and therefore the dimensions of the tube as well as the microphone positions are fixed.

It is called the Spot Method because it measures the sound absorption coefficient over an area of 0.08 m^2, whereas the Extended Surface Method, discussed in the next subsection, covers an area of approximately 3 m^2.

The next section gives some method details, that differ to ISO 10534-2, and remarks are given.

2.5.2 *Method Details*

The theory behind the Spot Method and the Two Microphone Transfer Function method are the same, and therefore are not going to be repeated in this section. However there are a few differences that arise due

to the intended use of the method. The method is to used to determine the acoustic properties of road surfaces, which are highly reflected. The frequency range is set to be valid between 250 Hz and 1600 Hz, for this reason the physical dimensions of the tube, and the microphone positions are fixed.

Another consequence of measuring highly reflective surfaces is that internal energy loss of the system is not negligible and need to be accounted for. This is done by placing a totally reflective surface, for example a 10 mm thick steel plate, and measuring the absorption coefficient of the reflective surface. This is then subtracted from the measurement of the road surface.

2.5.3 *Remarks*

The advantages and disadvantages are the same as for the Two Microphone Transfer Function method, and will not be repeated.

2.6 EXTENDED SURFACE METHOD - ISO 13472-1

2.6.1 *Introduction*

The *Extended Surface Method*[25] is an *in-situ* method that is complimentary to *Spot Method*, ISO 13472-2. It determines the absorption coefficient over an area of approximately 3 m^2. Although the cepstral technique studied in this thesis is used to determine the absorption coefficient for surface areas comparable to the *Spot Method*, i.e 0.08 m^2, the *Extended Surface Method* is of interest as it is a single microphone technique.

2.6.2 *Method Details*

A MLS signal is generated and played through a loudspeaker that is located above the surface under test. A microphone is located at some known distance away from the loudspeaker, and some known distance above the surface. It captures the incident and reflected sound energy. Using the *Fast Hadamard Transform*, to cross correlate the received signal with the generated MLS signal, the measured impulse response is given. This process is repeated a number of times to improve the signal-to-noise ratio (SNR). The material's impulse response is separated from the measured impulse response, by measuring the impulse response free from reflections. In order to measure the reflection-free impulse response, the microphone and loudspeaker are pointed away from any surfaces (towards the sky). This reflection-free impulse response is subtracted from the measured impulse response containing the material's impulse response, leaving the material impulse response.

University of Cape Town

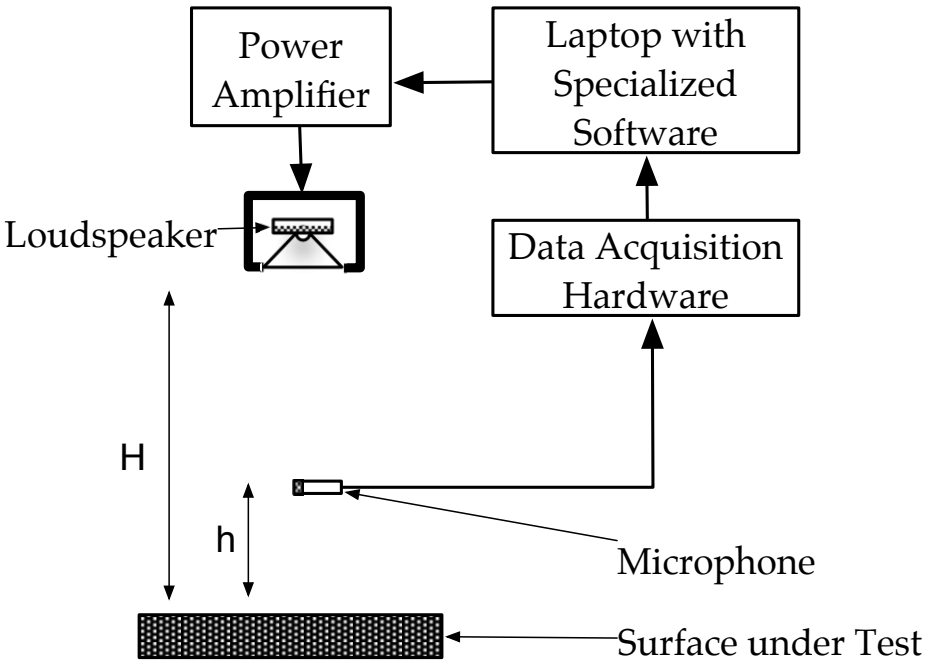

Figure 5: Sketch of apparatus used to determine the absorption coefficient using the extended surface method.

To determine the absorption coefficient, α, the reflection coefficient needs to determined. The scaled reflection coefficient is the squared magnitude of the ratio of the frequency response of the reflected path, $H_r(f)$, to the frequency response of the incident path, $H_i(f)$,

$$R(f) = \frac{1}{K_r^2}\left|\frac{H_r(f)}{H_i(f)}\right|^2. \tag{8}$$

The scaling factor, K_r^{-2}, is due the geometrical spreading. This is because the sound energy is no longer contained in total inside the tube, but can spread spherically from the sound source. The geometrical spreading factor is given as

$$K_r = \frac{d_s - d_m}{d_s + d_m}. \tag{9}$$

Where d_s the distance from the speaker to the material under test, and d_m the distance from the microphone to the surface under test. The sound power absorption coefficient is then given as

$$\alpha(f) = 1 - R(f). \tag{10}$$

2.6.3 *Remarks*

The *Extended Surface Method*, although not a spot method, is a single microphone method that requires no calibration and therefore could be

used by unskilled operators. However, it measures the average absorption over a large area and does not fulfil the requirement of measuring small areas.

2.7 CONCLUSION

Four methods to determine the sound power absorption coefficient have been discussed in this chapter, each that are designed to work in specific environment, or for specific measurements. ISO 13472-1, the extended surface method, is used for outdoor measurements used to measure the average absorption coefficient over an approximately 3 m^2 surface area. The spot method, ISO 13472-2, is also used for outdoor measurements but is measures a small surface area - 0.08 m^2. Finally, ISO 10534-1, the standing wave tube method, is used for a small surface area but requires measurements to be performed in a laboratory environment.

The next chapter is going to discuss the theory of the method of determining the absorption coefficient using the cepstral technique, which is the focus of this research. The measurements obtained with the cepstral method will be correlated with the standing wave tube method.

University of Cape Town

3

THEORY OF THE CEPSTRAL TECHNIQUE

3.1 INTRODUCTION

The history of the *cepstrum* dates back to Bogert, Healy and Tukey's paper titled *"The Quefrency Alanysis of Time Series for Echoes: Cepstrum, Psuedo-Auto-covariance and Saphe Cracking"*[3, 33]. The idea comes from noting that an echo can be modelled as

$$x(t) = s(t) + \alpha \cdot s(t - \tau), \tag{11}$$

where $x(t)$ is a captured signal, $s(t)$ is a non-specific signal, α is the attenuation coefficient of a partial reflector, and τ is the delay before the arrival of the reflection. Then the Fourier spectral density of $x(t)$, $|X(f)|^2$, is

$$|X(f)|^2 = |S(f)|^2 \left[1 + \alpha^2 + 2\alpha \cdot \cos(2\pi f \tau)\right]. \tag{12}$$

If the logarithm of the Fourier spectral density is taken, the multiplications are transformed into additions,

$$\begin{aligned} C(f) &= \ln |X(f)|^2 \\ &= \ln |S(f)|^2 + \ln \left|1 + \alpha^2 + 2\alpha \cdot \cos(2\pi f \tau)\right|. \end{aligned} \tag{13}$$

The resulting logarithmic spectrum, $C(f)$, can be viewed as a waveform with an additive periodic component. The periodic component has a fundamental frequency that is equal to the time delay of the echo. If this logarithmic spectrum is Fourier transformed again, the periodic component becomes a spike corresponding to the time delay of the echo, τ. This twice Fourier transformed waveform is no longer in the time domain, nor is it in the frequency domain. Bogert et al. referred to this domain as the *quefrency* domain. They also named this twice Fourier transformed waveform the *cepstrum.* Table 1 gives a list of some of the terms Bogert et al. created in their paper.

Table 1: Terms coined by Borgert et al, and their frequency domain equivalent.

CEPSTRUM		SPECTRUM
quefrency	$\longrightarrow$	frequency
rahmonic	$\longrightarrow$	harmonic
saphe	$\longrightarrow$	phase
lifter	$\longrightarrow$	filter

University of Cape Town

Cepstral analysis is in use in a large variety of fields, from speech recognition, detecting echoes in seismic signals, and analysing radar signal returns[33].

This present thesis is based on work performed by Bolton and Gold[6, 4, 7, 5]. Bolton, in his PhD thesis, explored using the cepstral technique to determine the impulse response of foam materials in a free-field environment. The frequency range of interest was limited from 300 Hz to 19 kHz. Bolton highlighted some problems that would make using the cepstrum method with impedance tubes difficult.

Jongens[27] presented results he obtained using the cepstrum technique with the impedance tube. These results generally had a good agreement with measurements carried out with the impedance tube.

The theory to the cepstrum technique is given in the next section, methods of improving the accuracy of the results obtained are discussed, finally concluding remarks are made.

3.2 THEORY

To understand the theory of the cepstrum technique, consider the system shown in Figure 6. A loudspeaker is connected to a tube of that is L meters in length. At the other end is the material sample to be measured. The microphone is located l meters from the sample. The loudspeaker emits a signal, $s(t)$, which impinges on the sample. The sample modifies the signal by presenting a frequency transfer function, $H(f)$, with associated impulse response, $h(t)$. The signal captured by the microphone, $p(t)$, is

$$p(t) = s(t) - s(t) \otimes h(t - \tau), \tag{14}$$

with $\otimes$ the convolution operator, $h(t)$ the impulse response of the sample, and τ the time it takes for the sound wave to propagate $2 \cdot l$ meters. For simplicity of illustration, the delay for the signal to travel the $L - l$ meters from the loudspeaker to the microphone is ignored.

University of Cape Town

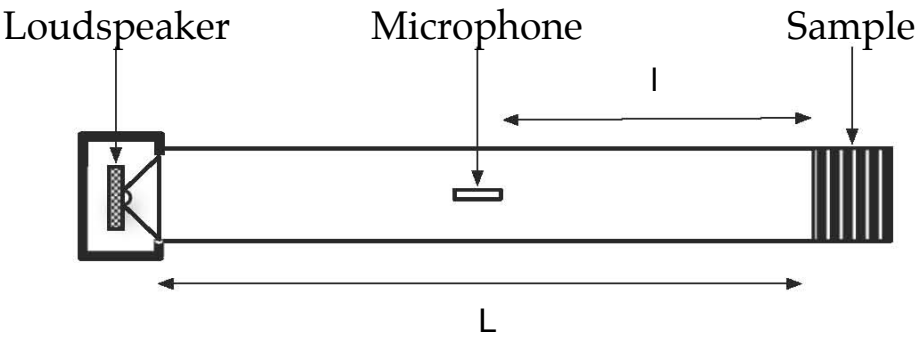

Figure 6: Sketch of measurement geometry used to determine the acoustic absorption coefficient of a material using a loudspeaker and a single microphone.

The Fourier spectral density of $p(t)$ is obtained by taking the square modulus of the Fourier transform of Equation 14

$$|P(f)|^2 = |S(f)|^2 \left[1 + H(f)\, e^{-j2\pi f\tau}\right] \left[1 + H^*(f)\, e^{+j2\pi f\tau}\right], \tag{15}$$

here $|P(f)|^2$ is the power spectral density (PSD) of $p(t)$, $|S(f)|^2$ is the PSD of the input signal $s(t)$, $H(f)$ is the frequency response of the sample and $H^*(f)$ its conjugate.

The logarithm of the total PSD converts the multiplications into additions, therefore

$$\ln|P(f)|^2 = \ln|S(f)|^2 + \ln\left|1 + H(f)\, e^{-j2\pi f\tau}\right| + \ln\left|1 + H^*(f)\, e^{+j2\pi f\tau}\right|. \tag{16}$$

The power series expansion of the natural logarithm, known as the *Mercator* series is

$$\begin{aligned} \ln(1+x) &= \sum_{n=1}^{\infty} \frac{(-1)^{n+1}}{n} x^n \\ &= x - x^2/2 + x^3/3 - \cdots, \end{aligned} \tag{17}$$

this holds so long as $|x| \leq 1$ and $x \neq -1$.

The frequency response of the sample, $|H(f)|$ is equal to the sound power reflection coefficient, α_r, of the sample. For passive reflectors, $|H(f)|$ is going to be less than 1, and therefore the Mercator series representation can be used.

The inverse Fourier transform of the logarithmic power spectrum, Equation 16, results in the cepstrum of the total pressure, $\hat{p}(t)$,

$$\begin{aligned} \hat{p}(t) =& \hat{s}(t) + h(t-\tau) - h(t-\tau) \otimes h(t-\tau)/2 + \cdots \\ &+ h(-t-\tau) - h(-t-\tau) \otimes h(-t-\tau)/2 + \cdots, \end{aligned} \tag{18}$$

University of Cape Town

with $\hat{p}(t)$ the total cepstrum, $\hat{s}(t)$ the power cepstrum of the direct signal, and $h(t)$ the impulse response of the sample. The terms where the impulse response of the sample is convoluted with itself a number of times, are referred to as *rahmonics.* The cepstrum illustrated in Figure 7, shows the direct cepstrum, the impulse response and subsequent *rahmonics*.

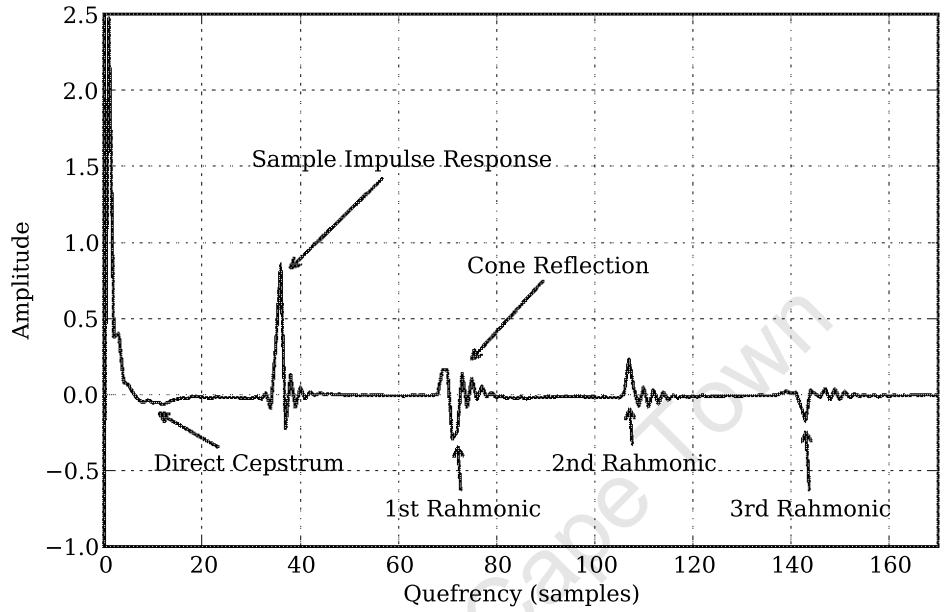

Figure 7: Annotated cepstrum for a reflective sample, showing the direct cepstrum, the impulse response of the material, the reflection from the cone and the *rahmonics.*

From the total cepstrum, in Equation 18, it can be seen that the impulse response of the sample can be *liftered* directly from the cepstrum, as long as the cepstrum of the direct signal is at negligible values at τ seconds. The limit on the length of the *lifterer* is determined by the arrival of the first *late* reflection - the reflection from the loudspeaker cone.

3.3 IMPROVING THE CEPSTRUM

3.3.1 *Zero Padding*

Zero padding refers to the technique of appending zeros to the end of a signal. It is usually used to extend the signal, so that the length is a power of 2, so that an efficient FFT algorithm can be utilised[44]. Zero padding is also used to decrease the frequency spacing of the resulting FFT bins. This is useful for presenting the data as the process interpolates between the original frequency points to present a continuous curve.

University of Cape Town

It is important to note, that although there is a perceived improvement in frequency resolution, the real frequency resolution is not improved[32].

A reason for using zero padding which pertains to cepstral analysis, is that it can be used to reduce the effect of *cepstral aliasing*. From Equation 18, it can be seen that the cepstrum contains the direct cepstral, $\hat{s}(t)$, the impulse response of the sample, $h(t)$, as well as higher order rahmonics. The addition of impulse response, and the higher order rahmonic converge to the Fourier transform of $\ln|1+H(f)|$, where $H(f)$ is the frequency response of the sample. The *rate of convergence* of this series depends how close $H(f)$ is to the *radius of convergence* of Mercator series, which is 1. The rate of convergence decreases as $H(f)$ approaches 1, and therefore is at its slowest rate when the sample is a reflective surface.

The effect of slow rate of convergence is that the negative rahmonics, terms in Equation 18 with negative t, may overlap the positive rahmonics. The overlapping rahmonics may interfere with the impulse response, and therefore making it impossible to lift it from the cepstrum.

3.3.2 *Background Subtraction*

Bolton[4] mentions the use of background subtraction to improve the results obtained using the cepstral technique. Background subtraction relies on a separate measurement of the system in an anechoic environment. The recorded pressure of the system, $p_s(t)$, is then

$$p_s(t) = s(t), \tag{19}$$

where $s(t)$ is the signal captured by the loudspeaker, which is a convolution of the components of the signal generating and acquisition chains,

$$s(t) = x(t) \otimes h_{DAC}(t) \otimes h_{PA}(t) \otimes h_{LS}(t) \otimes h_{MIC}(t) \otimes h_{ADC}(t), \tag{20}$$

where $x(t)$ is the excitation signal, $h_{DAC}(t)$ is the impulse response of the digital to analog converter, $h_{PA}(t)$ is the impulse response of the power amplifier, $h_{LS}(t)$ is the impulse response of the loudspeaker, $h_{MIC}(t)$ is the impulse response of the microphone, and $h_{ADC}(t)$ is the impulse response of the analog to digital convertor.

From the previous section it can be seen that the power cepstrum of the system, $\hat{p}_s(t)$, is

$$\hat{p}_s(t) = \hat{s}(t). \tag{21}$$

University of Cape Town

Therefore subtracting the power cepstrum of the system in an anechoic environment from the power cepstrum of the measurement of the sample, $\hat{p}(t)$ from Equation 18

$$\begin{aligned}\hat{p}(t) - \hat{p}_s(t) = (&\hat{s}(t) + h(t-\tau) - h(t-\tau) \otimes h(t-\tau)/2 + \cdots \\ &+ h(-t-\tau) - h(-t-\tau) \otimes h(-t-\tau)/2 + \cdots) \\ &- \hat{s}(t) \\ = &\, h(t-\tau) - h(t-\tau) \otimes h(t-\tau)/2 + \cdots \\ &+ h(-t-\tau) - h(-t-\tau) \otimes h(-t-\tau)/2 + \cdots\end{aligned} \quad . \tag{22}$$

Unfortunately, it is a non-trivial task to measure the system separately when using an impedance tube. Jongens[27] attempted this by creating an anechoic termination, but there was still some energy being reflected from the termination which would distort the impulse response of the sample being measured. Another option is to increase the length of the tube in order to increase the length of time before the arrival of the first reflection. The problem that arises from this is that unless the connection between the two pipes is completely acoustically transparent - that is, no sharp edges, no air leakage or slight difference in diameter between the two pipes - there will be a reflected wave at the point of connection.

Fortunately, if only part of the sound generating chain and acquisition chain is measured separately, it can be used to improve the cepstrum. If the output of the digital to analog converter is connected directly to the digital to analog converter, the electrical generator-acquisition chain, $p_{ga}(t)$ can be captured.

The logarithmic power spectrum of the total system, $P_s(\omega)$ is obtained by taking the Fourier transform of $p_s(t)$,

$$\begin{aligned}\ln|P_s(f)|^2 &= \ln|S(f)|^2 \\ &= \ln|X(f) \cdot H_{DAC}(f) \cdot H_{PA}(f) \cdot H_{LS}(f) \cdot H_{MIC}(f) \cdot H_{ADC}(f)|^2 \\ &= \ln|X(f)|^2 + \ln|H_{DAC}(f)|^2 + \ln|H_{PA}(f)|^2 + \\ &\quad \ln|H_{LS}(f)|^2 + \ln|H_{MIC}(f)|^2 + \ln|H_{ADC}(f)|^2,\end{aligned} \tag{23}$$

where $X(f)$, $H_{DAC}(f)$, $H_{LS}(f)$, $H_{MIC}(f)$ and $H_{ADC}(f)$ are the frequency responses of the excitation signal, the digital to analog convertor, the loudspeaker, the microphone and the analog to digital converter, respectively. The logarithmic power spectrum of the electrical generator-acquisition chain, $P_{ga}(f)$ is,

$$\ln\left|P_{ga}(f)^2\right| = \ln|X(f)|^2 + \ln|H_{DAC}(f)|^2 + \ln|H_{LS}(f)|^2 + \ln|H_{ADC}(f)|^2. \tag{24}$$

Thus, if the electrical generator-acquisition chain is subtracted from the measurement signal, the direct cepstrum becomes dependent on the impulse response of the loudspeaker and microphone alone.

University of Cape Town

Since the Fourier transform and its inverse transform are linear operators, the electrical generator-acquisition chain can be subtracted from the measurement signal in either the logarithmic spectrum domain or in the cepstral domain.

The cepstrum for the captured microphone and signal generating signals are shown in Figure 8. It can be seen that the generators cepstrum is superimposed in the microphone cepstrum.

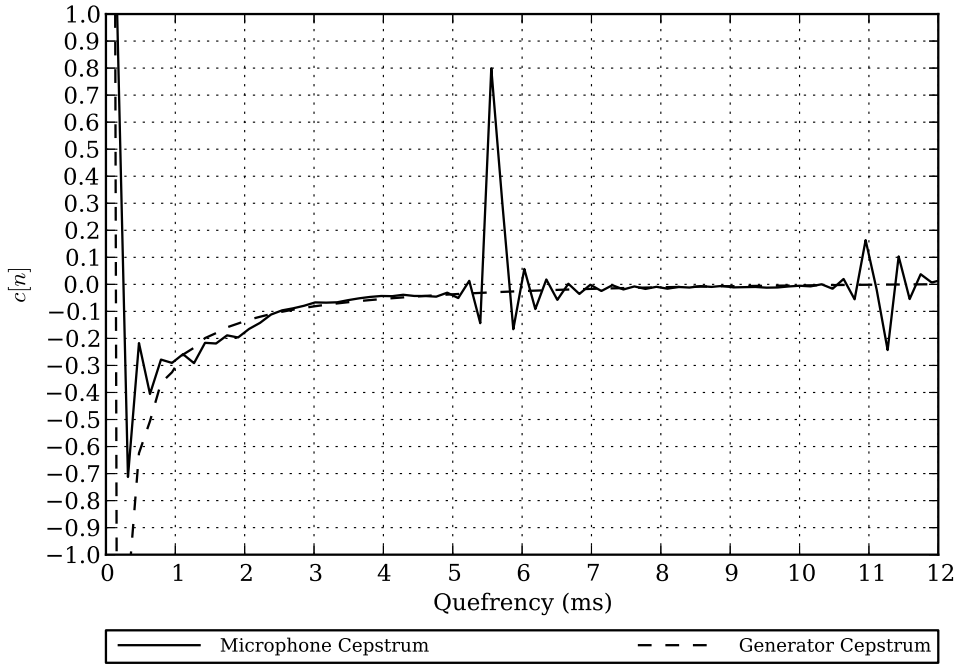

Figure 8: The *cepstrum* for the captured microphone and generator signals.

3.3.3 *Low Frequency Synthesis*

Green et al. [18] found it necessary to implement low frequency synthesis to improve the correlation of the absorption coefficient obtained in a free field measurement with a measurement using the impedance tube. This is due to the importance of having a smooth spectrum down to DC, which is an impossible requirement for a real measurement system. Instead of using the actual spectrum below 20 Hz, a spectrum was synthesised by assuming the material was a perfect reflector. For details on the process, refer to Bolton [4].

Attaching a tube to the front of a loudspeaker has the effect of boosting the low frequency performance of the speaker (refer to Subsection 6.2.1). For this reason, it was found that there were negligible gains implementing the low frequency synthesis. This is consistent with the findings of Groll[19].

3.3.4 *Loudspeaker Response Shaping*

The direct cepstrum, $\hat{s}(t)$, is a combination of the cepstrum of the signal, digital-to-analog convertor, the amplifier, the loudspeaker, the microphone and the analog-to-digital convertor. In order to reduce the length of the of the cepstrum due to the loudspeaker, without requiring a flat spectrum down to DC, an alternative target spectrum for the loudspeaker is given by Bolton[4]. The argument presented by Bolton is as follows. The log modulus of the Discrete Fourier Transform of a real sampled signal is itself real and even. It can therefore be represented by a sum of Fourier cosines

$$\log |S[k]|^2 = \sum_{m=0}^{M} a_m \cos\left(\frac{2\pi km}{N}\right), \qquad k = 0, 1, \ldots, N-1, \tag{25}$$

where a_m are the real coefficients of the cosine series, N is the length of Fourier Transform, and M is the specific number of terms in the series expansion. The inverse Discrete Fourier Transform is calculated, which results in the power cepstrum. The result of the transformation is

$$\hat{s}[n] = \begin{cases} a_0, & n = 0 \\ \frac{1}{2}\sum_{m=0}^{M} a_m \left(\delta[n-m] + \delta[n+m-N]\right), & n = 1, 2, \ldots N-1. \end{cases} \tag{26}$$

Therefore, the resulting power cepstrum is limited in samples to the number of terms used in the cosine series expansion.

Figure 9 shows the target spectrum using a sampling rate of 8000 Hz, M = 10, a_0 set to -1, and a_1 to a_9 set to 1. The shape of the target spectrum corresponds well to the typical frequency response of a loudspeaker. Using this target spectrum will not make undue demands on the loudspeaker. The resulting cepstrum using this target spectrum is shown Figure 10. It can be seen that the cepstrum is limited to 1.125 ms.

University of Cape Town

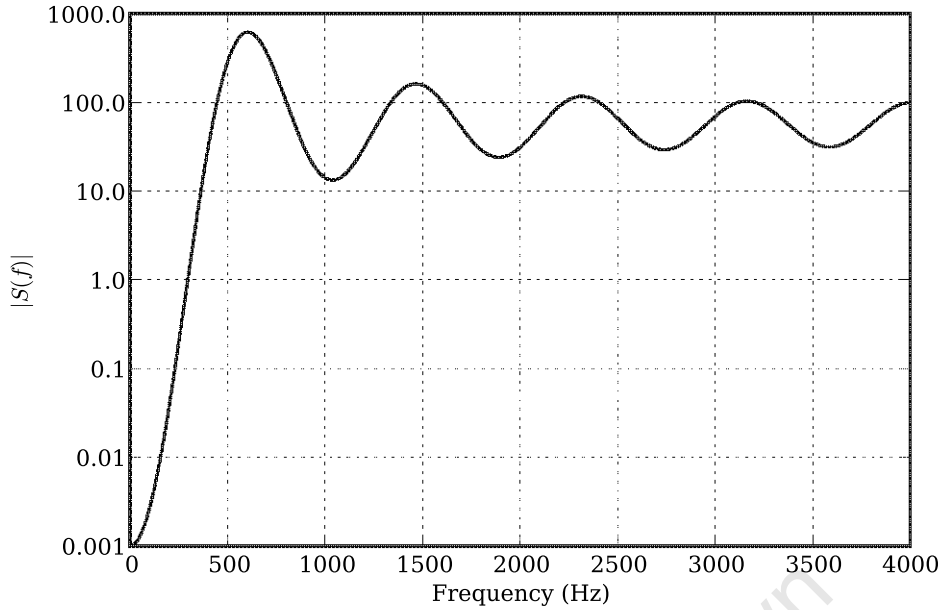

Figure 9: The modulus of the target spectrum.

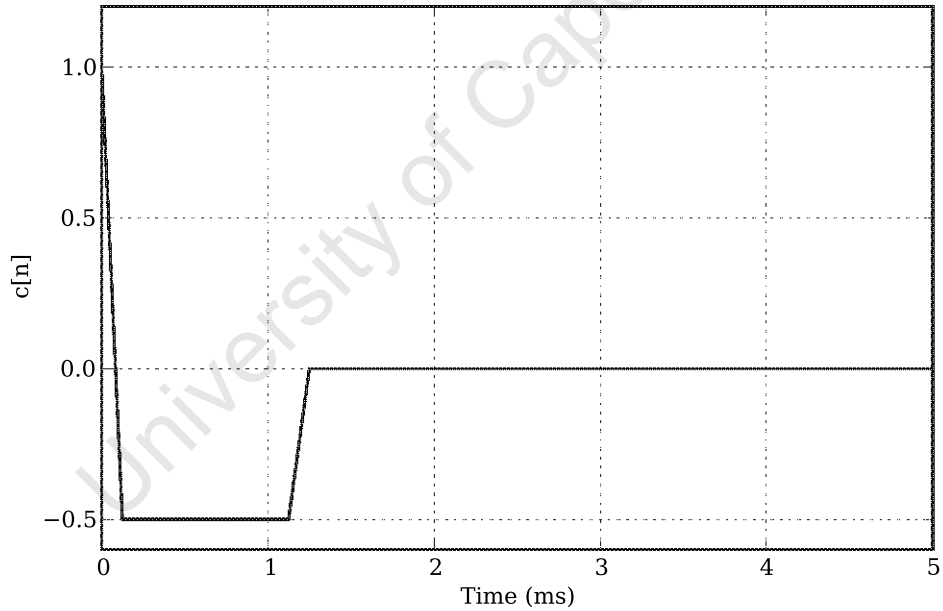

Figure 10: The resulting cepstrum from the target spectrum shown in Figure 9.

Although no improvement was found by implementing the spectrum shaping algorithm, it is likely that it will be needed to improve the frequency resolution, discussed below.

University of Cape Town

3.3.5 *Improving Frequency Resolution*

If the cepstrum of the direct signal, $\hat{s}(t)$, falls to negligible values before the arrival of the first reflection, then the delay, τ may be made shorter. This is achieved by moving the microphone closer to the sample under measurement. From 18, it can be seen that the first *rahmonic* occurs at 2τ. Thus, moving the microphone may seem to reduce the frequency resolution - as only the time between τ and 2τ can be *liftered*. However, if the microphone's global impulse response is forced to zero where the first *late* reflection occurs, then it's possible to extract not only the sample's impulse response, but also the subsequent *rahmonics*. Noting that the *rahmonics* arise from taking the logarithm of response of the system to the excitation. If the impulse response and the *rahmonics* are exponentiated, and remembering the *Mercator series*, the result will be

$$\exp\left(h'(t) + \sum_{n=2}^{\infty} \frac{(-1)^{n+1}}{n} \left(h'(t)\right)^n\right) = 1 + h(t), \tag{27}$$

where $h'(t)$ is the *rahmonic*-time limited impulse response of the sample. The time limit is imposed by the arrival of the first *rahmonic*. $h(t)$ is the reflection-impulse response of the sample, where the frequency resolution of the impulse response is limited by the arrival of the reflection off the loudspeaker cone.

3.4 CONCLUSIONS

This chapter introduced the theory of using properties of the cepstrum, to extract the impulse response of a sample under test - and therefore determine the sound power absorption coefficient. Five methods were introduced that could enhance the accuracy of the measurement. These methods were zero padding the signal, background subtraction, low frequency synthesis, loudspeaker response shaping and a method to improve the frequency resolution.

The cepstral processing technique allows for the measurement of the normal incident sound power absorption coefficient, without the need to handle the microphone. It will be shown that the measurements achieved with the cepstral technique correlate closely with the impedance tube. It is therefore a suitable method to meet the criteria highlighted in Section 1.2.

Zero padding the signal, and using background subtraction to improve the cepstrum were found to significantly improve the results. It found that, due to the low frequency emphasis gained by attaching a tube in front of the loudspeaker, low frequency synthesis offered little to no improvement in the results.

University of Cape Town

It was also found that it was unnecessary to shape the loudspeaker frequency response, as discussed in Subsection 3.3.4. Instead, two simple filters - one high pass and one low pass filter - were enough to ensure the direct cepstrum, primarily due to the loudspeaker, falls to negligible levels before the arrival of the impulse response of the material.

Attempts were made to improve the frequency resolution of the results using the theory in Subsection 3.3.5. Further research should be undertaken into improving the frequency response, as it is one of the significant offerings of the cepstrum technique.

The next section is going to discuss excitation signals that can be used with the cepstral method to determine the sound power absorption coefficient.

University of Cape Town

4

EXCITATION SIGNALS

4.1 INTRODUCTION

The cepstrum is defined to be the inverse Fourier transform of the logarithmic squared modulus of the spectrum. The frequency response of the system is defined by the modulus of the spectrum, as well as the phase of the spectrum. The scope of this research focuses on the power that is absorbed by the sample under measurement, therefore the phase is not of great importance. Further work will be done on determining the impedance of the sample, where the phase will play an important role. With phase ignored, the system impulse response, $h_s[n]$, can be determined by taking the inverse Fourier transform of modulus of the Fourier transform of the system output,

$$h_s[n] = \mathfrak{F}^{-1}\{|\mathfrak{F}\{s[n]\}|\}, \tag{28}$$

where $s[n]$ is the output of the system captured by the microphone, and $\mathfrak{F}\{\cdot\}$ and $\mathfrak{F}^{-1}\{\cdot\}$ is the Fourier Transform operator and its inverse, respectively.

The system impulse response may directly be determined by using an impulse signal,

$$x[n] = \begin{cases} 1, & n = 0 \\ 0 & otherwise, \end{cases} \tag{29}$$

but this signal has severe limitations. The problem is that most systems limit the amplitude of the input signal. This in turn limits the Signal-to-Noise Ratio (SNR) that can be achieved with the impulsive signal. This may be remedied to a degree by averaging successive tests on the system, which increases the time of the measurement.

The system impulse response can also be determined by using other excitation signals, and using the advantages these signals offer - such as a low crest factor, and increasing the SNR by increasing the length of the signal without having to be limited by the arrival of the first reflection. The crest factor is the ratio of the peak energy of a signal to the average energy of the signal.

The remainder of this chapter will discuss two excitation signals, and modifications to these signals. The signals discussed are the swept sine signal, its modification, the low pass swept sine and the Maximum Length Sequence, and its modification, the Inverse Repeat Sequence.

University of Cape Town

4.2 SWEPT SINE

The swept sine is created by sweeping the frequency up and/or down in one measurement period[40], and is generated by,

$$x[n] = \sin\left[(a \cdot n + b) \cdot \frac{n}{f_s}\right], \quad 0 \leq n \leq N \tag{30}$$

where f_s is the sampling frequency, N is the number of samples in one measurement period, b is the offset,

$$b = 2\pi f_1, \tag{31}$$

and a is the sweep rate,

$$a = \frac{\pi (f_2 - f_1)}{N}. \tag{32}$$

Here f_1 and f_2 are the low frequency and high frequency range, respectively, that the swept sine sweeps between. Figure 11 illustrates the swept sine from 0 Hz to the Nyquist frequency, 22050 Hz in 100 ms.

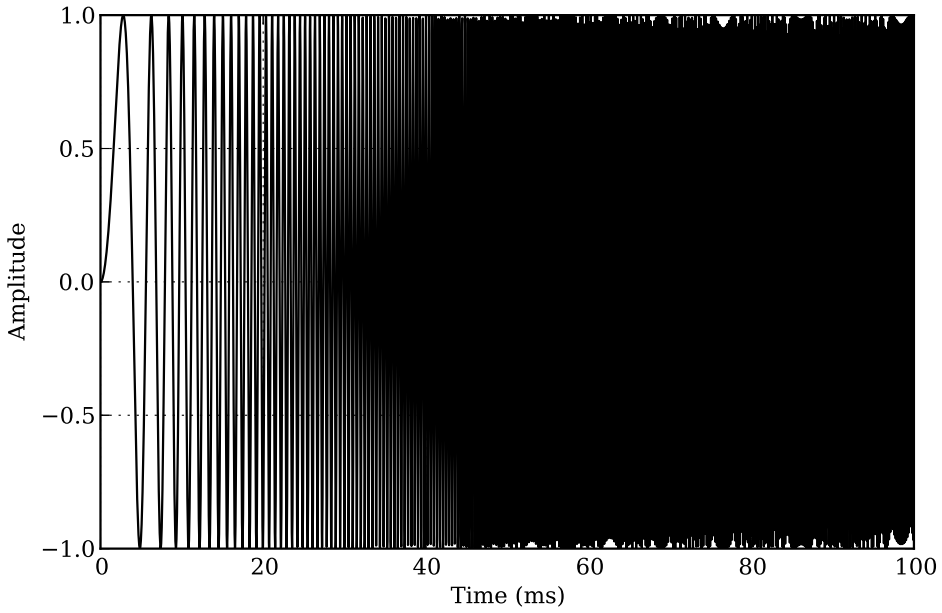

Figure 11: Swept sine sweeping between 0 Hz and 22050 Hz, the Nyquist frequency, in 100 ms.

The crest factor of the swept sine signal is approximately 1.45 [40]. It will be shown in the next subsection that the amplitude of the spectrum is not flat, due to the frequency changing in steps between each sample. To improve the situation, an inverse filtering technique will be used to create a flat spectrum at the cost of the crest factor - and hence the SNR - the resulting signal is known as the *low pass swept sine.*

4.3 LOW PASS SWEPT SINE

The swept sine has some attractive properties, including a low crest factor and being able to generate the signal up to a specific frequency. One major disadvantage is that the resulting spectrum is not flat or smooth. It has been shown that the cepstrum technique requires a flat spectrum, or at least a smooth spectrum without peaks and notches. This requirement makes the swept sine a bad signal choice. Fortunately, making use of inverse filtering techniques it is possible to generate a signal that is similar to the swept sine but has a flat spectrum. This signal is known as the low pass swept sine [6].

The algorithm, in block diagram form, to generate the minimum phase signal is shown in Figure 12. The algorithm is not limited to swept sine input signals and can be used to generate signals with arbitrary spectrum shape. To generate a low pass swept sine the input signal, $x[n]$, to the algorithm is the swept sine signal from 0 Hz to the Nyquist frequency (half the sampling frequency). The discrete spectrum of the input signal, $X[k]$, is calculated using the DFT. The k variable indicates that the spectrum is in the discrete frequency domain. A function similar to the cepstrum is then obtained. First the logarithm of the inverse modulus of the spectrum, $\ln|X[k]|^{-1}$ is calculated. This is shown in Figure 13. The inverse Fourier transform is then performed on $\ln|X[k]|^{-1}$ to give $c_p[n]$.

The *minimum phase* block in Figure 12 takes $c_p[n]$ as an input. This signal is then windowed in the following manner to produce, $m[n]$

$$m[n] = \begin{cases} c_p[n], & n = 0, N/2 \\ 2c_p[n], & 1 \leq n < N/2 \\ 0, & N/2 < n \leq N-1. \end{cases} \tag{33}$$

Here N is the length of $c_p[n]$. Now, $m[n]$ has the following properties; the real part of the Fourier transform of $m[n]$ is equal to $\ln|X[k]|^{-1}$, and the imaginary part is the minimum phase function, $\phi_{mp}[k]$. The exponential of Fourier transform of $m[n]$ results in the transfer function of the minimum phase inverse filter, $X_{mp}^{-1}[k]$. Multiplying the original input spectrum, $X[k]$, with the minimum phase inverse filter, $X_{mp}^{-1}[k]$, the result is a flat spectrum up to the Nyquist frequency. A low pass filter is applied to the resulting spectrum to attenuate frequencies above the highest frequency of interest. The low pass filter used was an 8^{th} order Butterworth digital low pass filter. If the cut off frequency is f_c Hz, then the new signal length is going to be approximately f_c/f_s times the length of the original signal. The filtered spectrum is finally inverse Fourier transformed to give the minimum phase signal $x_m[n]$. Figure 14 compares the spectra of the low pass swept sine to the original swept sine. It

University of Cape Town

can be seen that the spectrum of the low pass swept sine is significantly smoother than the spectrum of the original swept sine.

Figure 15 shows the resulting low pass swept sine compared to the original swept sine. It is of interest to note that the resulting minimum phase signal $x_m[n]$ is similar in appearance to the original swept sine signal except there is a noticeable 'hump'. This 'hump' increases the crest factor, and hence lowers the SNR. The cost of the lower SNR is outweighed by the benefit of the flat spectrum of the resulting low pass swept sine signal.

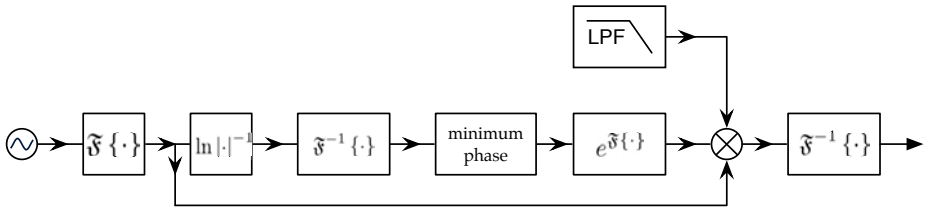

Figure 12: Algorithm to obtain the minimum phase signal from an input signal.

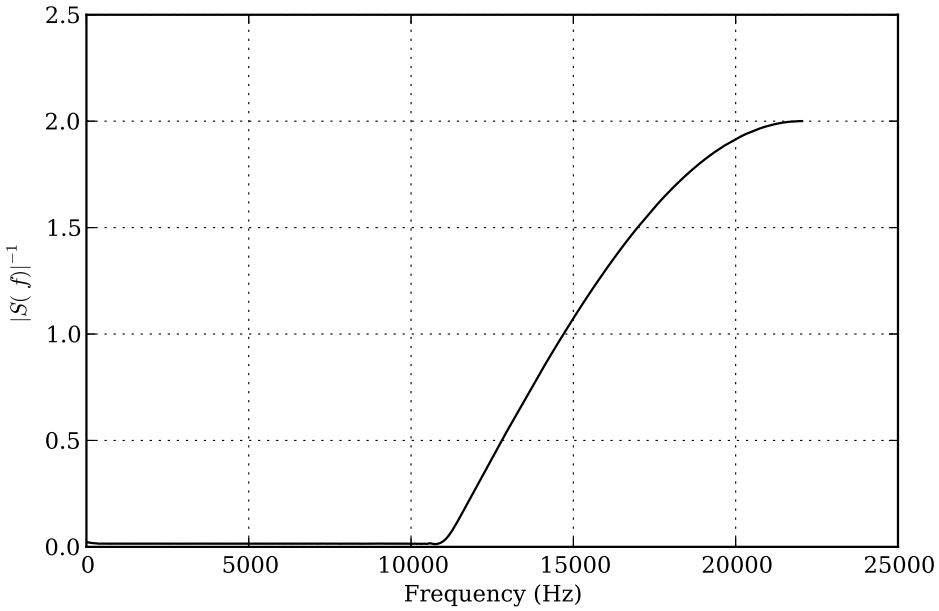

Figure 13: The inverse logarithmic spectrum of the swept sine signal shown in Figure 11.

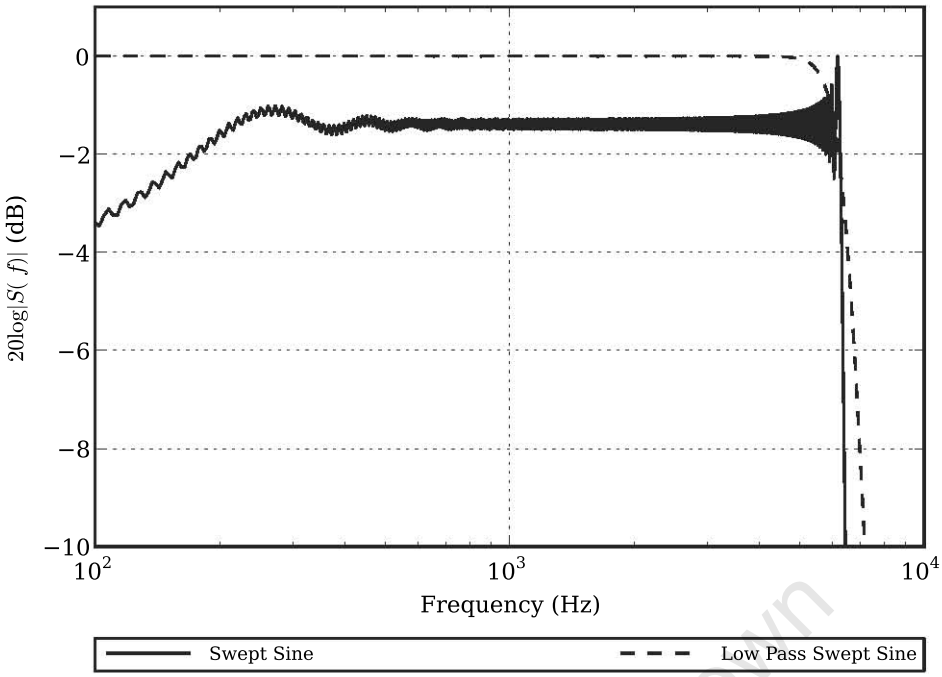

Figure 14: The spectrum of the input swept sine input signal compared to the resulting spectrum of the low pass swept sine.

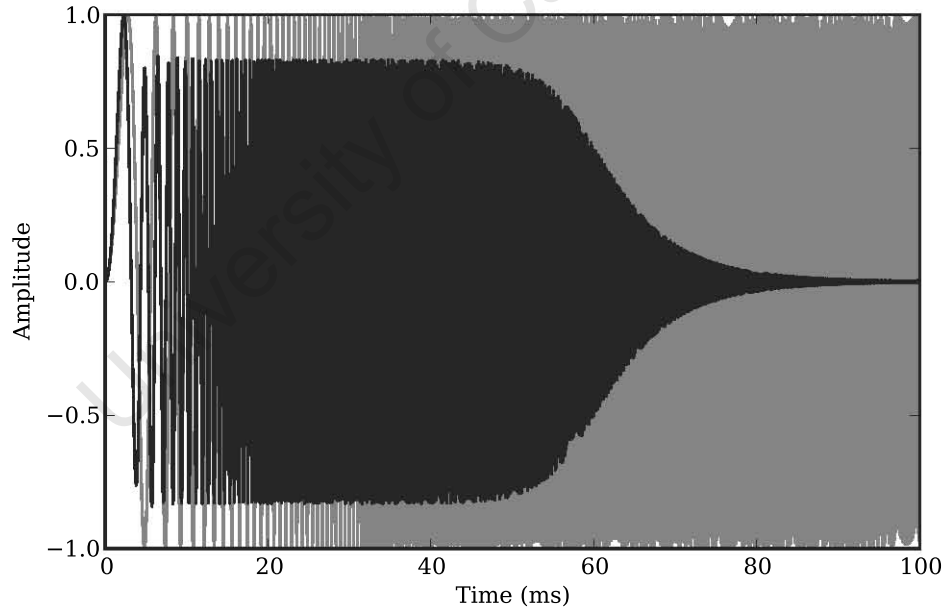

Figure 15: The resulting minimum phase signal, shown in black, after applying the algorithm in Figure 12 to the swept sine signal, shown in grey.

University of Cape Town

4.4 MAXIMUM LENGTH SEQUENCE

4.4.1 *Introduction*

Maximum Length Sequence (MLS) signals are binary signals, that can be used to determine the periodic impulse response of a system using circular convolution. A MLS generator generates a sequence of length $P = 2^N - 1$, with N the size of the generator, and P the periodicity of the sequence.

In order to determine the impulse response of a system, an analog version of the generated MLS signal is applied to the system. The response is then cross-correlated with the original MLS signal, resulting in the system impulse response.

4.4.2 *Generating Maximum Length Sequences*

Maximum Length Sequences can efficiently be generated using one-bit linear feedback registers[21]. A Maximum Length Sequence, shown in Figure 16, is generated using the following recursive relationship, for a 4 bit generator,

$$s_{\{0,1\}}[n] = a_0[n], \tag{34}$$

with

$$a_k[n+1] = \begin{cases} a_0[n] + a_1[n] & k = 3 \\ a_{k+1}[n] & otherwise, \end{cases} \tag{35}$$

where k is the bit register position, n is the time index, and $+$ is modulo-2 addition, the *XOR* operator. This relationship is shown in Figure 17, with $N = 4$. MLS signals are periodic, with the shift registers cycling through each possible binary value from 1 to 2^N. If all the registers are 0 then the generator will get stuck in that state. This is the reason it does not generate a sequence of 2^N bits.

University of Cape Town

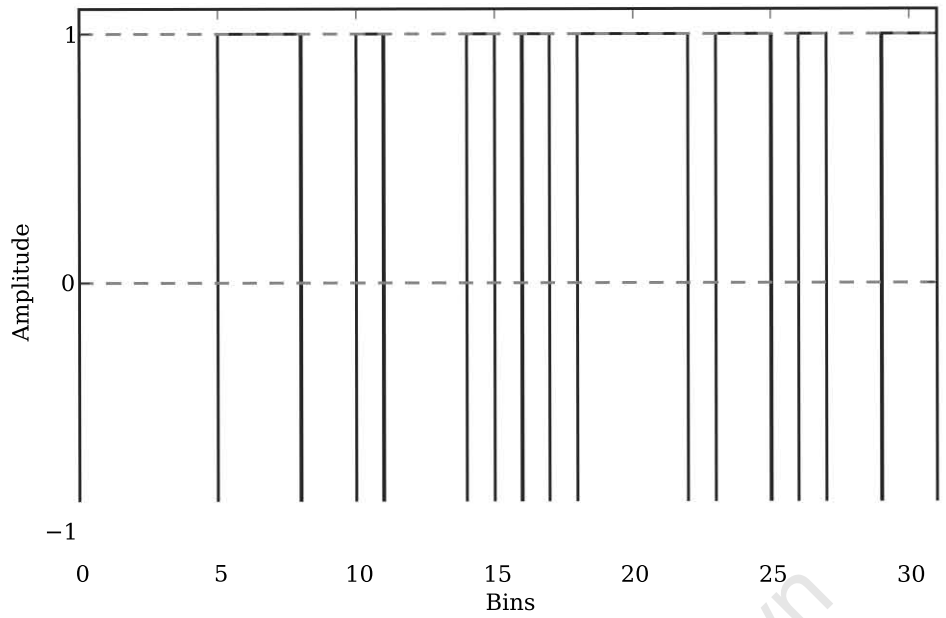

Figure 16: An example MLS generated with a 5-bit feedback register.

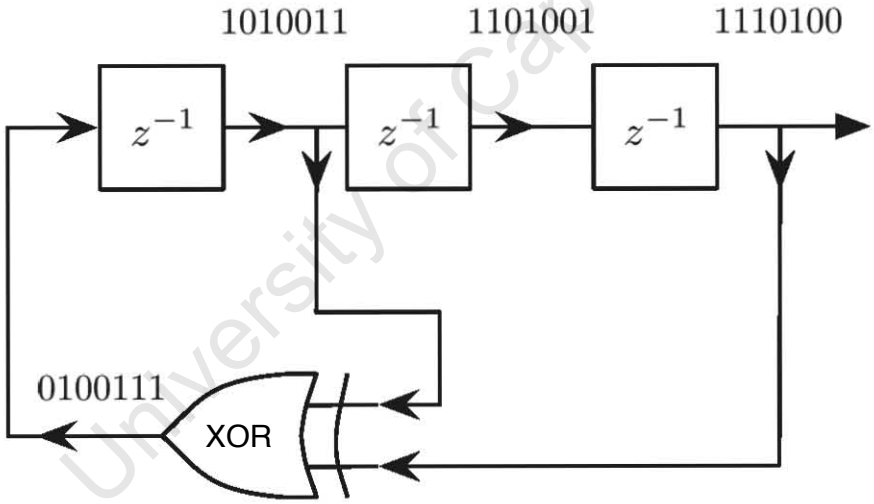

University of Cape Town

Figure 17: System of binary feedback shift registers used to generate a maximum length sequence, with $P = 7, N = 3$.

Equation 35 is dependent on the number of bits in the register. To determine which taps of the shift register are fed to the *XOR* gate, a polynomial of degree N is associated with a N bit shift register. The coefficient of the polynomial are either 1, if the tap is fed to the *XOR* gate, or 0. The class of polynomials used to generate the maximum number of bits, 2^N, are called primitive polynomials. If the polynomial is not primitive, the periodicity of the sequence will be less than 2^N. Generat-

ing primitive polynomials is difficult, but fortunately tables with high degree polynomials are available in literature [21].

In order to output the signal to the speaker, the output needs to be mapped from $\{0,1\} \rightarrow \{1,-1\}$, which can be achieved as follows,

$$s_{\{1,-1\}}[n] = 1 - 2 \cdot s_{\{0,1\}}[n]. \tag{36}$$

4.4.3 *Recovering the System Impulse Response*

In order to recover the system impulse response using MLS, the signal is generated using Equation 36, and passed to the power amplifier, which powers the loudspeaker. The output of the loudspeaker, as well as the impulse response of the system, is captured by the microphone,

$$y[n] = \sum_{k=-\infty}^{\infty} x[n] \otimes h[n-k], \tag{37}$$

where $y[n]$ is the captured signal, $h[n]$ is the system impulse response, $x[n]$ is the MLS signal generated by the loudspeaker and $\otimes$ is the discrete linear convolution operator. It is important to note that since MLS is periodic, linear convolution is not applicable, and circular convolution should be used. Circular convolution recovers the periodic impulse response of the system, $h'[n]$, which is related to the true impulse response of the system by,

$$h'[n] = h[n \bmod P], \tag{38}$$

where P is the period of MLS. A consequence of this fact is that the period of the MLS, P, should be chosen such that the tail of the true impulse response of the system, $h[n]$, is negligible. If the tail is not negligible, it will be overlapped to the beginning of the periodic impulse response, $h'[n]$, causing time aliasing, shown in Figure 18.

University of Cape Town

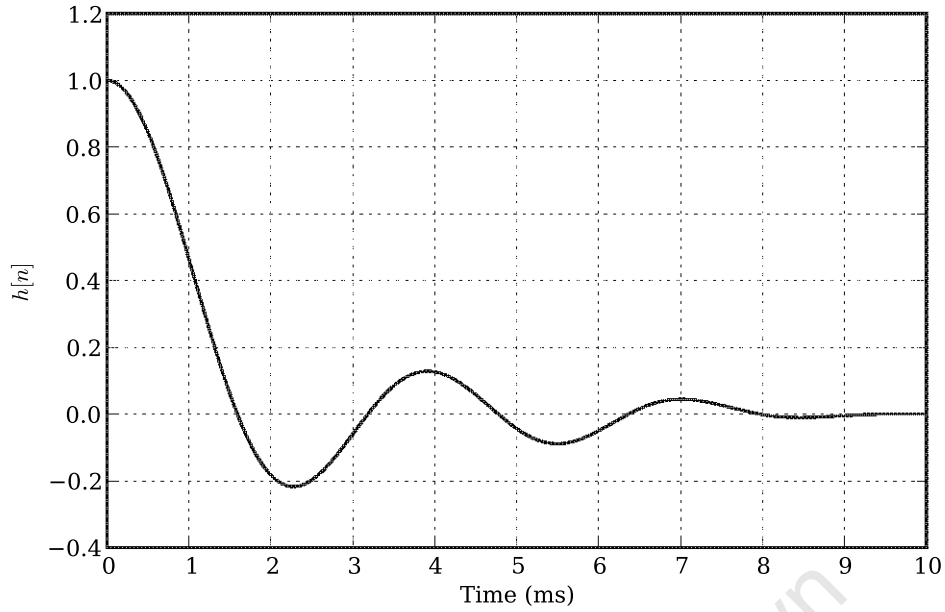

(a)

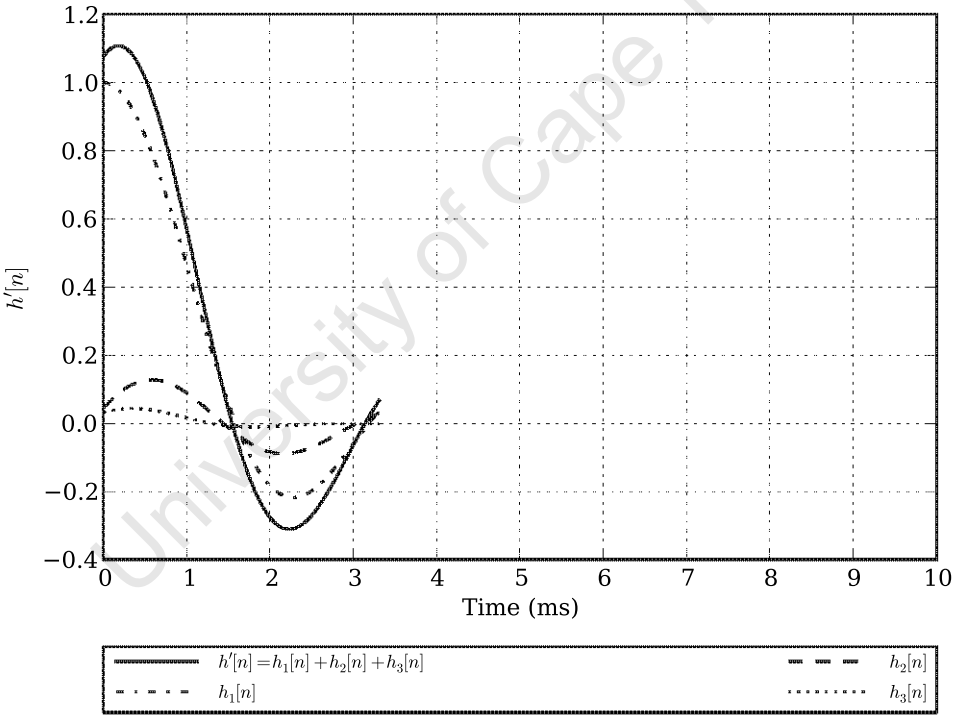

(b)

University of Cape Town

Figure 18: a) The actual impulse response, lasting 10 ms. b) The time aliased impulse response, $h'[n]$, made up of the sum of the three aliased impulse response, $h_1[n]$, $h_2[n]$ and $h_3[n]$.

Another important consequence of using a periodic signal, is that it must exist for all time. This is not true in any real system, but if the system impulse response stabilises in M samples, with $M < P$, then

an additional L samples should be applied, and those L samples analysed to determine the system impulse response. In practice it is easier to generate a MLS with $P \gg M$, and apply the signal at least twice, and analyse the response to the second signal.

An important property of MLS is that the autocorrelation of an MLS, $\Omega_{ss}[n]$, is

$$\begin{aligned}\Omega_{ss}[n] &= s'[n] \circledast s'[n] \\ &= \frac{1}{L}\sum_{k=0}^{L-1} s'[k]\, s'[k+n],\end{aligned} \tag{39}$$

where $s'[n]$ is the periodic MLS with periodicity of L, and $\circledast$ is the circular convolution operator. This results in

$$\Omega_{ss}[n] = \begin{cases} 1 & n = 0 \\ \frac{-1}{L} & 1 \leq n < L. \end{cases} \tag{40}$$

It is useful to re-normalise Equation 39 by $(L+1)$ instead of L, which leads to

$$\begin{aligned}\Omega_{ss}[n] &= s'[n] \circledast s'[n] \\ &= \frac{1}{L+1}\sum_{k=0}^{L-1} s'[k]\, s'[k+n].\end{aligned} \tag{41}$$

The autocorrelation of the MLS can now be written as

$$\Omega_{ss}[n] = \begin{cases} \frac{L}{L+1} & n = 0 \\ \frac{-1}{L+1} & 1 \leq n < L. \end{cases} \tag{42}$$

This allows $\Omega_{ss}[n]$ to be expressed as

$$\Omega_{ss}[n] = \delta'[n] - \frac{1}{L+1}, \tag{43}$$

where $\delta'[n]$ is the periodic unit sample function, with period L. From Equation 43 it can be seen that as L increases, $\Omega_{ss}[n]$ approaches the ideal periodic unit sample function, $\delta'[n]$.

Now, applying a periodic MLS, $s'[n]$, to a system with periodic impulse response, $h'[n]$, which results in the output, $y'[n]$,

$$y'[n] = s'[n] \circledast h'[n]. \tag{44}$$

The cross correlation of $y'[n]$ with $s'[n]$, $\Omega_{sy}[n]$, and re-normalising with $L+1$ instead of L, is

$$\begin{aligned}\Omega_{sy}[n] &= s'[n] \circledast y'[n] \\ &= s'[n] \circledast \left(s'[n] \circledast h'[n]\right) \\ &= \Omega_{ss}[n] \circledast h'[n].\end{aligned} \tag{45}$$

University of Cape Town

This states that the cross correlation of the output signal $y'[n]$ with the MLS, $s'[n]$, is equal to the auto-correlation of the MLS convolved with the periodic impulse response of the system, $h'[n]$. Substituting the normalised autocorrelation of the MLS Equation 43 into Equation 45 results in

$$\begin{aligned}\Omega_{sy}[n] &= \left(\delta'[n] - \frac{1}{L+1}\right) \circledast h'[n] \\ &= h'[n] - \frac{1}{L+1}\sum_{k=0}^{L-1} h'[k] \\ &= h'[n] - \frac{1}{L}\sum_{k=0}^{L-1} h'[n] + \frac{1}{L(L+1)}\sum_{k=0}^{L-1} h'[n].\end{aligned} \tag{46}$$

The second term in Equation 46 is the mean value of the system response, the *DC* value, and the third term is the same DC value scaled by $\frac{1}{L+1}$. Therefore the cross correlation of the output of system excited by a MLS, results in the AC coupled periodic impulse response of the system.

4.5 INVERSE REPEAT SEQUENCE

The Inverse Repeat Sequence (IRS) is an extension to the MLS, and is generated from an MLS as follows

$$x_{IRS}[n] = \begin{cases} x_{MLS}[n] & n \text{ even}, \quad 0 \leq n < 2L \\ -x_{MLS}[n] & n \text{ odd}, \quad 0 \leq n < 2L, \end{cases} \tag{47}$$

where $x_{MLS}[n]$ is the MLS with period L. The primary advantage of using the IRS over the MLS is that the IRS offers complete immunity to even-order nonlinearity[13].

To illustrate how the IRS signal can be used to recover the impulse response of a system, consider applying $x_{IRS}[n]$, to an unknown system $h[n]$ to produce the output signal, $y[n]$,

$$y[n] = x_{IRS}[n] \otimes h[n]. \tag{48}$$

Here $\otimes$ is the convolution operator. Now it can be shown [38] that convoluting the MLS signal, $x_{MLS}[n]$, with itself results in an impulse at $n = 0$ as well as a small DC offset

$$\begin{aligned}\Omega_{MLS}[n] &= x_{MLS}[n] \circledast x_{MLS}[n] \\ &= \delta[n] - \frac{1}{L+1}.\end{aligned} \tag{49}$$

University of Cape Town

For the IRS signal, the circular convolution becomes

$$\begin{aligned}\Omega_{IRS}[n] &= x_{IRS}[n] \circledast x_{IRS}[n] \\ &= \begin{cases} \Omega_{MLS}[n] & n \text{ even} \\ -\Omega_{MLS}[n] & n \text{ odd} \end{cases} \\ &\delta[n] - \frac{(-1)^n}{L+1} - \delta[n-L], \qquad 0 \leq n < 2L.\end{aligned} \tag{50}$$

The above equation has an impulse at the origin, and an inverted impulse at L samples. It also has an oscillation at half the sampling frequency, which is due to the $-\frac{(-1)^n}{L+1}$ term. It can be shown that this impulse response has complete even-order non-linearity immunity[13], however the swept sine signal offers greater odd-order distortion immunity.

4.6 NOISE IMMUNITY

Green [18] noted that the cepstral technique is very sensitive to noise in the measuring environment. It has been shown that using the cross-correlation property of psuedorandom signals offers a high degree of noise immunity [45, 16]. The reason for this noise immunity is that the background noise will have a very low correlation with the psuedorandom excitation signal. To determine the system impulse response the output of the system is cross correlated with the input to the system. Due to the low correlation with the input signal, the background noise is significantly reduced.

To illustrate the advantage of this noise immunity two measurements were done on an asphalt sample using the low pass swept sine and the IRS signals. The first measurement was performed in normal laboratory conditions, and the second measurement was performed with a loud sound source present. The sound source was a loudspeaker located close to the middle of the cepstral tube. The excitation signal for this loudspeaker was a recording of ambient traffic noise, and had a similar noise spectrum that could be expected with *in-situ* measurements. The results are shown down to 100 Hz, although the frequency range of interest is only down to 200 Hz, so that the sound level could be adjusted. This process is explained in Section 9.1.

Figure 19 show the results of the two measurements using the low pass swept sine. The results from the measurement in the quiet environment are shown with a solid line. The dashed line represents the results with the noisy sound source switched on. It can be seen that there is a maximum difference of 0.05 at 200 Hz between the two measurements.

The results of the two measurements using the IRS signal are shown in Figure 20. There is a close correlation between the measurement in the

University of Cape Town

quiet and the measurement in the noisy environment. There is however a maximum difference of 0.03 at 200 Hz and 1600 Hz. There is also a difference of 0.02 at 1000 Hz.

The power spectral density of the the environment with and without the noise source present is shown in Figure 21. It can be seen that the cepstral tube reduces the noise level by 20 dB at approximately 270 Hz, compared to 170 Hz. The increased noise levels below 300 Hz is the reason for the variation between the measurements in the noisy and quiet environments in the low frequency region.

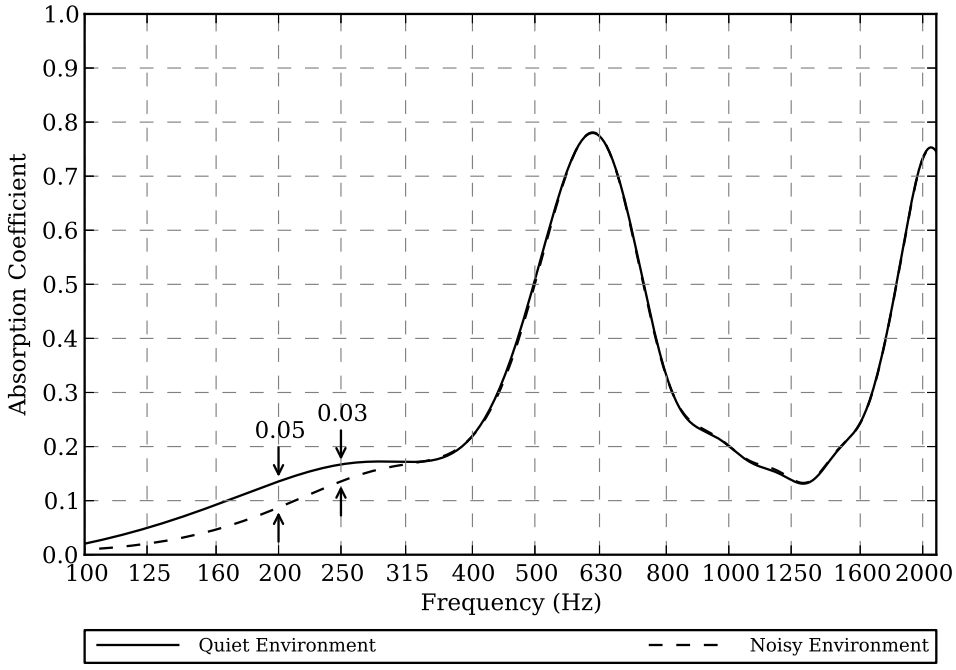

Figure 19: The absorption coefficient of an asphalt sample measured in a quiet environment (solid line) and in a noisy environment (dashed line) using the low pass swept sine signal.

Univers.

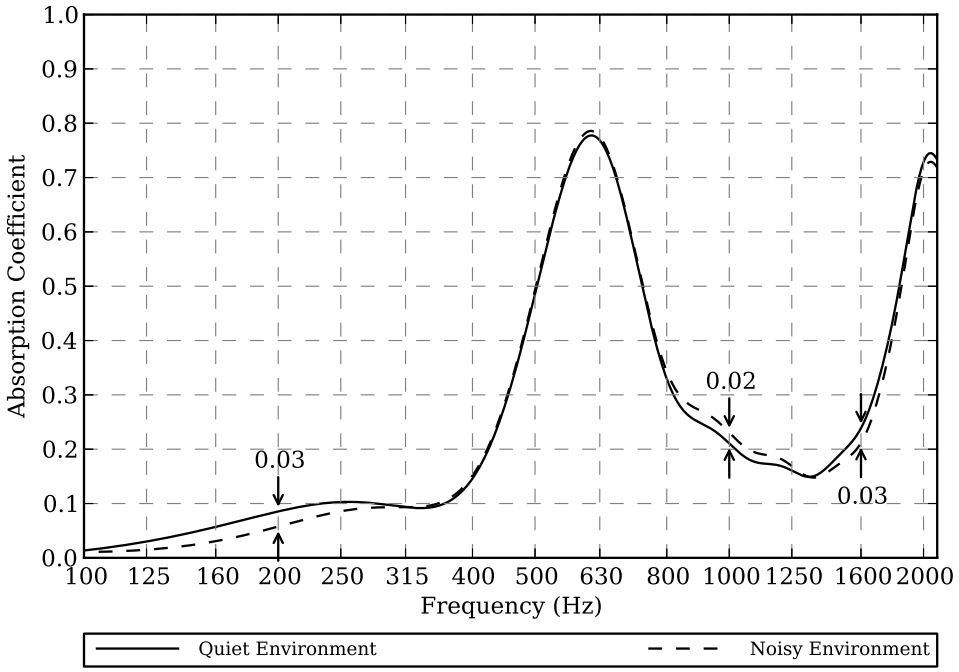

Figure 20: The absorption coefficient of an asphalt sample measured in a quiet environment (solid line) and in a noisy environment (dashed line) using the Inverse Repeat Sequence signal.

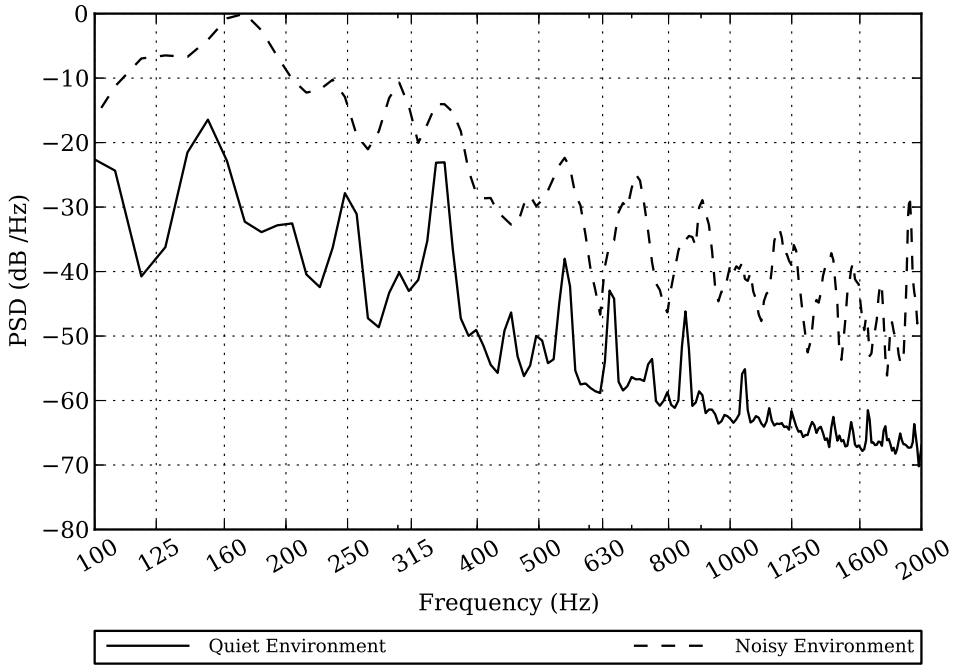

Figure 21: The power spectral density captured by the microphone of the quiet environment, solid line, and the noisy environment, shown with a dashed line.

4.7 CONCLUSIONS

This section presented four excitation signals to determine the transfer function of a system. Jongens [27] used the Low Pass Swept Sine signal, and obtained results that correlated closely with the impedance tube method.

It was shown that noise affects the low pass swept sine measurement more than the IRS measurement between 200 Hz and 315 Hz, however the low pass swept sine measurement was negligibly affected over the range 315 Hz to 2000 Hz. The maximum difference between the measurement in the noisy environment and the quiet environment was 0.03 for the IRS measurement, and 0.05 for the low pass swept sine measurement.

It will be shown in Section 6.2.1 that connecting a tube to the front of the loudspeaker driver increases the impedance on the loudspeaker. This has the effect of emphasising low frequencies, which increases the crest factor of the swept sine signals. It was therefore decided that the IRS signal should be used as the excitation signal.

University of Cape Town

5

THE LOUDSPEAKER

5.1 INTRODUCTION

The loudspeaker converts electrical energy into acoustical energy. It is also the weakest link in the measurement chain. The loudspeaker's low frequency roll off and high frequency roll off dominate the response of the system. If the high frequency roll off is above the frequency range of interest, the loudspeaker can be treated as a high pass filter. Above the first ring anti-resonant frequency, the loudspeaker's cone begins to break up introducing peaks, notches and fine structure into the frequency response. The mechanics of the loudspeaker produce non-linear distortion.

The frequency response of the *ApartAudio OVO5T,* shown in Figure 22, was obtained using the cepstral tube apparatus. The 2 meter tube was extended to 8.5 meters by attaching a 6.5 meter tube to the end of the 2 meter tube. The connection between the two pipes was not seamless, therefore some of the sound energy was reflected back towards the microphone at the connection. This reflected energy also introduces undulations into the frequency response.

of Cape Town

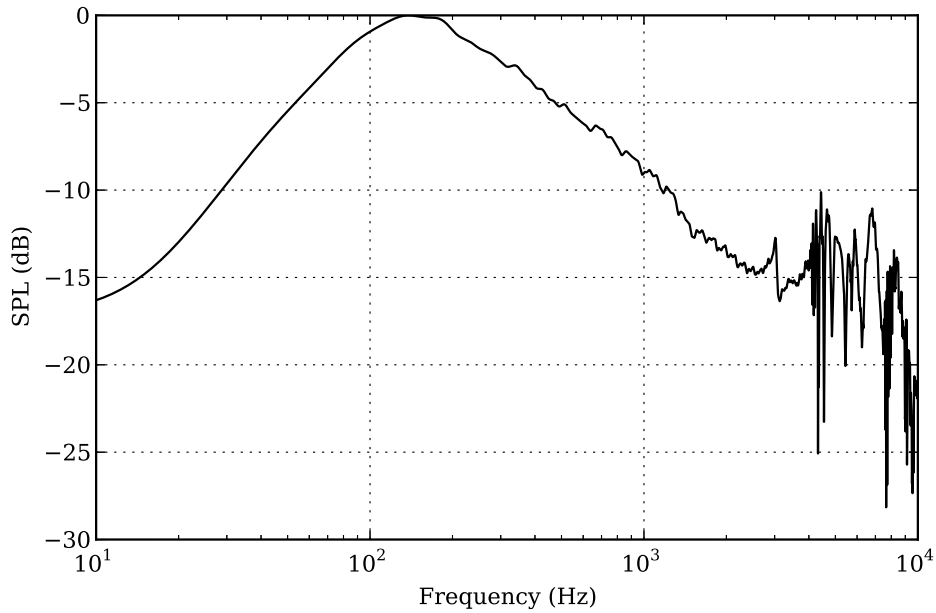

Figure 22: The frequency response of the *ApartAudio OVO5T* loudspeaker driver coupled to a 110 mm diameter pipe.

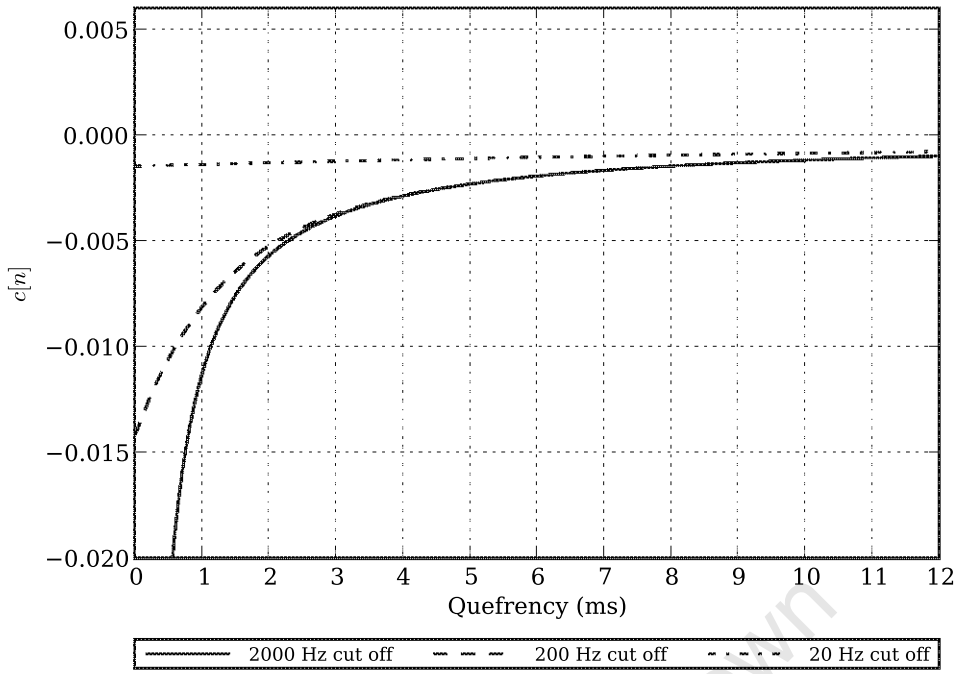

Figure 23: Zoomed direct cepstrum of three theoretical loudspeakers with low frequency cut offs of 2000 Hz, 200 Hz and 20 Hz.

This section discusses these issues, and presents a method to reduce the influence of the notch in the frequency response.

5.2 SOURCES OF UNCERTAINTIES

5.2.1 *Low Frequency Roll Off*

The low frequency roll off of the loudspeaker dominates the overall system's response. Figure 23 shows the direct cepstrum of three theoretical loudspeakers with low frequency cut offs of 2000 Hz, 200 Hz and 20 Hz, each have a 6 dB/octave roll off. It can be seen that the low frequency roll off of the loudspeaker has two effects. It introduces a small DC offset, and it extends the tail of the direct cepstrum. The effect of the DC offset is discussed in Section 7.7.

5.2.2 *Cone breakup*

A cone acts as a rigid object, which can be modelled as a piston, up to a cut off frequency. Above this cut off frequency two wave types appear simultaneously on the cone, and the cone's transverse velocity is no longer uniform over its surface[14]. A longitudinal wave appears at the top of the cone, while a bending wave appears at the base of the cone. Bending waves have displacements that are normal to the surface

University of Cape Town

of the cone, and longitudinal waves have displacements in the plane of the cone. In paper cones, these waves can appear simultaneously, and one type has no effect on the other.

The bending and longitudinal waves have the effect of superimposing peaks, notches and a fine structure onto the frequency response curve of the loudspeaker. These effects introduce noise into the cepstrum.

The frequency at which the cone break occurs starts at the ring anti-resonant frequency, f_{ra}, and occurs approximately at [14],

$$f_{ra} \approx \frac{c \cos \theta_{\mathrm{LS}}}{2\pi R_b}, \tag{51}$$

where c is the speed of sound, θ_{LS} is the angle of the cone makes with the axial-axis - half of the *opening angle* of the cone, and R_b the outer edge radius. The geometry of the cone is shown in Figure 24, showing the quantities θ_{LS} and R_b. A point to make regarding the above formula is, increasing the radius and the opening angle, decreases the frequency of cone break up.

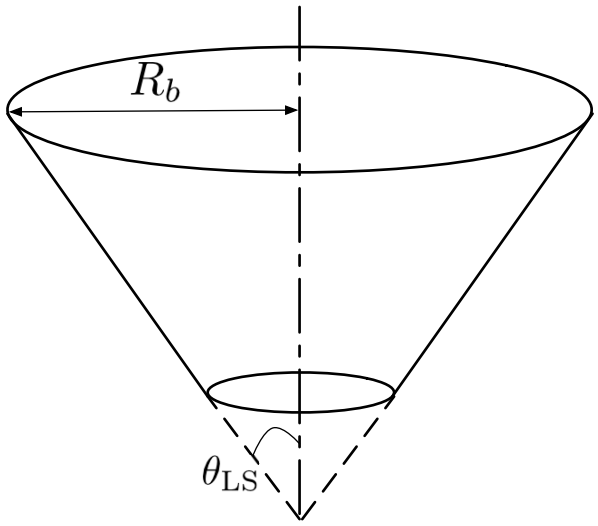

Figure 24: Cone geometry, illustrating the geometric quantities that determine the ring anti-resonant frequency.

5.2.3 *Driver Nonlinearities*

Nonlinearities in the loudspeakers driver's response should be noted when measuring the impulse response of the loudspeaker. This is due to the fact that methods employed to measure the impulse response are under the assumption that the device under test (DUT) is a linear-time-invariant (LTI) system. Depending on the severity of the nonlinearity, this may have a significant influence on the measured response.

The major source of non-linearities of the driver lie in the electro-dynamic motor[39], and are due to the non-linearity of the spider (a flexible suspension attached to the voice coil to ensure the cone remains centered), the non-uniformity of the radial induction, B, in the air-gap and the variation of self inductance in relation to both the instantaneous position of the voice coil, and the current flowing through it.

The non-linearities due to the spider and the radial induction in the air gap are mainly an issue around the resonant frequency of the loudspeaker. This is where the loudspeaker diaphragm movement is at a maximum. The typical magnitude of the second and third order distortions for these nonlinearities are between 1 and 4%[39].

The non-linearity due to the self inductance becomes decisive in the mid-range frequencies, and second and third order distortions is of the order of between 0.1 and 1%.

The non-linearities of the the *ApartAudio OVO5T* loudspeaker were measured using the apparatus for the cepstral measurement, discussed in Section 8.3. The Total Harmonic Distortion (THD) was measured by applying a sinusoidal signal to the loudspeaker, and measuring the signal generated by the loudspeaker. The measurement procedure was repeated to measure the THD over the range of 100 Hz to 2000 Hz in 50 Hz increments. The Power Spectral Density (PSD) was estimated using *Welch's Method*[49]. The THD, in percentage, of the loudspeaker is then given by

$$\text{THD} = 100\sqrt{\frac{\sum_{i=2}^{N} P_i}{P_1}}, \tag{52}$$

where P_1 is the power of fundamental frequency, P_i is power the i^{th} harmonic and N is the order of the highest harmonic. Figure 25 shows the measured THD of the *ApartAudio OVO5T* loudspeaker. It is to be noted that the results below approximately 500 Hz are significantly influenced by the background noise.

University of Cape Town

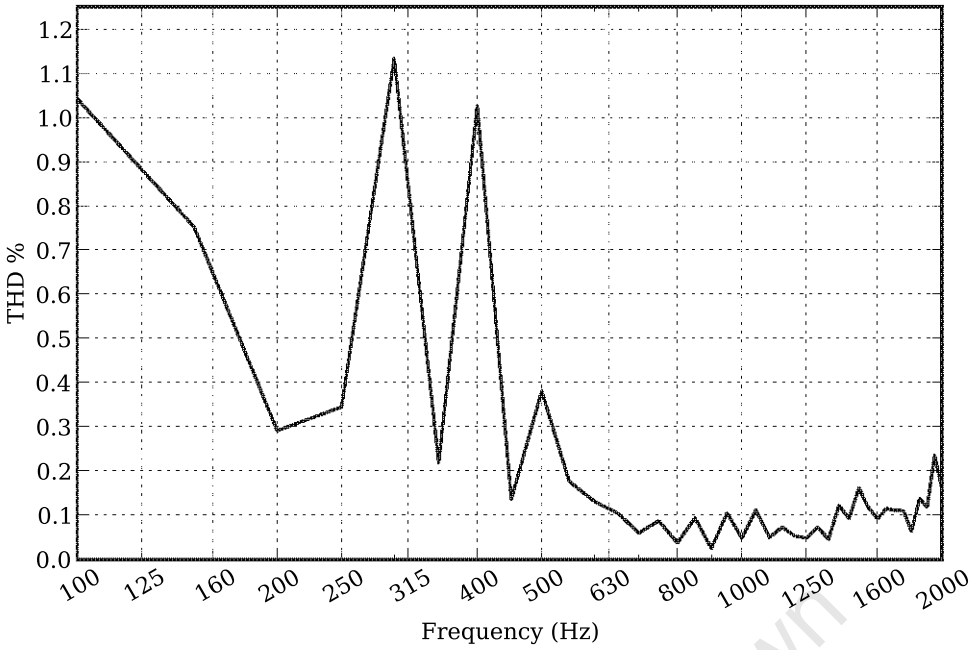

Figure 25: The Total Harmonic Distortion, in percentage, of the *ApartAudio OVO5T.*

Figure 26 shows the effect that a 0.1% second order distortion has on the direct cepstrum. In Figure 26 it can be seen that a 0.1% second order distortion results in a small offset in the direct cepstrum. The effect of this offset will be discussed in Chapter 7.

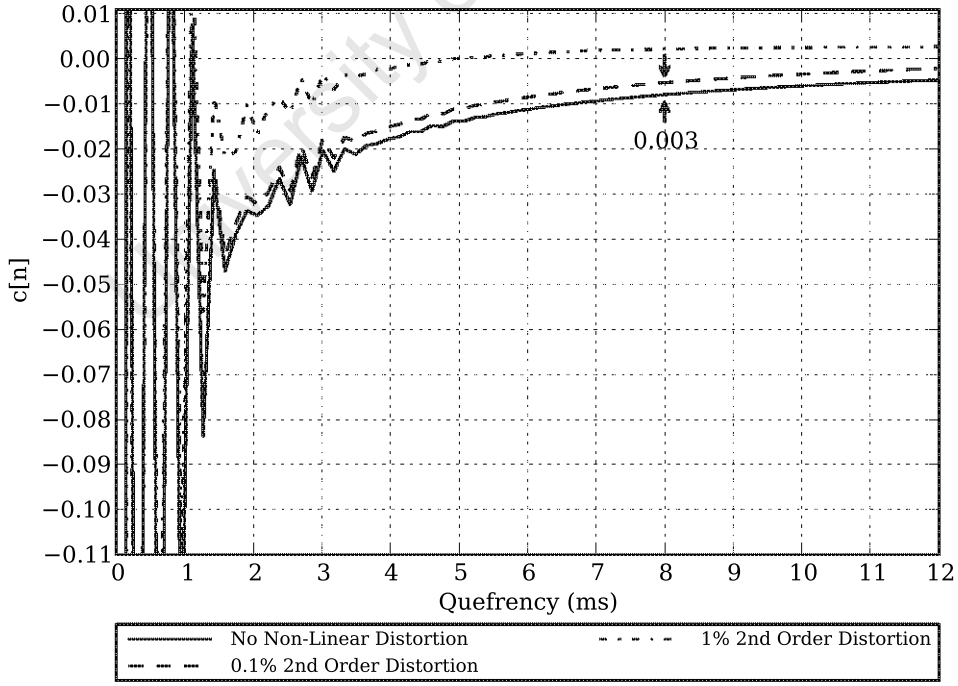

Figure 26: A 0.1% 2nd order distortion results in the direct cepstrum being offset by approximately 0.003.

University of Cape Town

5.3 REDUCING UNCERTAINTIES

The frequency response of the loudspeaker used in the measurements is shown in Figure 22. At approximately 3000 Hz a sharp peak can be seen, followed by a sharp notch. This is due to the uncontrolled cone breakup discussed in Section 5.2.2. Placing lightweight fibrous material, shown in Figure 27, significantly reduces these peaks and notches. The glass fibre acts as a low pass filter which reduces the energy at the high frequencies, and hence the sharp peaks and notches.

Figure 27: Placing fibrous material on the loudspeaker cone smooths the frequency of response

6

INFLUENCE OF THE TUBE

6.1 INTRODUCTION

The tube has a significant influence on the ability to accurately measure the plane wave sound absorption coefficient. The impedance loading effect on the loudspeaker emphasises the low frequency response of the loudspeaker. The coupling of the tube to the loudspeaker can introduce sharp discontinuities. These edges cause an impinging wave to scatter. Above a cut off frequency, the assumption of plane wave propagation in the tube falls. This is because higher order modes are activated, and pressure along a cross-sectional plane is no longer constant. Wave guides are dispersive mediums, which means the velocity of a wave is dependent on its frequency. There are two consequences of this, the first is that high frequency oscillations are introduced into the impulse response of the system. And, two, modes do not propagate at their respective cut off frequency causing sharp notches in the frequency response of the system.

This chapter will deal with these influences, and methods employed to overcome them.

University of Cape Town

6.2 INFLUENCES ON THE SYSTEM

6.2.1 *Change in radiation resistance due to the impedance tube*

The low frequency emphasis has two major influences on the accuracy of the measurements. The low frequency cut off of the loudspeaker is reduced, increasing the length of the impulse response of the loudspeaker. The low frequency emphasis also significantly increases the crest factor of the swept-sine based excitation signal. Increasing the crest factor decreases the SNR. This effect can be seen in Figure 22 between approximately 180 Hz to 2000 Hz.

A loudspeaker can be modelled as a piston at low frequencies, that is, frequencies where the cone of the loudspeaker moves as a rigid object[28]. The radiation impedance of a piston attached to an infinite baffle is given as $Z_r = R_r + jX_r$, where the radiation resistance R_r and reactance X_r are

$$R_r = \pi a^2 \rho_0 c R_1 (2ka) \tag{53}$$

and

$$X_r = \pi a^2 \rho_0 c X_1 (2ka) . \tag{54}$$

Where a is the radius of the piston, ρ_0 is the density of air, c is the speed of sound in air. R_1 is the *piston resistance function* and X_1 is the *piston reactance function*, they are defined as

$$R_1(x) = 1 - \frac{2J_1(x)}{x} \tag{55}$$

and

$$X_1(x) = \frac{2H_1(x)}{x}. \tag{56}$$

Where $J_1(x)$ is the *Bessel* function of the first order, and $H_1(x)$ is the *first order Struve* function. Figure 28 gives the plots of these resistance and reactance functions.

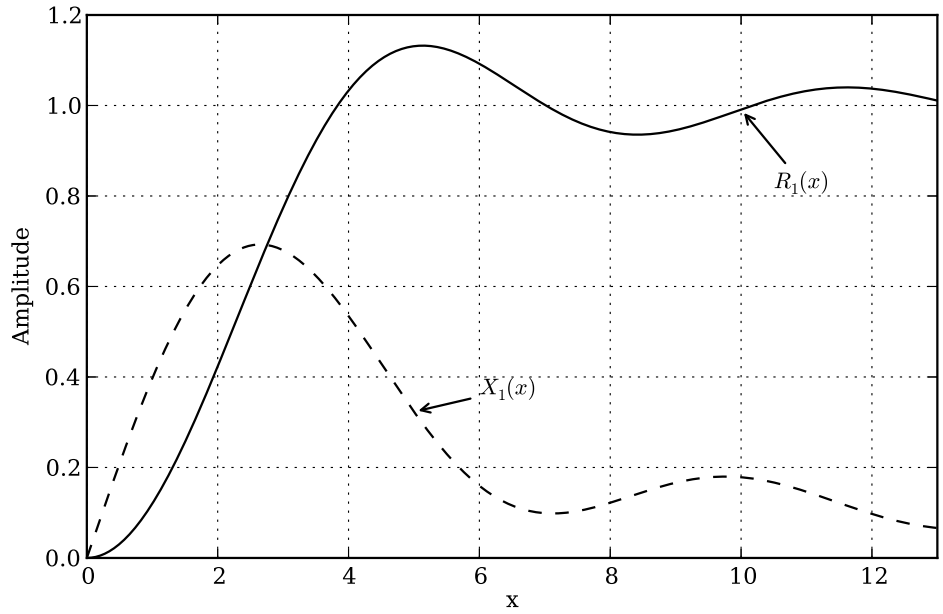

Figure 28: Piston resistance and reactance functions for a circular piston.

The sound power, W, radiated into free air by a circular piston is given as,

$$W = \frac{1}{2} R_r U_0^2, \tag{57}$$

where R_r is the radiation resistance of the circular piston, defined by Equation 53, and U_0 is the velocity amplitude of the piston. Since the radiation resistance is dependent on frequency, the sound power radiated is also dependent on frequency. The piston resistance function for a 100 mm diameter piston is shown in Figure 29. It can be seen that the resistance, is reduced by approximately 6 dB / octave, for decreasing frequency below 1600 Hz.

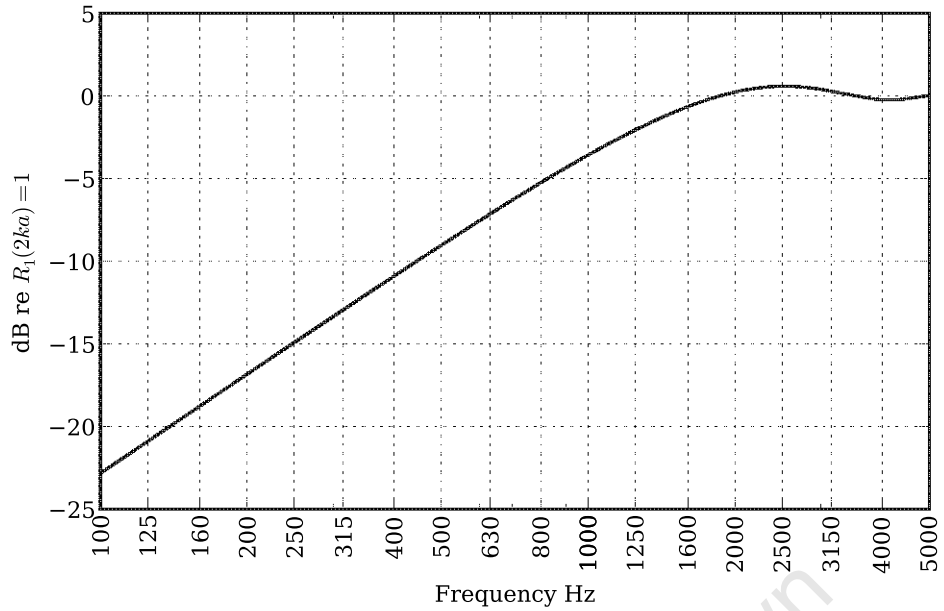

Figure 29: Piston resistance for a 100 mm diameter piston in an infinite baffle radiating into free air.

The velocity amplitude of the piston, U_0, is determined by the mechanical impedance of the loudspeaker, Z_m[28]. The change in radiation resistance is, almost exactly, balanced by the change in mechanical impedance - down until the resonance frequency of the the loudspeaker. Therefore there is a flat frequency response above the low frequency cut-off of the loudspeaker.

Placing a tube in front of the loudspeaker has the effect of creating a loading impedance on loudspeaker[1, 28]. The sound power radiated from the loudspeaker into the tube is determined by the Acoustic resistance,

$$R = \frac{\rho_0 c}{S}, \tag{58}$$

where ρ_0 is the density of air, c is the speed of sound, S the cross sectional area of the tube. The above equation is valid so long as plane waves propagate in the tube, which is valid up until the cut-off frequency of the tube. It can be seen by the above equation that acoustic resistance is independent of frequency. Since the mechanical impedance of the loudspeaker, Z_m, is the same regardless of whether the loudspeaker is propagating into free air or into a tube, the sound power will increase, with decreasing frequency, below 1600 Hz.

6.2.2 *Construction of Waveguide*

The loudspeaker is mounted on the inner face of the enclosure. The tube is coupled to the loudspeaker enclosure with a PVC flange. It can be seen

University of Cape Town

in Figure 30, th
and the input to
generating edge
field in the tube
incident sound

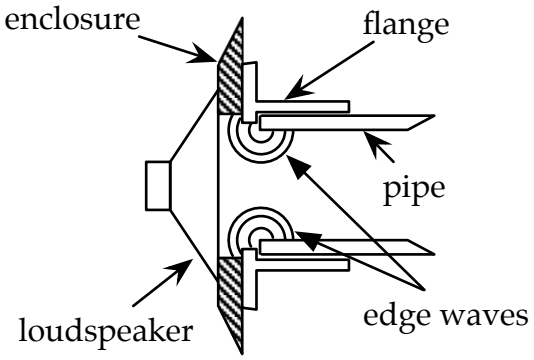

Figure 30: The connection of the loudspeaker to the tube. The loudspeaker is mounted on the inside of the enclosure, a flange is mounted on the outside of the enclosure, and the tube is placed inside the flange. The edge waves generated by the sharp edges are identified.

6.2.3 *Cross mode propagation in circular wave-guide*

The excitation of higher order modes set the upper limit of the frequency range so that the normal incident sound power absorption coefficient can be determined. Above the cut off frequency of the first mode, it can no longer be assumed that plane waves propagate in the tube.

Waves propagating in the impedance tube are complicated by the fact that wave guides are dispersive systems[9]. A dispersive system is one where the wave velocity is dependent on the frequency of the wave. The sound waves propagate at c, the speed of sound of the medium, up until the cut-off frequency of the first cross-mode. Above this frequency, the sound wave no longer propagates as a plane wave - one where the pressure across the cross section of the wave guide is constant. For a circular wave guide with a diameter of $2a = 110$ mm, the first cut-off frequency is 1993 Hz, above this frequency the $(0,1)$ cross-mode wave propagates. The contours of the $(1,0)$ cross-mode wave are shown in Figure 31. It is of interest to note that at the centre of the plane, there is a zero change in pressure and therefore, if an infinitesimally thin microphone is assumed, the effects of the $(1,0)$ mode will be negligible.

University of Cape Town

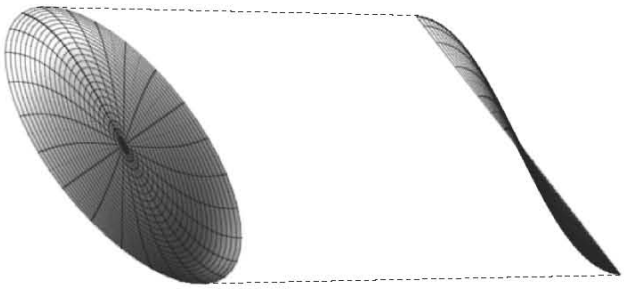

Figure 31: The $(1,0)$ mode which propagates above 1993 Hz in a circular waveguide with a diameter of 110 mm.

The derivation of the pressure distribution across the cross-mode plane, as well as the values of the cut-off frequencies for the various cross-modes are given in Appendix D. The general solution for the cut-off frequency for the (m,n)-mode is given by

$$f_{mn} = \frac{\beta_{mn} c}{2\pi a}, \tag{59}$$

where c is the speed of sound in the medium, a is the radius of the waveguide and βmn is the n^{th} root of the solution of the equation,

$$\frac{\partial J_m(\beta_{mn})}{\partial r} = 0, \tag{60}$$

where $J_{m(\cdot)}$ is the Bessel function of the m^{th} order. Values for β_{mn} are given in Table 2, and the corresponding cut-off frequencies are given in Table 3.

Table 2: Values for β_{mn}, values which satisfy the equation $\frac{\partial J_m(\beta_{mn})}{\partial r} = 0$.

m \ n	0	1	2
0	0	3.831705970	7.015586670
1	1.841183781	5.331442774	8.536316366
2	3.054236928	6.706133194	9.969467823

University of Cape Town

Table 3: The specific cut-off frequencies for the (m, n)-modes up to the $(2, 2)$-mode.

m \ n	0	1	2
0	0Hz	4147Hz	7593Hz
1	1993Hz	5770Hz	9238Hz
2	3305Hz	7258Hz	10790Hz

6.2.4 *Frequency Dependent Wave and Group Velocity*

The previous subsection discussed the cross-mode wave propagation. This section will discuss another consequence of the dispersive nature of wave guides. Figure 32 shows the impulse response of the loudspeaker coupled with the tube. A high frequency oscillation is noted in the response. The reason for this oscillation will be discussed in this subsection. It is to be noted that although the frequency of these oscillations are above the measurement frequency of interest, they have the effect of introducing sharp peaks and notches into the frequency response of the system, shown in Figure 22 above approximately 4100 Hz. This corrupts the cepstrum with noise, which makes it harder to identify the impulse response.

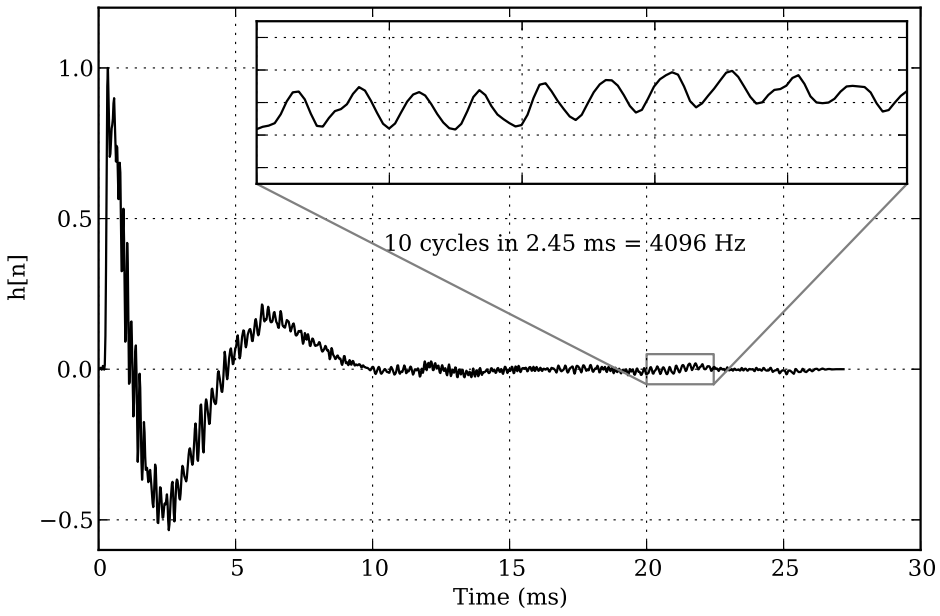

Figure 32: Impulse response of the loudspeaker coupled to the tube, showing the oscillations due to the dispersive nature of the tube.

A dispersive system is one where the wave velocity is dependent on its frequency. Up until the first cross mode, the wave propagates as a plane wave, and at a constant group and wave velocity[9]. Above the $(0,0)$-mode, the wave velocity, $\mathcal{V}$, is dependent on its frequency. The wave velocity is given as:

$$\mathcal{V} = c\sqrt{1 - \left(\frac{f_n}{f}\right)^2}, \tag{61}$$

where c is the speed of sound, f is the frequency of the wave, and f_n is the frequency of the cut-off mode. Equation 61 is plotted in Figure 33. It is of interest to note that at the cut-off frequency, f_n, the wave velocity is 0. Another phenomena, worth mentioning, that occurs is that waves tend to travel in *wave packets*. A *wave packet* usually contains a small range of component frequencies near a central frequency. The centre of the *wave packet* travels at the group velocity.

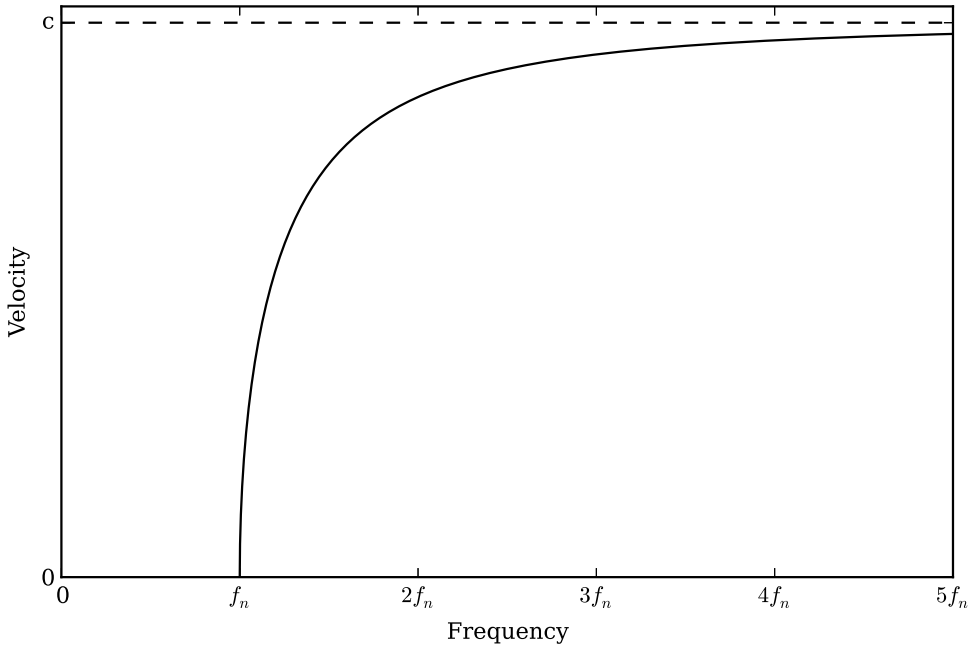

Figure 33: Wave velocity of cross-modes in a wave-guide, above the $(0,0)$ mode. The velocity of the $(0,0)$ mode is constant.

The fact that waves propagate at different velocities in a wave guide means that there is going to be a distortion on the impulse response of the wave guide. The impulse response in one mode will first be discussed, then the impulse response of the addition of modes will be discussed at the end of the section.

In a wave guide with perfectly reflecting walls, the impulse response for one mode is determined by the function[9],

$$\frac{\cos\left(k_n\sqrt{c^2t^2-d^2}\right)}{k_n\sqrt{c^2t^2-d^2}}, \tag{62}$$

where c is the speed of sound, t is the time variable, d is the distance from the sound source, and k_n is the wave-number of the cut-off frequency. Figure 34 shows the impulse response described by the above equation. It can be seen that, as expected, there is no sound at the receiver that travels faster than the speed of sound, c. At the time, $t = {}^{d}/_{c}$, there is a sudden jump in signal amplitude, which is the arrival of the components of greatest frequency in the signal. These components, occurring to Equation 61, travel at close to the speed of sound. The components of frequencies that are close to the cut off frequency of the mode begin to arrive at a time, $t > {}^{d}/_{c}$. The signal then oscillates at a decreasing frequency that tends to the frequency of the cut off frequency of the mode. It can be shown that the frequency at an instant of time, $t \gg {}^{d}/_{c}$, is approximately equal to the that of a wave which would travel with group velocity ${}^{p}/_{t}$. The impulse response of one mode then, approximately, becomes,

$$\frac{1}{2\pi f_n t}\cos\left(2\pi f_n t\right). \tag{63}$$

The signal therefore then oscillates at the cut off frequency of the mode, f_n. The reason for the decay of t^{-1}, is due to the fact that the cross-modes do not propagate parallel to the axial direction of the waveguide, and become heavily dispersed.

University of Cape Town

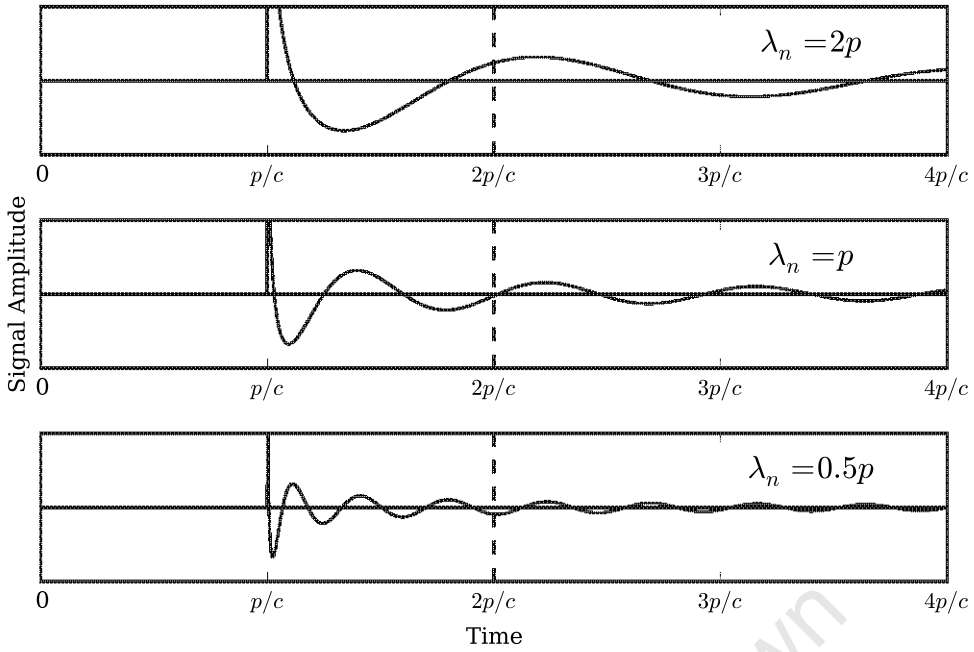

Figure 34: The impulse response for one mode in a waveguide with perfectly reflecting walls. Each plot is for a mode with a cut off frequency proportional to the distance the receiver is from the source.

6.3 REDUCING THE INFLUENCES

6.3.1 *Dense fibreglass in the tube*

Placing dense fibreglass inside the tube, in-front of the loudspeaker, has two effects. First, it reduces the standing waves that appears in the tube. More importantly, in terms of creating a smoother frequency response, it reduces the magnitude of the higher order propagation modes.

6.3.2 *High pass filter*

Coupling of the tube and loudspeaker, specifically the impedance loading on the loudspeaker, has the effect of emphasising the low frequency response of the loudspeaker. A high pass filter can be utilised to reduce the emphasis, which shortens the transient response of the loudspeaker. The knee of the emphasis, shown in Figure 29, is approximately 1600 Hz. This was used as the cut off frequency of the high pass filter. Placing fibreglass in the tube also has the effect of emphasising low frequencies, by more efficiently absorbing sound energy with increasing frequency. A second order filter was used to equalise the effect of the impedance loading and fibreglass absorption.

University of Cape Town

6.3.3 *Low pass filter*

The use of the low pass filter has two purposes. Firstly, the IRS signal rapidly oscillates from a maximum positive value to a maximum negative value and back again. This implies the signal has a very high slew rate, and the signal will get distorted by the system being unable to handle the rapid change[47].

The more physical reason for using the low pass filter is to do with the higher order modes that propagate in the tube. A low pass filter is used to minimise the amount of energy at frequencies above the cut-off frequencies, especially ones that have significant effects on the frequency response of the loudspeaker. It will be seen that (0,1) mode at 4197 Hz, and modes with cut off frequencies above, introduce peaks and notches into the frequency response of the loudspeaker. These high order modes reduce the smoothness of the frequency response above the respective cut off frequency.

An 8th order Butterworth filter with cut off frequency of 3500 Hz was used to reduce the high frequency energy.

6.4 CONCLUSIONS

This chapter discuss the effect that connecting the tube in front of the loudspeaker has on the system response. It was shown that the low frequencies, below 1600 Hz, are emphasised. It was also shown that the wave guide is a dispersive medium, and therefore the speed of sound is frequency dependent. This introduces sharp notches into the system's frequency response.

Three methods that were employed to reduce these factors were presented. Placing fibreglass in the tube reduces the standing wave that appear in the tube. The fibre glass, along with the low pass filter, also reduces the magnitude of the higher order propagation modes. The high pass filter reduces the low frequency emphasis created by the tube's impedance loading on the loudspeaker.

Approximately 80 mm of glass fibre was placed inside the tube, in front of the loudspeaker cone. An 8th order Butterworth low pass filter with cut off frequency of 3500 Hz was used to reduce the high frequency energy. A 2nd order Butterworth high pass filter with cut off frequency of 1600 Hz was used to reduce the low frequency emphasis.

University of Cape Town

7

LIFTERING

7.1 INTRODUCTION

In order to extract the impulse response of the sample under measurement, it needs to be *lifted* from the cepstrum. *Liftering* in the cepstrum is the cepstral equivalent of windowing in the time domain. The *liftering* process is going to be discussed in terms of time domain windows.

The function of the window in *liftering* the impulse response will be explained. The *Equivalent Noise Bandwidth* (ENBW) will then be introduced and related to the frequency resolution of the window. The shape of the window, and the effect of the shape on the spectrum of the signal windowed, will then be discussed.

7.2 THE FUNCTION OF THE WINDOW

The window acts as a bandpass *lifter* in the cepstral domain. It is used to *lift* the impulse response of the measured sample from the cepstrum of the system. Figure 35 shows the use of the *lifter* to extract the impulse response of a reflective sample from the cepstrum. The first rahmonic is clearly visible at approximately 10.5 ms, and care needs to be taken to ensure that it is not *liftered* along with the impulse response.

University of Cape Town

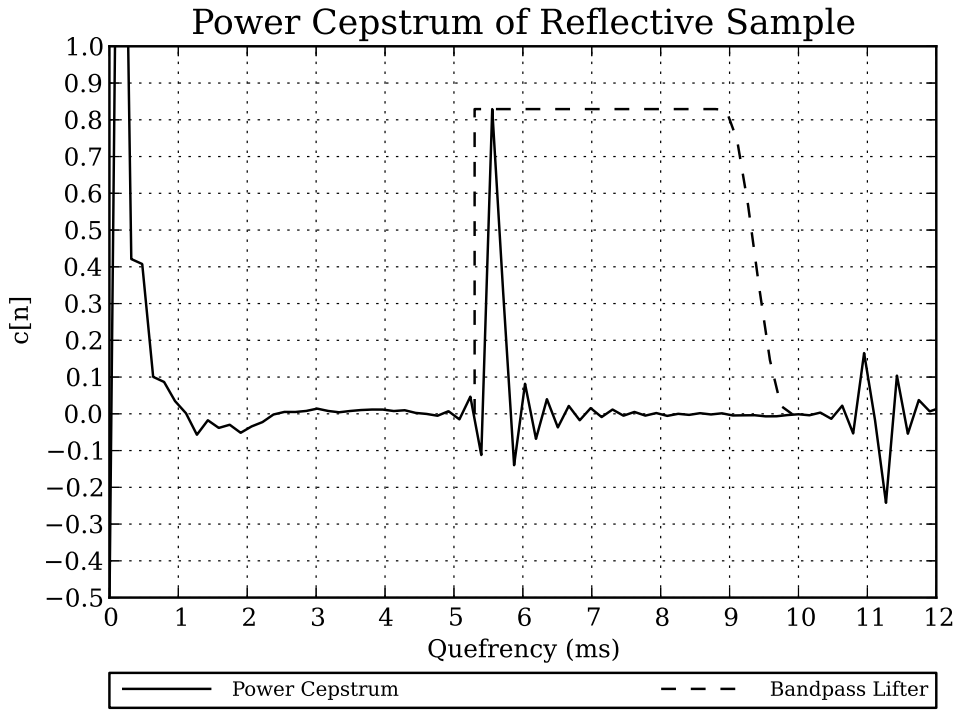

Figure 35: The use of a bandpass *lifter*, or window, to extract the impulse response from the cepstrum.

Due to the nature of the Discrete Fourier Transform (DFT), discontinuities at the boundary of the extracted signal result in spectral leakage across the entire frequency domain[20]. The purpose of the window function is to smoothly force the boundaries to zero, and therefore reduce the negative effects of the spectral leakage.

If the extracted impulse response, including samples before the actual impulse response, is $h[n]$, then the windowed impulse response, $\tilde{h}[n]$, is

$$\tilde{h}[n] = h[n] \cdot w[n], \tag{64}$$

where $w[n]$ is the window function. The frequency response of the extracted impulse response, $\tilde{H}(f)$, is

$$\tilde{H}(f) = \mathfrak{F}\{h[n]\} \otimes \mathfrak{F}\{w[n]\}, \tag{65}$$

where $\mathfrak{F}\{\cdot\}$ is the Fourier Transform operator, and $\otimes$ the convolution operator.

7.3 LENGTH OF WINDOW

The window length should be as long as possible. The low time limit is the tail of the direct cepstrum, and the high time limit is either the arrival of the impulse response of the loudspeaker cone, or the first *rahmonic*.

University of Cape

There is no advantage to having the window start before the arrival of the impulse response of the sample. Setting the start of the window to the arrival of the impulse response of the sample allows the direct cepstrum more time to fall to negligible levels. Therefore the window should start at the arrival of the material impulse response.

If the microphone is positioned exactly halfway between the loudspeaker and the material sample, then the window could end at twice the delay of the arrival of the sample impulse response. However, since the impulse response does not necessarily arrive at an integral number of samples, the impulse response is convolved by a *Sinc* function. This result gives the appearance of acausal behaviour of the impulse in the spectrum. It also limits the length of the window, since there is energy of the *rahmonic* - and loudspeaker cone reflection - before the expected arrival of the *rahmonic*[34, 6].

7.4 EQUIVALENT NOISE BANDWIDTH

In order to illustrate the concept of the Equivalent Noise Bandwidth (ENBW), consider the case where the signal, $x(t)$, is a monotonic sinusoidal with frequency f_0,

$$x(t) = \sin(2\pi f_0 t), \tag{66}$$

and the window used to extract the signal, $w(t)$, is the rectangular window of length L,

$$w(t) = \begin{cases} 1 & |t| < L \\ 0 & \text{otherwise.} \end{cases} \tag{67}$$

The resulting spectrum of the windowed signal, $x(t) \cdot w(t)$, is a convolution of the spectrum of $x(t)$ and the spectrum of the window, $w(t)$

$$X(f) = \mathfrak{F}\{x(t)\} \otimes \mathfrak{F}\{w(t)\}. \tag{68}$$

The resulting spectrum is shown in Figure 36. It can be seen that the spectrum is a Sinc signal centred at the sinusoidal frequency.

University of Cape Town

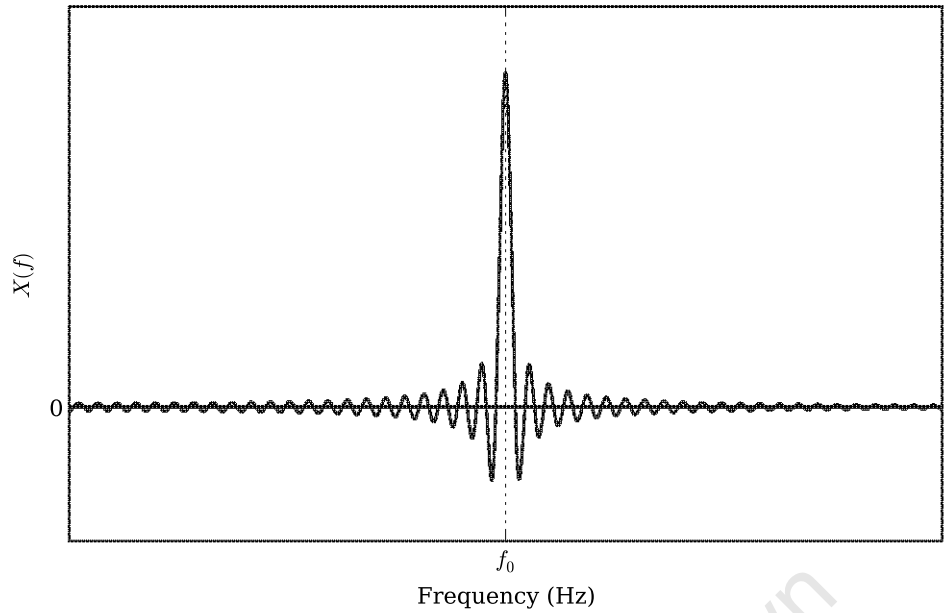

Figure 36: The spectrum of a windowed sinusoidal signal with a frequency of f_0 Hz.

Theoretically, the spectrum of a sinusoidal signal is transformed into an impulse located at frequency of the signal in the spectrum. Figure 36 shows that energy has been spread over the entire frequency domain.

The ENBW of a window is width of a rectangular filter with the same peak power of the window containing the same noise power as introduced by the window[20]. Figure 37 shows an illustration of this rectangle.

University of Cape Town

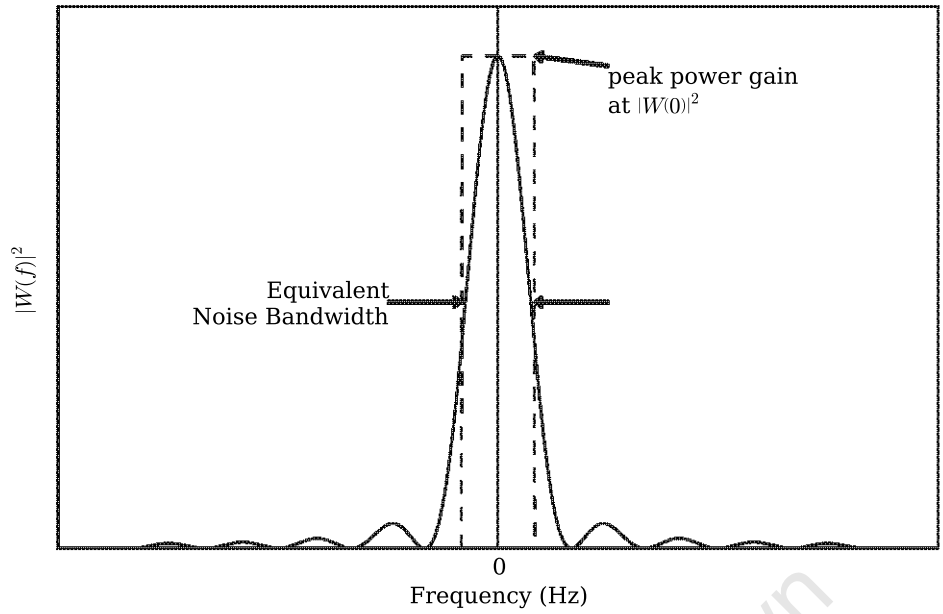

Figure 37: Illustration of Equivalent Noise Bandwidth, the rectangle has the same height as the peak power of the window, and the width is determined by the noise power introduced by the window.

The normalised noise power of the window is defined as [20]

$$\text{Noise Power} = \int_{-1/T}^{1/T} |W(f)|^2 \, df, \tag{69}$$

where T is the length of the window, and $|W(f)|^2$ is the power spectral density of the window.

Using Parsval's theorem, the normalised noise power can be determined by the time-domain representation of the window,

$$\text{Noise Power} = \sum_n w^2[n]. \tag{70}$$

At 0 Hz, the power gain of the window is at a peak, and therefore is given as

$$\text{Peak Power Gain} = W(0) = \left(\sum_n w[n] \right)^2. \tag{71}$$

The ENBW is then defined as the normalised noise power divided by the peak power gain, or

$$\text{ENBW} = \frac{\sum_n w^2[n]}{\left(\sum_n w[n]\right)^2}. \tag{72}$$

The significance of the ENBW will be shown in the next subsection, which discusses the frequency resolution of the window.

University of Cape Town

7.5 SPECTRAL RESOLUTION

The spectral resolution of the DFT is the measure of how close the frequency of two sine waves can be, and still be detected. The spectral resolution Δf is defined as [20]

$$\Delta f = \beta \left(\frac{f_s}{N} \right), \tag{73}$$

where f_s is the sampling frequency, N is number of lines used in the DFT, f_s/N is the width of the DFT bin, and β is a coefficient relating to the scaling of the resolution due to the selected window. β is generally chosen to be equal to the ENBW of the chosen window[20].

The spectral resolution should not be confused with the frequency resolution, which is related to the length of signal extracted. Zero padding the extracted signal, to increase N, does not result in a greater frequency resolution, with the best case frequency resolution obtainable is[32],

$$\text{best case frequency resolution} = \frac{1}{T}, \tag{74}$$

where T is the time, in seconds, of the extracted signal.

University of Cape Town

7.6 WINDOW SELECTION

It was shown in the previous subsection, that the spectral resolution of the DFT is determined by the number of lines used in determining the DFT, N, and the choice of the window used to reduce the effects of spectral leakage. This section will discuss the effects that different shapes of windows have on the frequency response. From Equation 68, the frequency response of an extracted signal is the frequency response of the signal convolved with the frequency response of the window.

Three types of windows will be compared, the first is the Rectangle window. *Liftering* the impulse response from the cepstrum is the equivalent of multiplying the impulse response with the Rectangle window. The window is symmetrical about the origin, and is defined as

$$w[n] = 1, \qquad |n| \leq N/2, \tag{75}$$

where N is the length of the window.

The next window is the Hanning window, which is given by

$$w[n] = 0.5 + 0.5 \cos \left[\frac{2\pi n}{N} \right], \qquad |n| \leq N/2, \tag{76}$$

again N is the length of the window.

Tukey windows are used to force the data at the edges of the window to zero. A parameter of the window, ρ, transforms the window from a

Rectangle window - $\rho = 0$ - to a Hanning window - $\rho = 1$. The window is given by

$$w[n] = \begin{cases} 1, & 0 \leq |n| \leq \rho\frac{N}{2} \\ 0.5\left[1 + \cos\left[\pi\frac{n-\rho\frac{N}{2}}{2(1-\rho)\frac{N}{2}}\right]\right], & \rho\frac{N}{2} \leq |n| \leq \frac{N}{2}, \end{cases} \tag{77}$$

where ρ is the percentage of taper of the window, between 0 and 1. It can be shown that the Tukey window is the result of a Rectangle window of length $\left(1 - \frac{\rho}{N}\right) N$ convolved with a Hanning window of length $\frac{\rho N}{2}$.

Figure 38 shows the shape of the windows for the Rectangle window, Hanning window and Tukey windows with $\rho = 0.25, 0.50, 0.75$.

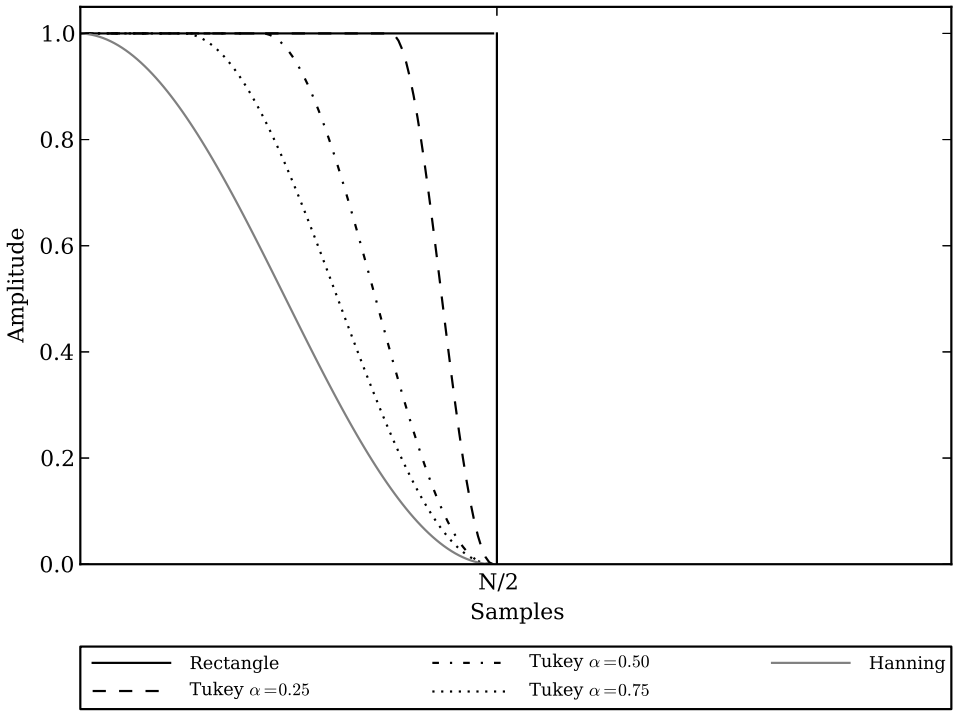

Figure 38: Shapes of different windows, showing only the second half of the window.

It was shown in Subsection 7.5 that the spectral resolution of a window is proportional to the ENBW of the window. The ENBW was shown, in Subsection 7.4, to be equal to the ratio of the sum of the square of the the window points to the square of the sum of the window points. The ENBW and the spectral resolution of the Rectangle, Hanning and Tukey windows are given in Table 4. It can be seen that the resolution ranges from 200 Hz, for the Rectangle Window, to 300 Hz for the Hanning window.

Table 4: The Equivalent Noise Bandwidth, and spectral resolution of various DFT windows. The spectral resolutions are for a sampling frequency of 44100 Hz and 220 DFT lines.

Window	ENBW	Spectral Resolution
Rectangle	1.00	200 Hz
Tukey $\rho = 0.25$	1.10	221 Hz
Tukey $\rho = 0.50$	1.22	245 Hz
Tukey $\rho = 0.75$	1.36	273 Hz
Hanning	1.50	301 Hz

Figure 39 shows the frequency response of the various windows. A significant oscillation, arising from the $sinc\,(x)$ function - the Fourier transform of the Rectangle window. The effect on increasing frequencies is reduced for increasing ρ, but there is significant effect below approximately 300 Hz.

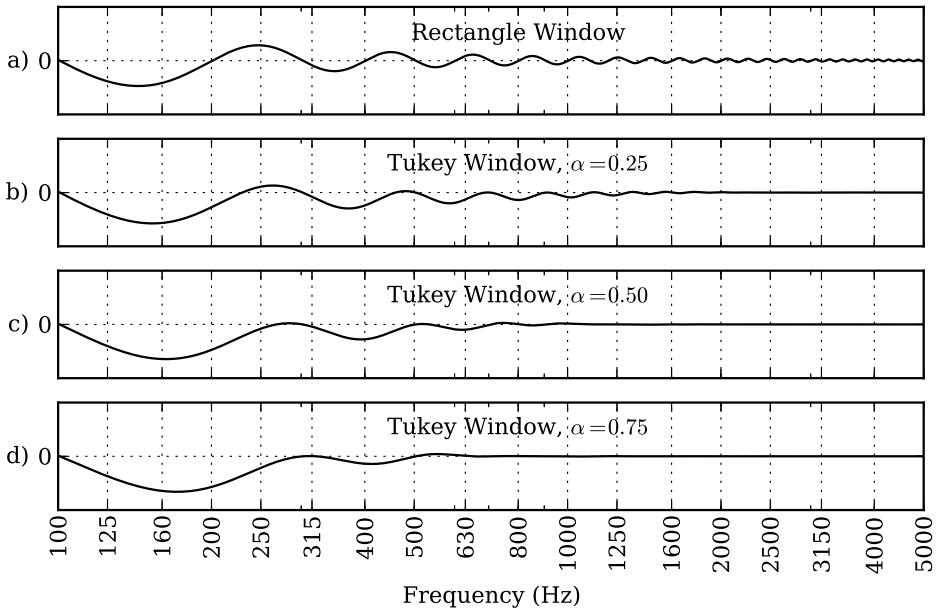

Figure 39: The frequency response of the a) Rectangle window and Tukey windows with b) $\rho = 0.25$, c) $\rho = 0.50$, d) $\rho = 0.75$. The frequency response is determined by using a window length of $N = 220$, and a sampling frequency of 44100 Hz.

7.7 OFFSET IN THE CEPSTRUM

To illustrate the effects of an offset in the cepstrum it will be assumed that the offset is constant. The *liftered* impulse response, $h'[n]$, with a small DC offset, ε, is

$$h'[n-\tau] = (h[n-\tau] + \varepsilon) \cdot w[n-\tau], \tag{78}$$

where $h[n]$ is the "true" sample impulse response, and $w[n]$ the band pass $lifterer$ and τ the delay before the arrival of the impulse response. The *liftered* frequency response, $H'(f)$, is found by taking the Fourier Transform,

$$H'(f) = [(\Re\{H(f)\} + \Im\{H(f)\}) + \varepsilon \cdot W(f)] \cdot e^{-j2\pi f\tau}, \tag{79}$$

where $\Re\{H(f)\}$ and $\Im\{H(f)\}$ are the real and imaginary components of the "true" frequency response of the material, respectively. $W(f)$ is the frequency response of the band pass *lifterer.* Expanding the exponential in terms of sines and cosines, the following is obtained

$$\begin{aligned} H'(f) = {} & [(\varepsilon \cdot W(f) + \Re\{H(f)\}) \cdot \cos(2\pi f\tau) + \Im\{H(f)\} \cdot \sin(2\pi f\tau)] + \\ & j[\Im\{H(f)\} \cdot \cos(2\pi f\tau) - (\varepsilon \cdot W(f) + \Re\{H(f)\}) \cdot \sin(2\pi f\tau)]. \end{aligned} \tag{80}$$

The reflection coefficient is found by squaring the modulus of $H'(f)$,

$$\begin{aligned} |H'(f)|^2 &= \left[\Re\{H(f)\}^2 + \Im\{H(f)\}^2\right] + \left[\varepsilon^2 \cdot W^2(f) + 2\varepsilon \cdot W(f) \cdot \Re\{H(f)\}\right] \\ &= |H(f)|^2 + \varepsilon^2 \cdot W^2(f) + 2\varepsilon \cdot W(f) \cdot \Re\{H(f)\}. \end{aligned} \tag{81}$$

The resulting reflection coefficient is the sum of three terms, the "true" reflection coefficient, the square of the DC offset multiplied by the frequency response of the band pass *lifterer* and also twice the DC offset multiplied by the product frequency response of the band pass *lifterer* and the real component of the "true" reflection coefficient.

7.8 CONCLUSIONS

The purpose of the *bandpass lifterer* is to extract the sample's impulse response from the *power cepstrum*. The length of the *lifterer* determines the spectral resolution of the frequency response, and therefore the resolution of the absorption coefficient. It was shown that using a *lifterer* with tapers decreases the the spectral resolution, but reduces the amplitude of the side lobes. The extent that the effects of the *lifterer* influence the results is determined by the offset in the cepstrum.

The *bandpass lifterer* used in the experiments was a one sided *Tukey* 4.7 ms window with a 20 % taper. The length of the *lifterer* was determined by the arrival of the first reflection off the glass fibre in front of the loudspeaker.

University of Cape Town

8

EXPERIMENTAL METHOD

8.1 INTRODUCTION

This chapter presents the apparatus to measure the absorption coefficient using cepstral technique and the method of standing wave ratios. Sources of uncertainties that are due to the apparatus, as well as the material being tested, are described.

It was found that the signal level had to be adjusted to minimise the non-linearities in the system. The method used to adjust the levels is then discussed.

The software developed for this research is then introduced. The algorithm used to perform the measurement is then given, including the practical problem of synchronising the captured signals.

8.2 IMPEDANCE TUBE APPARATUS

The impedance tube measurements were performed with a *Bruel & Kjaer Type 4002 Standing Wave Tube*, shown in Figure 40. A material sample is placed in the steel sample holder and clamped to the end of the standing wave tube. A *HP 33120A Function Generator* was used to generate sinusoidal signals, which were then amplified by a laboratory amplifier. The output of the amplifier was connected to the loudspeaker in the standing wave tube apparatus. The microphone probe is then adjusted to locate the first pressure anti-node and a pressure node. The microphone signal is then fed to the input of the *Bruel & Kjaer Type 1614 Band Pass Filter Set*, allowing 1/3rd octave band pass filters to be selected. The output of the filter set was split, connecting to an *Agilent Technologies DSO3062A* digital oscilloscope, and an *Agilent Technologies 34410A* digital multimeter. The digital oscilloscope was used to help locate the nodes and anti-nodes. The multimeter was used to read the voltage corresponding to the nodes and anti-nodes. The values were recorded in a spreadsheet application, and the absorption coefficient was determined.

University of Cape Town

Figure 40: *Bruel & Kjaer Type 4002 Standing Wave Tube.*[46]

8.3 CEPSTRUM APPARATUS

The apparatus for the cepstral measurement is shown in Figure 41. The signal is generated using *Python 2.7* running on *Apple OS X 10.7*. The signal was then sent through PortAudio to the *Tascam US-122MKII* external sound card. The line out of the sound card was connected to the generic laboratory amplifier. The amplifier output was split, with one path connecting to the *ApartAudio OVO5T* loudspeaker driver, and the other path connecting to the sound card through a 50 : 1 voltage divider. The circuit diagram of the voltage divider is shown in Figure 42. The loudspeaker driver generates an acoustic wave which propagates down the 2 m long, 110 mm outer diameter PVC pipe. At the other end of the pipe, the material sample under test is placed in the cepstral sample holder and clamped to the pipe. Petroleum jelly was applied to the outer rim of the cepstral sample holder to ensure an airtight seal with the tube. A *Bruel & Kjaer Type 4134* microphone is connected to a *Bruel & Kjaer Type 2619* preamplifier, both are located 1 meter down the pipe. The microphone is centred in the pipe using a centring device. The preamplifier was connected to a *Bruel & Kjaer Type 2803* microphone power supply, which supplies the microphone with 200 V polarisation voltage, and the preamplifier with power. The output of the power supply is connected to the input of the sound card.

University of Cape Town

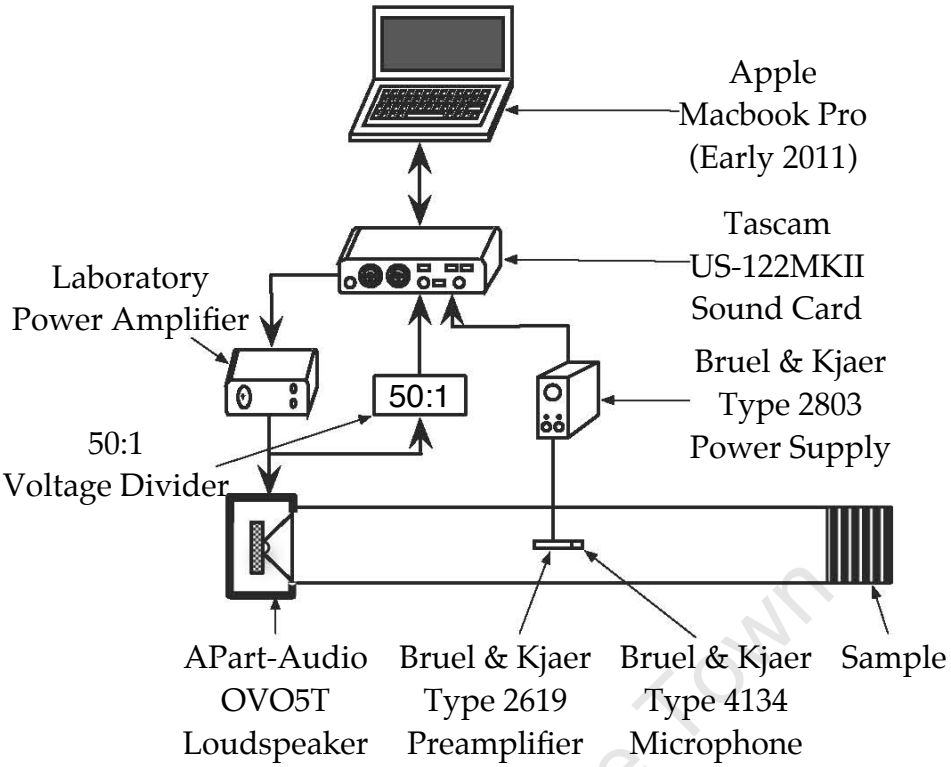

Figure 41: Apparatus used to determine the absorption coefficient using the cepstral technique.

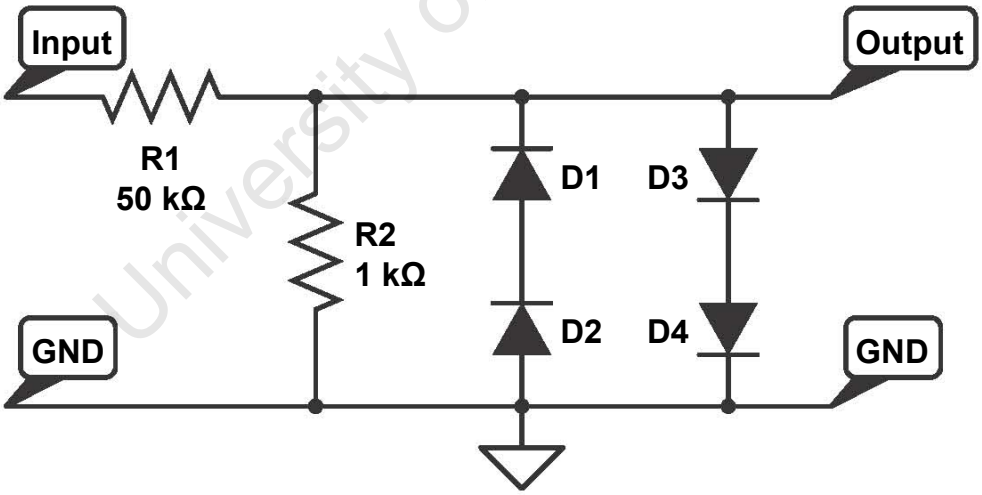

Figure 42: Voltage divider network used to measure the output of the power amplifier. The diodes are used to clip the voltage at 1.2 V, the maximum input voltage of the sound card.

University of Cape Town

8.4 SOURCES OF UNCERTAINTIES

8.4.1 *Equipment Malfunctions and Limitations*

It was noted that some of the equipment had a tendency to malfunction, specifically the *Bruel & Kjaer Type 2803* power supply, and the *Bruel & Kjaer Type 2619* preamplifier. The output of the power supply was monitored on the *Tektronix* oscilloscope. If the signal level became erratic, the power supply was switched off and back on again.

The *Agilent Technologies 34410A* was able to accurately read voltage levels down to 100 μV[17]. Below 100 μV the readings become non-linear, and lead to erroneous absorption coefficient measurements.

8.4.2 *Placing the Sample in the Sample Holder*

Cummings [12] found that any gap around the material sample has the effect of changing the resistance of the sample. This in turn has the effect of changing the absorption coefficient of the material. Therefore, when testing a material sample care was taken not to disturb the material when moving from the cepstral tube to the impedance tube.

Some materials samples needed tape wrapped around them to reduce the air gap around the sample.

8.4.3 *The Sample Under Test*

Morgan and Watts [31] discuss the accuracy of the MLS technique, used in the Extended Surface Method, relating to the surface being measured. It was found that the less sound energy that is absorbed by the material, the greater the uncertainty. This can be shown by noting the variance of the absorption coefficient, σ_α^2, is

$$\begin{aligned} \sigma_\alpha^2 &= \left(\frac{d\alpha}{dH}\right)^2 \sigma_H^2 \\ &= (-2H)^2 \sigma_H^2, \end{aligned} \tag{82}$$

where α is the absorption coefficient, H is the frequency response of the material, and σ_H^2 is the variance of the frequency response of the material. Figure 43 shows the fractional error, σ_α^2/α, of the absorption coefficient. It was assumed that the variance of the measured frequency response of the sample was 0.01. It can be seen from the graph that for highly reflective surfaces, the fractional error can become significant. This error reduces as $\alpha \to 1$.

University of Cape Town

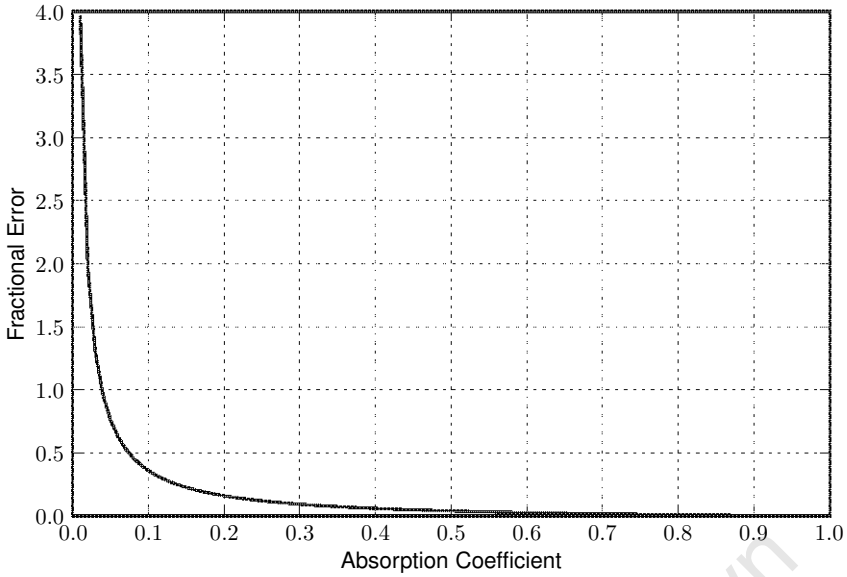

Figure 43: Fractional error of the absorption coefficient, assuming 1% variance in the measured frequency response of the sample.

The variance in the determined frequency response of the material is due to a combination of all the uncertainties in the system. This illustrates the importance of minimising the uncertainties, especially for measuring material with little absorption.

8.5 ADJUSTMENT OF THE SIGNAL LEVEL

The signal used for the measurements was the Inverse Repeat Sequence, discussed in Subsection 4.5. One of the disadvantages of pseudorandom signals, is that the signals are sensitive to non-linearities in the measurement system. In development of an easy, automated method to determine the sound power absorption coefficient, a *Tascam USB-122MKII* sound card was used to generate excitation signals and capture the microphone signal. It was found the the signal levels needed to be calibrated in order to have the ADC's and DAC's in the sound card operating in a linear region. It was also found necessary to lower the amplitude of the output signal to reduce the non-linearities in the loudspeaker.

Another need to adjust the signal level is that the microphone cepstrum, from Equation 20, contains the cepstrum of the signal as well as the cepstrum of the electronic signal generating and acquisition systems. The signal generating cepstrum, excluding the loudspeaker's cepstrum, is measured and subtracted from the microphone's cepstrum. But, the amplitude of signal generating cepstrum that resides in the microphone cepstrum is unknown. Adjusting the signal gain varies the amplitude

University of Cape Town

of the signal generating cepstrum, allowing for greater accuracy when subtracting from the microphone cepstrum.

The signal was adjusted so that the tail of the absorption coefficient between 100 Hz and 200 Hz was approximately constant. It was found that if the tail curved upwards, the signal level was too high, likewise, if the tail curved downwards the signal level was too low. The curve in the tail of the absorption coefficient is due to the ripple introduced by the band pass *lifterer.*

Future work will have to determine if it is possible to automate the adjustment process.

8.6 SOFTWARE

8.6.1 *Introduction*

A graphical user interface was developed to rapidly and simply measure the absorption coefficient of material samples. An example of the interface is shown in Figure 44. The software was developed using the *Python[37]* programming language.

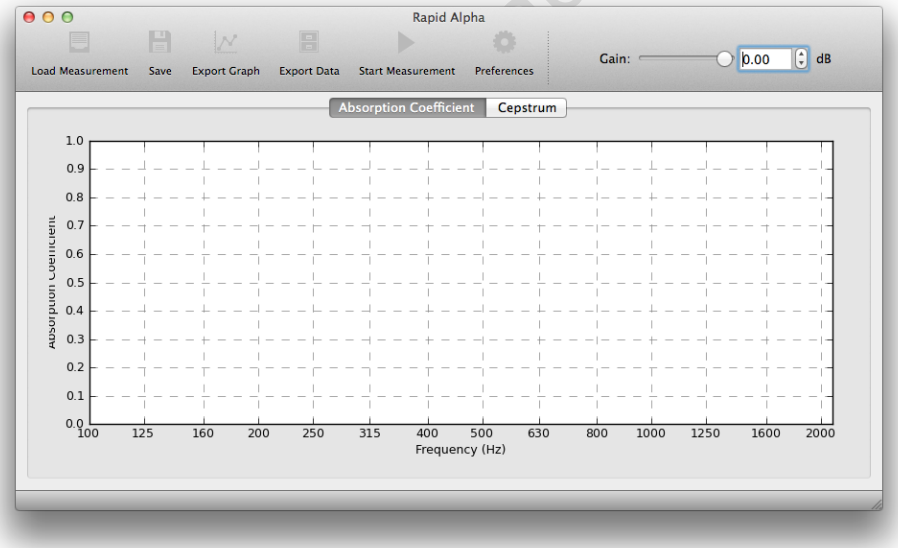

Figure 44: *Rapid Alpha*, the software created to rapidly measure the absorption coefficient of materials.

There is minimal interaction required to perform a measurement. The "Start Measurement" button, located in the tool bar at the top of the interface, will begin the measurement. After the measurement has been completed, a *save file* dialog will be displayed. The measurement will then be analysed, and the absorption coefficient will be displayed in the

plot area. The complete user manual is shown in Appendix F. The Gain slider is used to perform the calibration of the system before testing.

The remainder of this subsection will discuss the algorithm to determine the absorption coefficient, including some practical considerations of the measurement.

8.6.2 *Algorithm*

The algorithm used in *Rapid Alpha*, the software developed for this research, is shown in Figure 45. There are two significant components in performing the measurement. The first component is producing a signal and measuring the system's response to the signal. The second component is analysing the measurement to determine the absorption coefficient.

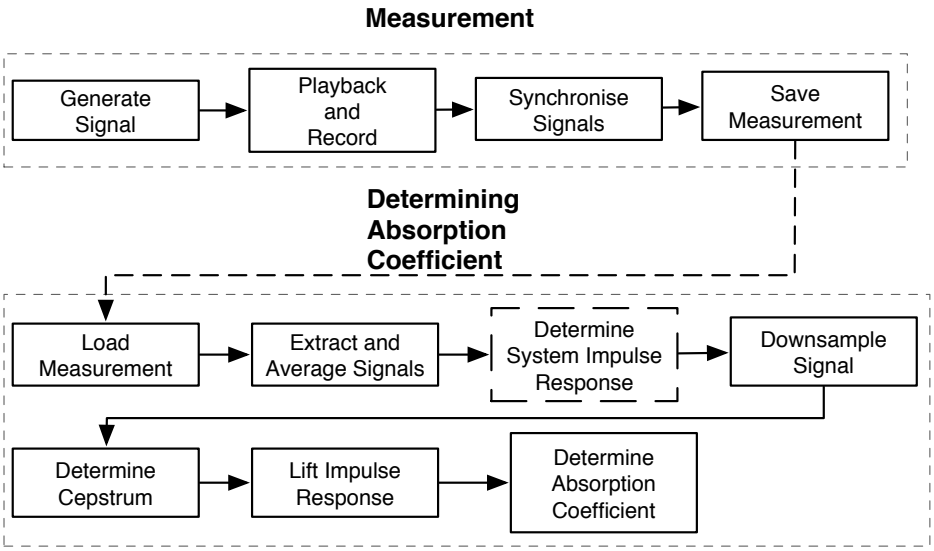

Figure 45: The algorithm used to determine the absorption coefficient of a material sample.

8.6.2.1 *Generating the Signal*

A signal is generated, dependent on the settings stored in the configuration database. The signal is appended with silence, this is to ensure that after a measurement the signal energy can decay and not interfere with the next measurement. Also, due to the measurement architecture, the software only measures as long as there is signal to output.

A unit impulse and a short silence is prepended to the signal. This unit impulse is then used to locate the signal in the recorded response.

The padded *signal frame* is then repeated a number of times, to create a *measurement frame*.

8.6.2.2 *Playback and Recording the Signal*

The *measurement frame* is then passed to the sound card. Communication with the sound card is handled by *PortAudio*[36], a cross platform audio input/output framework. The signal is captured by the microphone for the duration of the *measurement frame* being processed by the sound card.

8.6.2.3 *Synchronising the Signals*

There are two significant factors which make predicting the location of the signal in the captured system's response impossible. There is a non-deterministic delay from the time the software informs the operating system that there is a signal to output, to the time that the signal is finally generated by the loudspeaker[35]. There is also a delay from the time the loudspeaker driver begins to produce the signal to the time the microphone first receives the signal. This delay is dependent on the distance the microphone is from the loudspeaker, the speed of sound, which itself is dependent on the temperature, pressure, material the sound wave is propagating through, and in a wave guide it is also frequency dependent[28].

Since the generator response has a high SNR, a trivial threshold detection function can be used,

$$n_0 = \min_n \left(s\left[n\right] > \delta \right), \tag{83}$$

where n_0 is the start of the synchronisation signal, $s\left[n\right]$ is the recorded response and δ is the threshold. There is, however, one caveat that may lead to a misidentification of n_0. Low cost DAC, such as the one used in the *Tascam* sound card, use linear-phase digital anti-aliasing filters[29]. Linear-phase filters offer the advantage of having no group-delay, all frequencies are delayed equally and therefore the shape of the waveform remains undistorted, at the cost of introducing pre-ringing to the signal. Figure 46 shows the pre-ringing present in the signal captured when the output of the ADC is connected directly back to the input of the DAC.

To locate the peak of the impulse, the threshold is set relatively low. The index of the first sample that exceeds the threshold is noted, then the maximum value is located in the neighbourhood of the sample. This peak is used as the location of the synchronisation impulse.

University of Cape Town

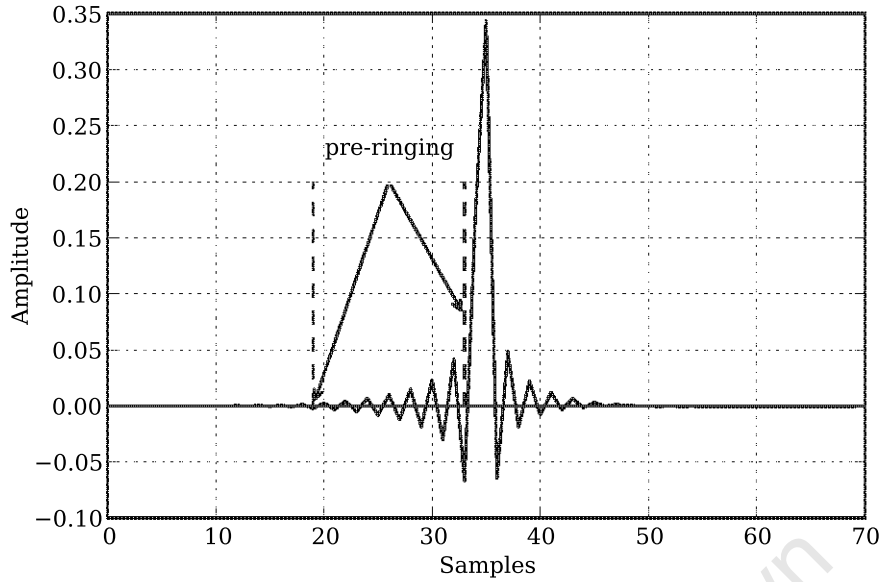

Figure 46: An impulse recorded by directly connecting the output of the ADC to the input of DAC. The pre-ringing is evident between samples 18 and 33, with the peak of the impulse at 35 samples.

The case is not as trivial for the output of the system captured by the microphone. Figure 47 shows the impulse received by the computer that was captured by the microphone. There are a number of problems with using the simple threshold detection with the impulse received by the microphone. The impulse waveform has been distorted by the effects of the loudspeaker's impulse response, the loudspeaker enclosure / pipe connection, and the glass fibre plug directly in front of the loudspeaker cone. The SNR has also been greatly reduced, as the peak amplitude in the signal captured by the microphone is less than 0.04 units compared to the 0.8 units of the signal captured at the output of the generator. There are 28 samples between the first peak on the main lobe and the onset of the impulse, therefore if a predetermined threshold was used, this may lead a misidentification of the onset by 28 samples.

University Of Cape Town

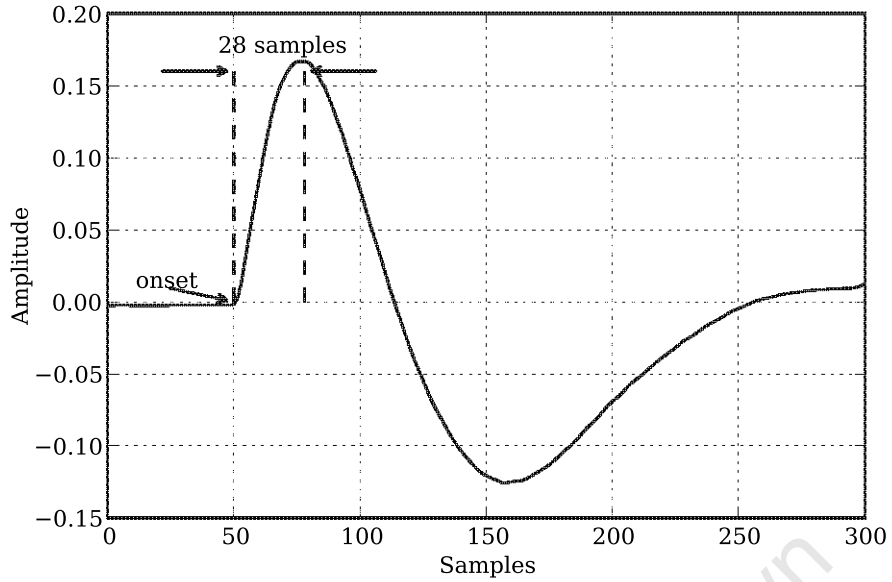

Figure 47: An impulse recorded by the microphone, generated by the loudspeaker that is connected to the tube with a fibre glass plug between the microphone and loudspeaker. It can be seen that there are 28 samples between the onset and the first peak on the main lobe of the impulse.

University of Cape Town

An improvement to this can be seen in Algorithm 8.1. The algorithm determines the forward difference of **signal**, the signal captured by the microphone, giving the rate of change between samples. This has the effect of removing low frequency components, such as a DC offset, that will effect comparing thresholds. The **noise** floor is then determined by assuming that the first **NOISE_SAMPLES** contain no signal components. This may be ensured by prepending the output signal with a delay of at least **NOISE_SAMPLES** samples. The maximum value and standard deviation of the noise floor is then determined. From the maximum value and standard deviation, the threshold, δ, used to detect the onset is calculated as

$$\delta = \max |\mathbf{noise}| + \xi\sigma, \tag{84}$$

where ξ is the **MULTIPLIER** and σ is the standard deviation of the noise. The onset is then determined to be the sample before the sample that crosses the threshold. The reason for using the sample before, is that the forward difference does not use the first sample. Figure 48 shows the detection algorithm with 1000 **NOISE_SAMPLES** and **MULTIPLIER** set to 2.5, refer to Appendix E for details on selecting these values.

Algorithm 8.1 Python code to detect the onset of an impulse of the signal captured by the microphone.

```
def detectImpulse(signal):
    """ Detects the onset to an impulse in the signal """
    delta_envelope = abs(signal[1:] - signal[:-1])
    noise = delta_signal[:NOISE_SAMPLES]

    max_noise = max(noise)  # maximum noise level
    std_noise = std(noise)  # standard deviation

    threshold = max_noise + MULTIPLIER * std_noise

    onset = where(delta_envelope > threshold)
    onset = onset[0] - 1

    return onset
```

TOWN

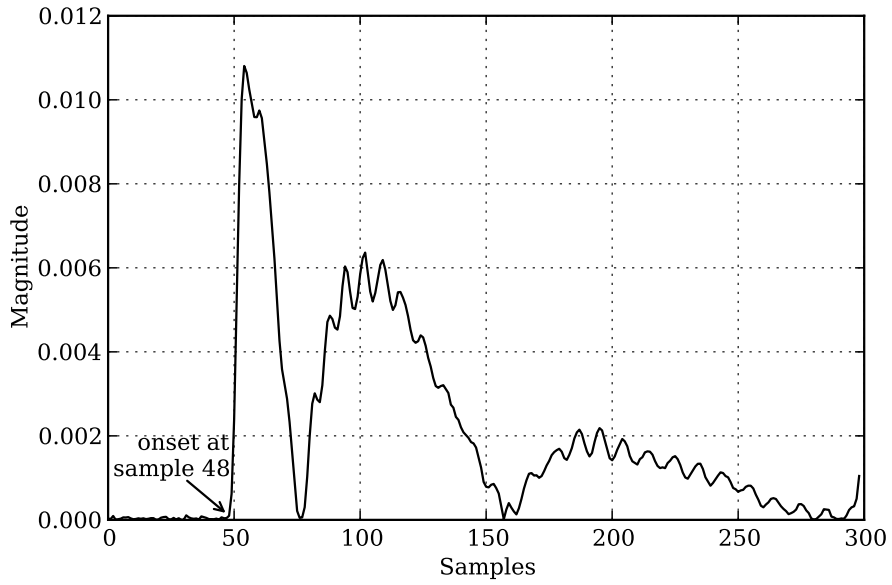

Figure 48: Onset detection in the forward difference domain, using the noise floor and standard deviation to determine the threshold. The onset is detected at 48 samples.

8.6.2.4 *Saving the Measurement*

Once the location of the synchronisation impulse have been found, the captured signal is split up into equal segments. The number of segments are equal to the number of times the signal is repeated in the measurement frame. Both the signal captured by the microphone, as well as the

signal captured from the output of the sound card is saved into a measurement database. The settings used in the measurement, including the type of excitation signal, and the filters used to condition the signal, are also saved in the database.

8.6.2.5 *Loading the Measurement*

The saved measurement database is then loaded back into the program.

8.6.2.6 *Extract and Average Signals*

The location of the impulse in the signal captured by the microphone as well as the signal captured at the output of the sound card is known, as is the delay from the impulse to the start of the actual excitation signal. From these two values, the part of the signal before the arrival of the actual excitation signal can be removed. The signals are then averaged together, improving the SNR.

8.6.2.7 *Determine System Impulse Response*

If the excitation is either the MLS or IRS signal, the system's impulse response is determined. The theory of determining the impulse response is discussed in Subsections 4.4 and 4.5. This is done to take advantage of the noise immunity that these excitation signals offer.

8.6.2.8 *Downsampling the Averaged Signal or System Impulse Response*

Once the signals have been averaged together, and the system impulse response has been determined, the signal is then decimated. Although down sampling is not necessary, if the signal is not decimated the resulting cepstrum will be corrupt with high frequency cepstral noise. This makes visually identifying the impulse response in the cepstrum more difficult than if the signal is resampled. This has negligible effect on the resulting absorption coefficient[6].

To decimate, the *decimate* function in the *Scipy* library is utilised. This function uses an order 8 Chebyshev Type I filter with a cut off frequency of 0.8 times the new Nyquist frequency[41]. Signal samples which are not multiples of the decimation factor are then dropped.

This is performed on both the captured microphone signal and output of the sound card.

8.6.2.9 *Determining the Cepstrum*

The cepstrum of the resampled microphone and sound card output signals are then transformed into the *quefrency* domain. The sound card's output cepstrum is then subtracted from the microphone cepstrum. This resulting cepstrum will be referred to simply as the power cepstrum.

University of Cape Town

8.6.2.10 *Liftering the Impulse Response*

The impulse response can then be directly *liftered* from the power cepstrum using a band pass *lifterer*. The band pass *lifterer* is equivalent to a time domain window. The starting sample of the window is sometime before the onset of the impulse response, to some time just before the onset of the first rahmonic or reflection from the loudspeaker cone - which ever arrives first. A one sided 4.7 ms *Tukey* window with a 20 % taper.

8.6.2.11 *Determining the Absorption Coefficient.*

Once the impulse response has been *liftered* from the power cepstrum, the absorption coefficient is then given by the squared magnitude of the Fourier transform of the impulse response which is subtracted from 1

$$\alpha(\omega) = 1 - |\mathfrak{F}\{h(t)\}|^2, \tag{85}$$

where $\alpha(\omega)$ is the frequency dependent absorption coefficient, $\mathfrak{F}\{\cdot\}$ is the Fourier transform operator and $h(t)$ is the materials impulse response.

8.7 MEASUREMENT PROCEDURE

The method of using the cepstral technique to automatically determine the absorption coefficient is tested in the following way:

1. A sample to be tested was placed, depending on its diameter, in the impedance tube sample holder, or the cepstral tube sample holder. The holder was then clamped to the cepstral tube.
2. Using *RapidAlpha* - the software developed for this project - the optimum gain was determined for sample. The procedure to determine the gain is discussed in Section 8.5.
3. The *iPython Notebook* was then used to perform 9 more measurements.
4. The absorption coefficient was determined using the standing wave tube method, discussed in Section 2.3.
5. After the measurements have been performed, they are then analysed using the *iPython Notebook* and the results are presented in the next chapter.

University of Cape Town

9 RESULTS

9.1 INTRODUCTION

This section displays the results obtained using the automated cepstral technique to determine the plane wave sound power absorption coefficient. Six different types of materials were selected to be measured. These were:

1. A highly reflective termination,
2. Porous Asphalt specimen 7 - 4,
3. 60 mm thick glass fibre sample,
4. Open pore foam sample, with an embedded 1 mm rubber panel,
5. Haraklith wood fibre ceiling panel,
6. Helmholtz resonator, with resonance at approximately 940 Hz.

The measurement was repeated 10 times in the cepstral tube, and once in the impedance tube. A cepstral measurement consists of 10 bursts of the IRS signal repeated twice. An example of the excitation signal is shown in Figure 49. The first measurement was then plotted as a solid black line, and the standard deviation of the 10 measurements were shown as an error bar at selected points along the line. The impedance tube measurements were displayed as black crosses, unless the reading was below 100 μV in which case the measurement is shown as a circle. *Geller Labs* [17] showed that below 100 μV, the voltage readings of the *Agilent 34410A Multimeter* become very non-linear. The magnitude of the error bar for the impedance tube measurements is obtained by the accuracy specifications of the *Agilent 34410A Multimeter*, which can be found in Appendix B.2.

The results obtained by the cepstral technique were then tabulated, along with the results obtained by the impedance tube, the standard deviation of the cepstral measurement, the error between the cepstral measurement and the impedance tube, and the standard deviation in the error between the two techniques. The criterion is for the absorption coefficient measured with the cepstral measurement to be within 0.05 of the impedance tube measurement over the range 200 Hz to 2000 Hz. Measurements that fail to meet this criteria are highlighted with bold print. The tables of results can be found in Appendix A.

University of Cape Town

Although the range of interest is between 200 Hz and 2000 Hz, the graphs are plotted down to 100 Hz. The shape of the absorption coefficient graph between 100 Hz and 200 Hz gives an indication of the DC offset present in the *liftered* impulse response. If the absorption coefficient between 100 Hz and 200 Hz is approximately constant, it can be assumed that there is little to no DC offset present.

9.2 MEASUREMENT SETTINGS

The measurement settings used for all the measurements are shown in Table 5. The excitation signal for the measurement is shown in Figure 49.

Table 5: Measurement settings used to determine the absorption coefficient using cepstral techniques.

Setting	Value
Signal	Inverse Repeat Sequence
Taps	14
High Pass Filter	1600 Hz, 2nd Order Butterworth
Low Pass Filter	3500 Hz, 8th Order Butterworth
Window Start	5.3 ms
Window End	10 ms
Window Function	One-Side Tukey with 1ms taper

University of Cape Town

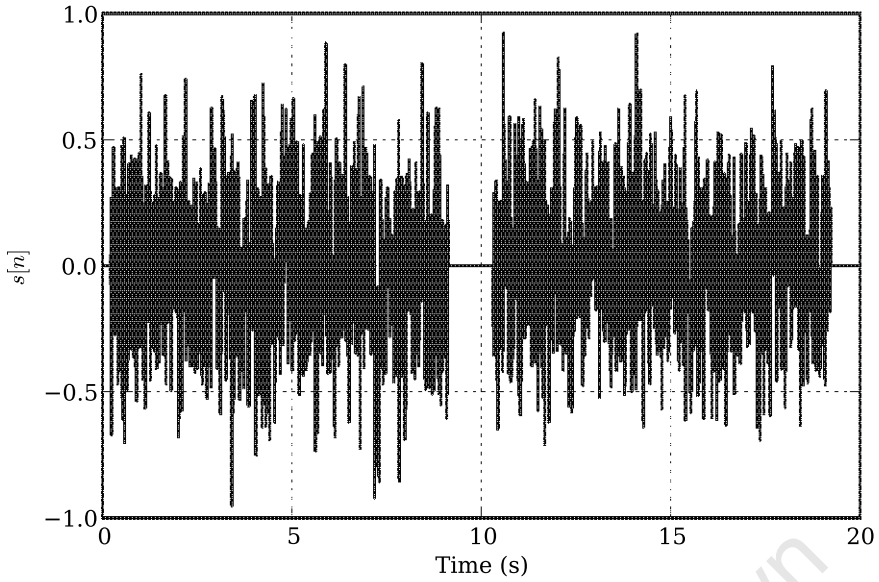

Figure 49: The full excitation signal used for a measurement.

University of Cape Town

9.3 REFLECTIVE

The reflective steel sample is one of the more interesting measurements. This is because it can be used to highlight problems with both the impedance tube measurement and the cepstral measurement, by clearly showing any inaccuracies. The reflector used for the measurement is shown in Figure 50. The theoretical absorption coefficient of the sample is 0 over the frequency range 100 Hz to 2000 Hz.

The impedance tube sample holder was placed inside the cepstral tube sample holder. Petroleum jelly was applied to the rim of the cepstral tube holder to minimise the possibility of any air leakage paths. Both the sample holders where then clamped to the cepstral tube.

The measured absorption coefficient is shown in Figure 51. A small oscillation is present throughout the absorption coefficient, which is an indication of contamination by the frequency response of the band pass *lifterer*. The reason for the contamination is that there is a small DC offset in the cepstrum. This was discussed in 5.2.1. Further contamination is due to the tail of the window including part of the first *rahmonic*. The arrival of the first *rahmonic* is earlier than expected due to the apparent acausal behaviour of the impulse response, explained in Section 7.3.

Errors with the impedance tube are also highlighted in the measured absorption coefficient. The absorption coefficient at 160 Hz, 170 Hz, 180 Hz, 280 Hz, and 550 Hz are unexpectedly above 0.1. These incorrect values are due to resonances in the impedance tube apparatus. The result at 710 Hz is uncertain due to the very low voltage of the pressure minimum, which is below the measurement capabilities of the *Agilent 34410A Multimeter*. The results are unexpected, as opposed to the values for 1600 Hz, 1800 Hz, 2000 Hz, because the *plane wave* sound power absorption coefficient for a steel reflector is expected to be 0. At above 1600 Hz, plane waves can no longer be assumed to be propagating.

The values for the absorption coefficient for the frequencies 160 Hz, 170 Hz, 180 Hz, 280 Hz, and 550 Hz will not be measured and presented for further measurements. It is to be noted that a resonance has been reported at approximately 315 Hz. Therefore, along with the 315 Hz, the absorption coefficient for 300 Hz and 330 Hz are measured and reported.

The power cepstrum of the measurement is shown in Figure 52. It can be seen that the direct cepstrum is not exactly zero at the arrival of the impulse response of the reflective sample. This offset is responsible for the undulations that are present in the absorption coefficient. The apparent acausal behaviour due to the nature of the DFT can be seen before the arrival of the impulse response of the sample. It can also be seen before the arrival of the first *rahmonic*. This puts a limit on the length of the *bandpass lifterer* that can be used to extract the impulse response.

University of Cape Town

Figure 50: Sample holder being used as reflective sample.

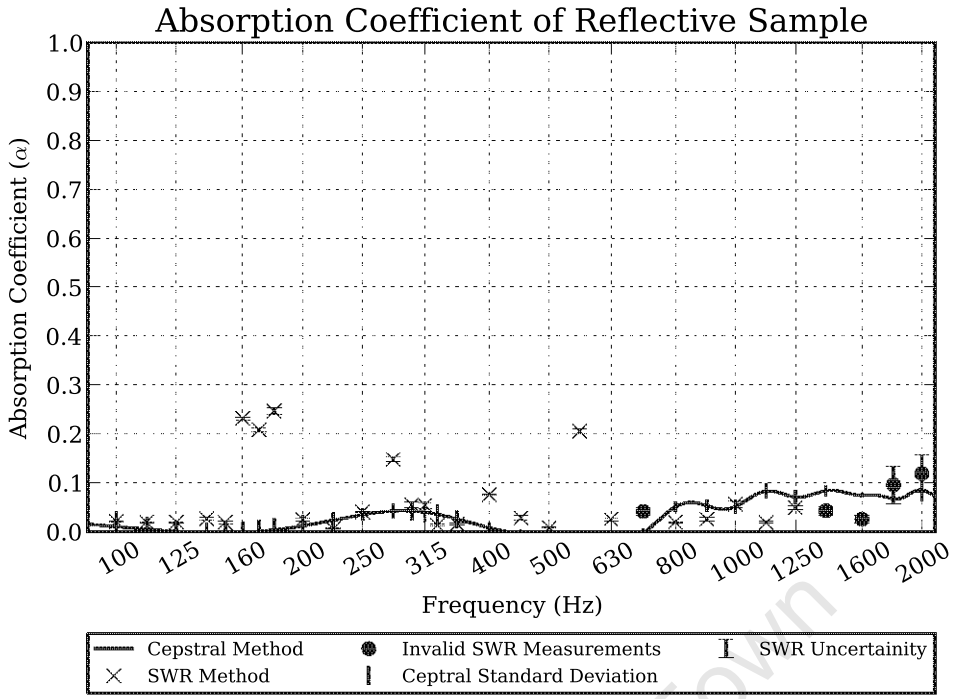

Figure 51: Absorption coefficient for the sample holder, which was used as a reflective sample.

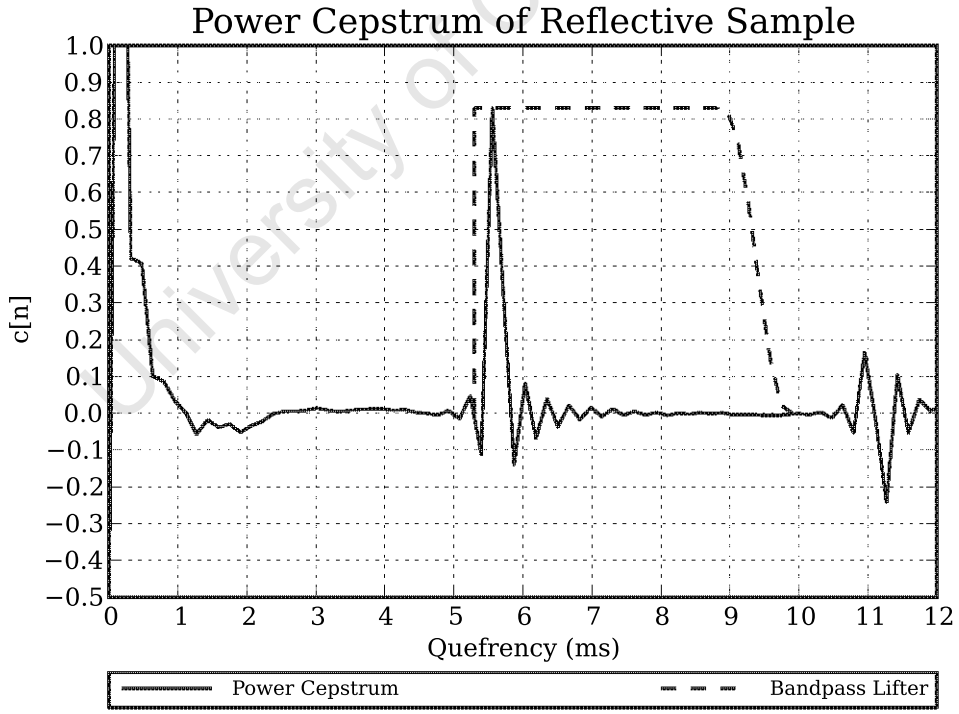

Figure 52: Power cepstrum for the sample holder, which was used as a reflective sample.

University of Cape Town

9.4 7-4 TWINLAY ASPHALT SAMPLE

The 7-4 TWINLay asphalt sample was a core taken from one of the road surface test sections at Welschap military airfield near Eindhoven, The Netherlands for an experimental project [48]. The 7-4 TWINLay sample is specimen 4 of asphalt type 7, shown in Figure 53, from the project. It contains two layers of different sized stone with two absorption maxima within the range 200 Hz to 2000 Hz.

Tape was wound around the asphalt sample, and some petroleum jelly was applied to the tape. The sample was then inserted into the cepstral tube sample holder. The thick steel lid of the impedance tube sample holder was used as a backing for the sample. Both the asphalt sample and the steel lid were then enclosed by the cover of the cepstral tube sample holder. The sample holder was then clamped to the cepstral tube.

The absorption coefficient measured with the cepstral technique and impedance tube are shown in Figure 54. There is a close correlation between the absorption coefficient obtained with the cepstral technique and the standing wave tube method. There were two frequency bins that were in error of more than 0.05 - 224 Hz and 1600 Hz. The difference at 224 Hz can be attributed to contamination of the band pass *lifterer.* The difference at 1600 Hz is likely due to pressure minimum being close to the limits of the *Agilent 34410A Multimeter.* It is to be noted that below 200 Hz, the standard deviation of the absorption coefficient determined with the cepstral method monotonically increases. This shows there is low confidence in the reported absorption coefficient below the frequency resolution of the band pass *lifterer.*

There is an uncertainty of 0.06 in the measurement at 1800 Hz due to both the minimum and maximum being very low, and therefore the SWR is sensitive to uncertainties in the multimeter readings. The pressure minimum of this measurement is close to the lower limits of the *Agilent 34410A* multimeter.

Figure 55 shows the power cepstrum obtained for the measurement. Like the power cepstrum for the reflective sample, there is a small offset in the cepstrum. It can also be seen that there is still energy present in the tail of the impulse response.

University of Cape Town

Figure 53: TwinLay asphalt sample.

University of Ge

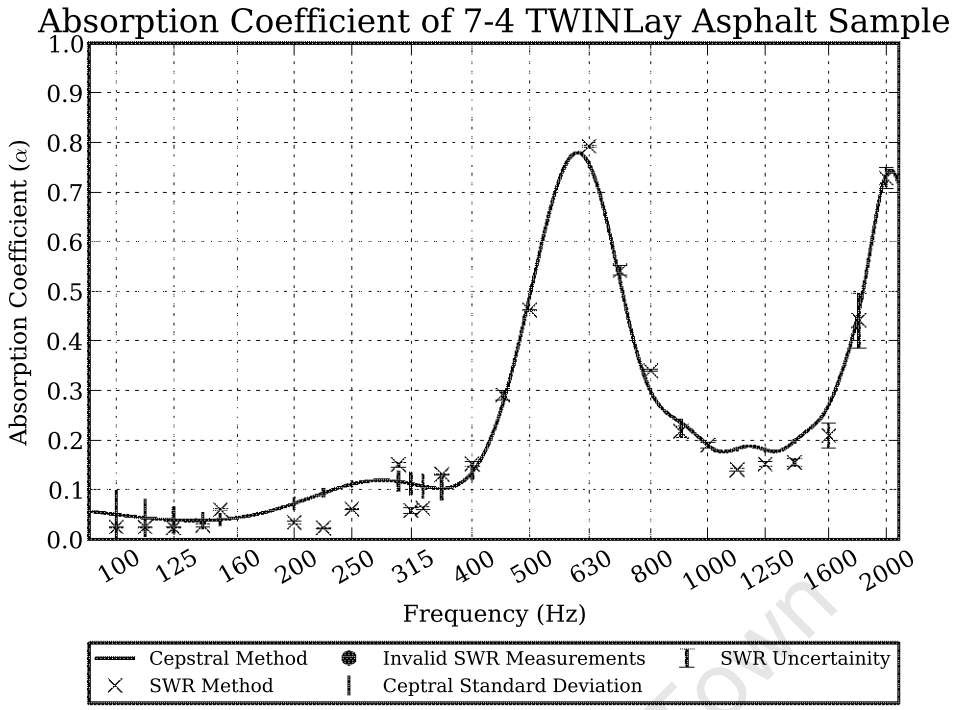

Figure 54: Absorption coefficient for specimen 4 of type 7 asphalt from Welschap military airfield near Eindhoven, The Netherlands.

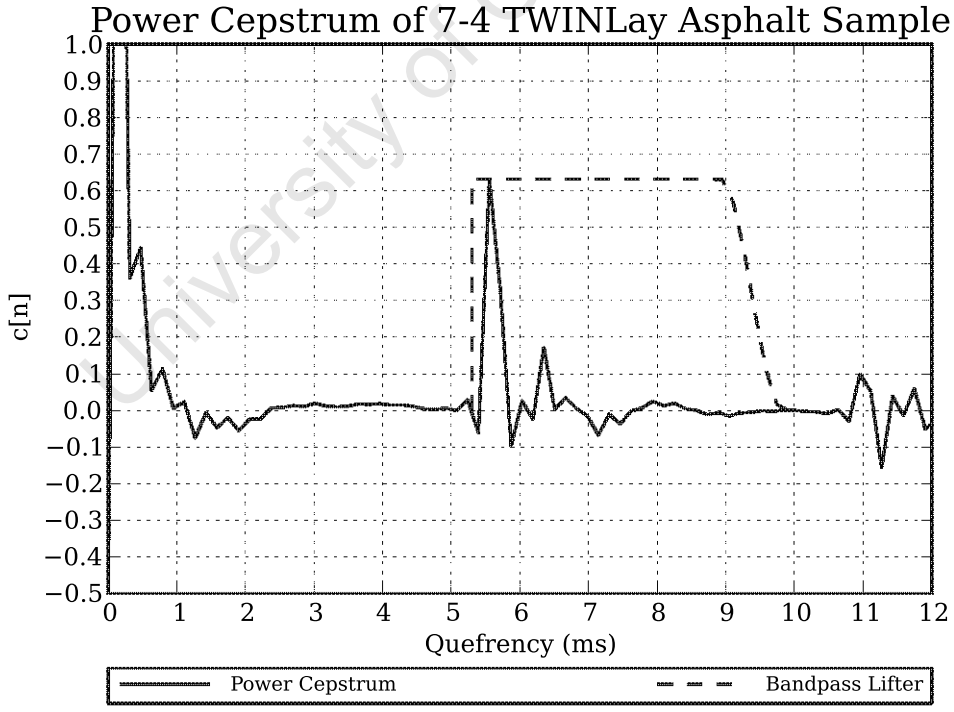

Figure 55: Power cepstrum for specimen 4 of type 7 asphalt from Welschap military airfield near Eindhoven, The Netherlands.

University of Cape Town

9.5 60 mm glass fibre

The glass fibre sample, shown in Figure 56, is porous, and made up of thin layers of long fibres. It is 60 mm in depth, and is cut to fit in the impedance tube sample holder - 96 mm in diameter. The sample was chosen as it represents a typical porous absorber.

The sample was placed inside the impedance tube sample holder. The impedance tube sample holder was then placed inside the cepstral tube sample holder. Both the sample holders were then clamped to the cepstral tube.

The measured absorption coefficient is shown in Figure 57. It shows there is a very close correlation between the cepstral technique and the standing wave tube measurement. The only measurement that failed to meet the criteria, was for the measurement at 250 Hz. Here the absorption coefficient between the two methods differ by 0.06. Excepting for the measurements at 100 Hz, 250 Hz, and 300 Hz, the agreement between the two methods were 0.03 or less. The impedance tube measurement at 300 Hz appears to be in error, as it is above the measurement for 315 Hz.

The power cepstrum for of the measurement is shown in Figure 58. It can be seen that the impulse response of the glass fibre sample falls to negligible levels in approximately 3 ms.

University of Cape Town

Figure 56: 60mm of glass fibre sample used in testing.

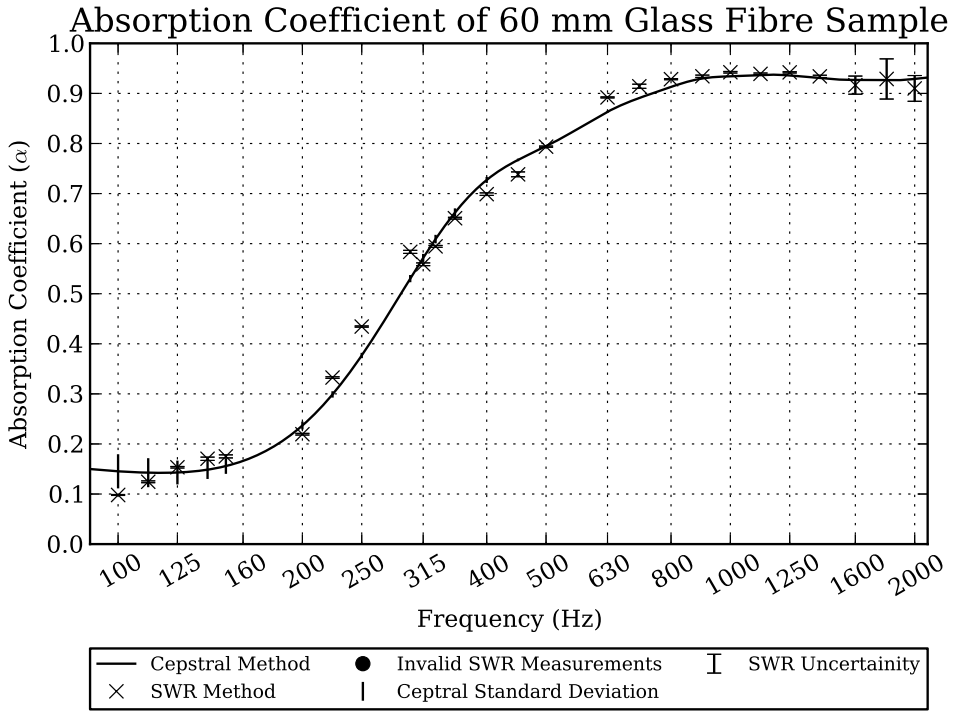

Figure 57: Absorption coefficient for 60mm of glass fibre.

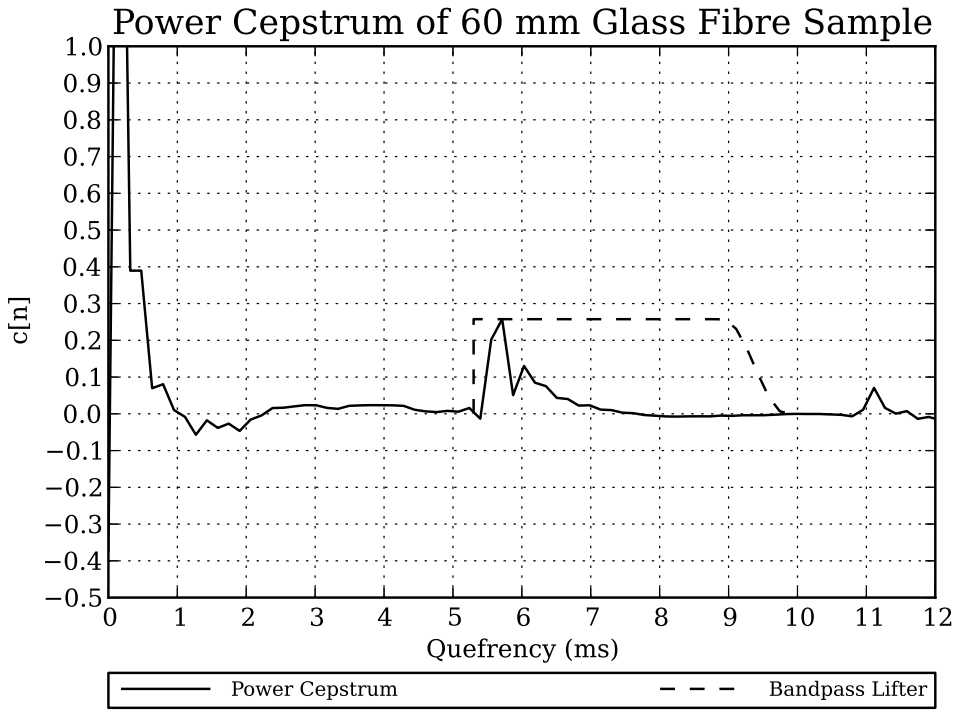

Figure 58: Power cepstrum for 60 mm of glass fibre.

University of Cape

9.6 POLYURETHANE FOAM SAMPLE WITH 1 MM RUBBER PANEL

The polyurethane foam sample selected was a 31 mm open pore sample, and is shown in Figure 59. It was selected as it contains a rubber membrane, which complicates the absorption coefficient curve with a resonant peak. The foam sample is cut to fit in the impedance tube sample holder, and has a diameter of 96 mm. It has a thin cloth covering the face of the sample. There is a 1 mm rubber panel embedded in the foam sample, 25 mm from the cloth face of the sample. The panel membrane embedded in the foam means there will be a local maximum at the resonant frequency of the panel in the foam.

The foam sample was placed inside the impedance tube sample holder, which was then placed inside the cepstral tube holder and clamped to the cepstral tube.

The absorption coefficient for the foam sample is shown in Figure 60. There is a very close correlation between the absorption coefficient measured using the cepstral tube and the impedance tube over the range 200 Hz to 2000 Hz. There are three measurements that differ more than 0.05. The absorption coefficient measured by the impedance tube at 300 Hz appears to be in error, which explains the difference. Around the resonance of the panel, between 450 Hz and 900 Hz, there is a superimposed ripple in the absorption coefficient line. Attempts were made to reduce this ripple by adjusting the signal level, without success. The power cepstrum for the measurement is shown in Figure 61. It can be seen that there is a small negative offset before the arrival of the impulse response. The tail of the impulse response of the sample extends past the length of the *lifterer*.

University of Cape Town

Figure 59: Polyurethane foam sample #1, an open pore foam sample with a 1 mm rubber panel embedded inside of it.

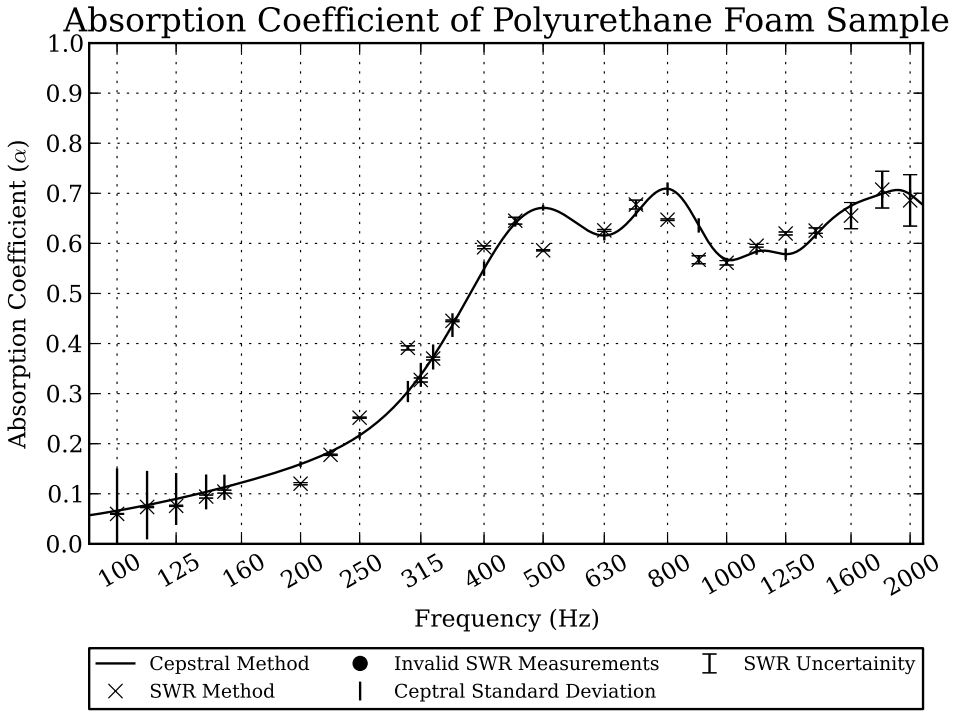

Figure 60: Absorption coefficient for polyurethane foam sample #1.

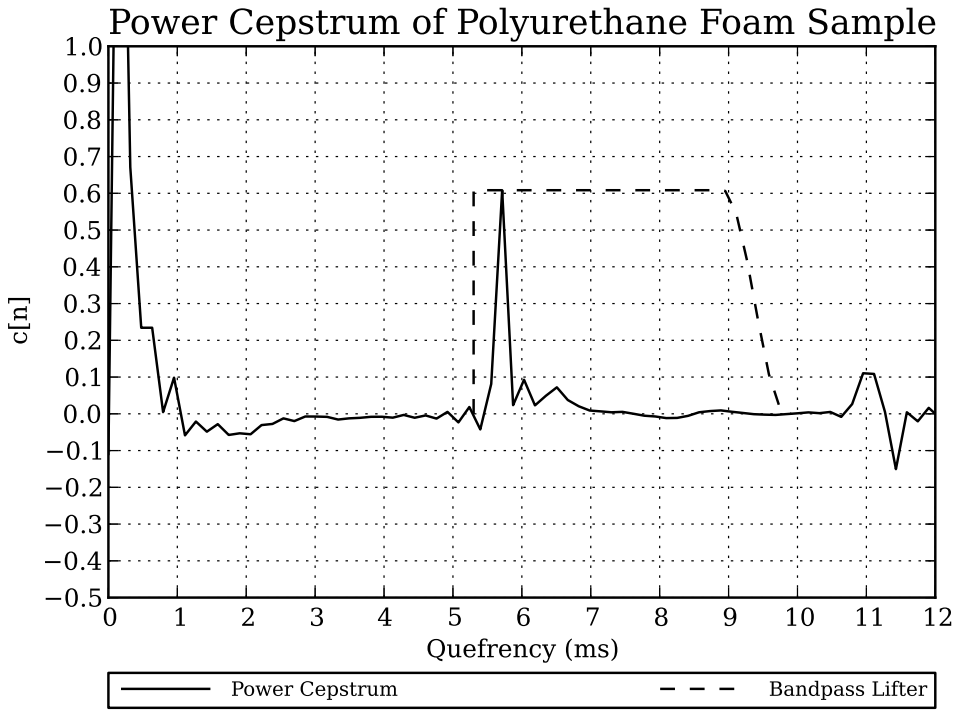

Figure 61: Power cepstrum for polyurethane foam sample #1.

University of Cape

9.7 WOOD FIBREBOARD SAMPLE

A 23 mm thick *Heraklith* wood fibreboard ceiling panel, shown in Figure 62, sample was chosen for its rapid increase in absorption between 400 Hz and approximately 1300 Hz, with very little absorption below 400 Hz. The sample was 102 mm in diameter, and was placed in the cepstrum tube holder. It is made of compressed wood shredding.

The wood fibreboard is placed directly in the cepstral tube sample holder. The impedance tube sample holder was placed behind the sample in the cepstral tube sample holder. The sample holders were then clamped to the cepstral tube.

The absorption coefficient is shown in Figure 63. There is a very close agreement between the cepstral tube and the impedance tube measurements. There are two points where the difference between the impedance tube and the cepstral tube measurements differ by more than 0.05. The error at 300 Hz is 0.07, but it appears this is due to an error in the impedance tube measurement. There is also an error of 0.07 at 710 Hz. This is due to the ripple caused by the band pass *lifterer*. The offset which causes the ripple is present in Figure 64. The impulse response decays to negligible levels within the length of the *lifterer*.

Figure 62: Haraklith wood fibreboard sample used in testing.

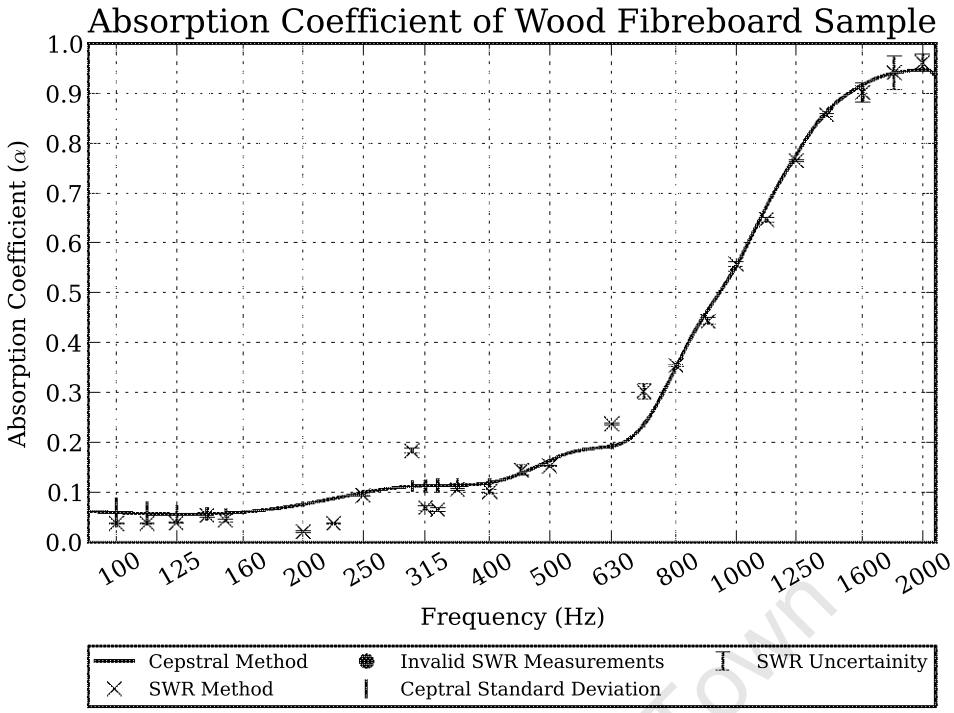

Figure 63: Absorption coefficient of Haraklith wood fibreboard sample.

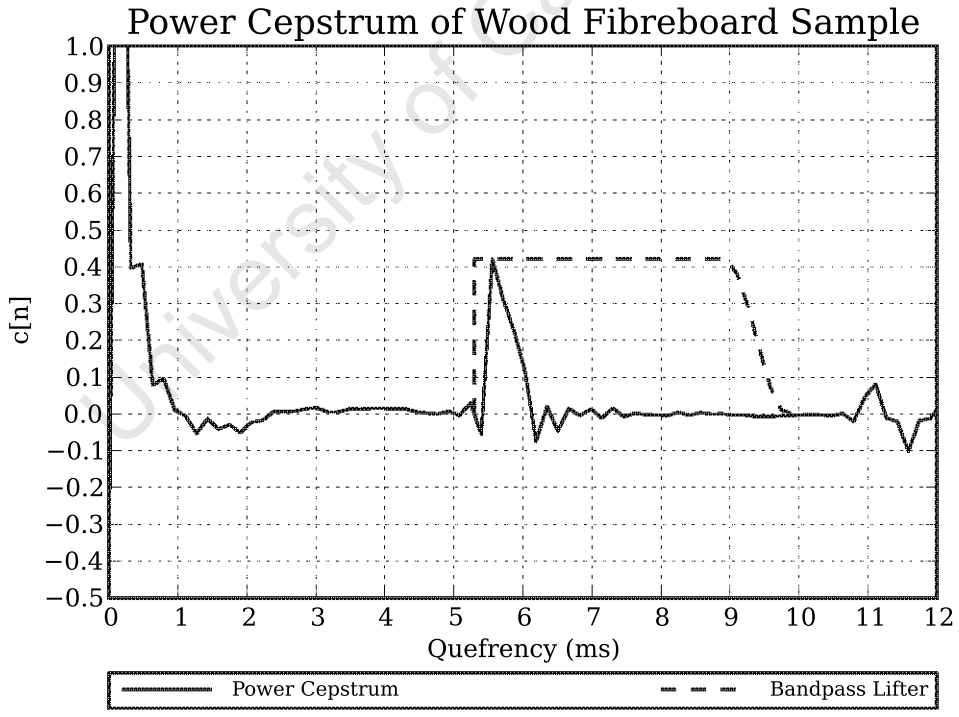

Figure 64: Power Cepstrum of Haraklith wood fibreboard sample.

University of Cape Town

9.8 HELMHOLTZ RESONATOR

A Helmholtz resonator absorber, shown in Figure 65, was created by placing a perforated hardwood sample with a diameter of 102 mm onto the impedance tube holder. A 40 mm air gap was created behind the hardboard face. The hardboard was 3 mm thick, with 52 holes. The holes were 5 mm in diameter. The resonator was chosen, as it was predicted to have a resonant peak beyond the measurement limits of the cepstral tube. This is because it has a high-Q absorption peak, with the peak bandwidth significantly less than the 200 Hz limit that a 2 meter tube imposes.

The absorption coefficient measured is shown in Figure 66. If one looks at the absorption coefficient measured by the impedance tube, it can be seen that there is little absorption in the range 100 Hz to 500 Hz, where the resonator begins to absorb the sound energy. The peak is reached at approximately 940 Hz. Above 940 Hz, the absorption coefficient falls from 0.35 to 0.15 between 1000 Hz to 2000 Hz.

The cepstral technique shows poor correlation with the impedance tube measurement over the range 100 Hz to 970 Hz. There is a close correlation from 970 Hz to 2000 Hz. It can be seen that the frequency of the peak in the absorption coefficient measured by the cepstral technique agrees with the peak in the absorption coefficient determined by the impedance tube. But, the peak of the absorption coefficient is only 0.42, as opposed to 0.61. This is due to the frequency resolution of the cepstral technique.

The power cepstrum for the Helmholtz resonator is shown in Figure 67. It can be seen that there is a small negative off set in the cepstrum before the arrival of the impulse response. The reason for the negative offset, when the other cepstrum have shown a small positive offset, is that the signal levels of the sound card inputs had been adjusted. This is responsible for the undulations in the absorption coefficient. It can also be seen that there is still energy present in the tail of the impulse response of the resonator.

University of Cape Town

Figure 65: The Helmholtz resonator created with the sample holder and a perforated hardboard.

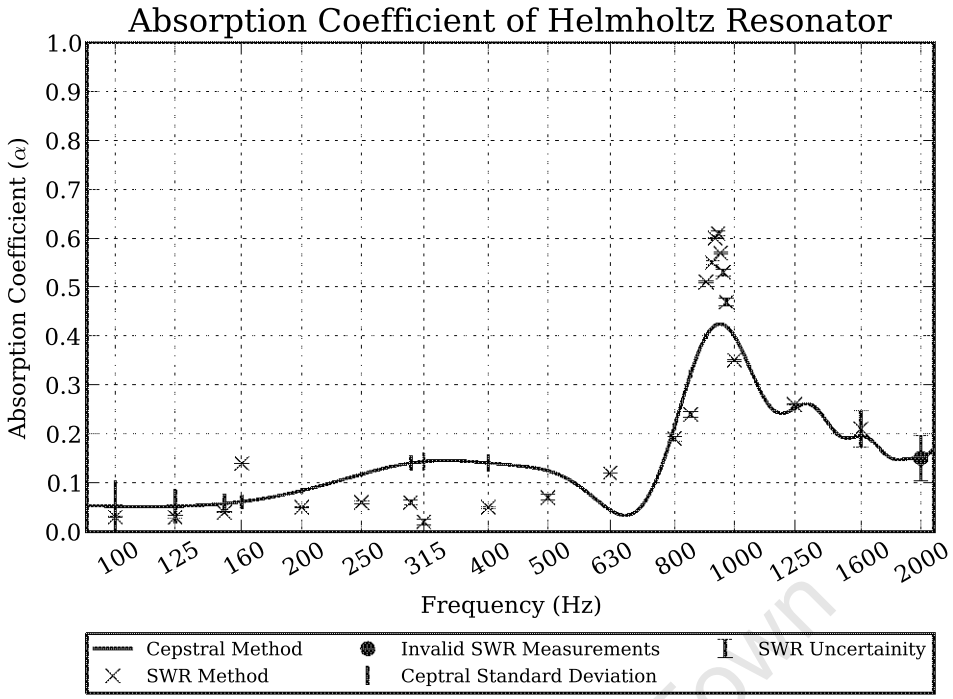

Figure 66: Absorption coefficient of the Helmholtz resonator.

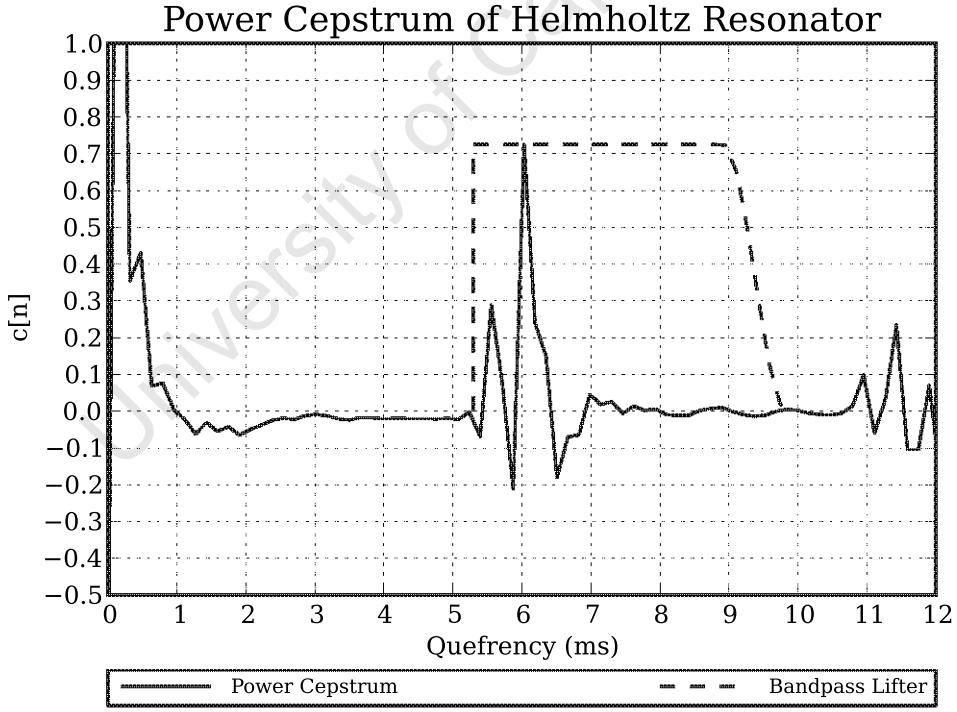

Figure 67: Power cepstrum of the Helmholtz resonator.

A thin layer of glass fibre is attached to the inside face of the hardboard of the resonator, shown in Figure 65. The glass fibre sample increases the range of frequencies that the resonator absorbs, and therefore increases

University of Cape Town

the bandwidth of the absorption peak. Figure 68 shows the absorption coefficient for the modified Helmholtz resonator. It can be seen that there is a good agreement with the cepstral technique measurements and the impedance tube measurements.

The corresponding power cepstrum obtained for the measurement is shown in Figure 69. The tail of the impulse response has decayed to negligible levels within the length of the *lifterer.*

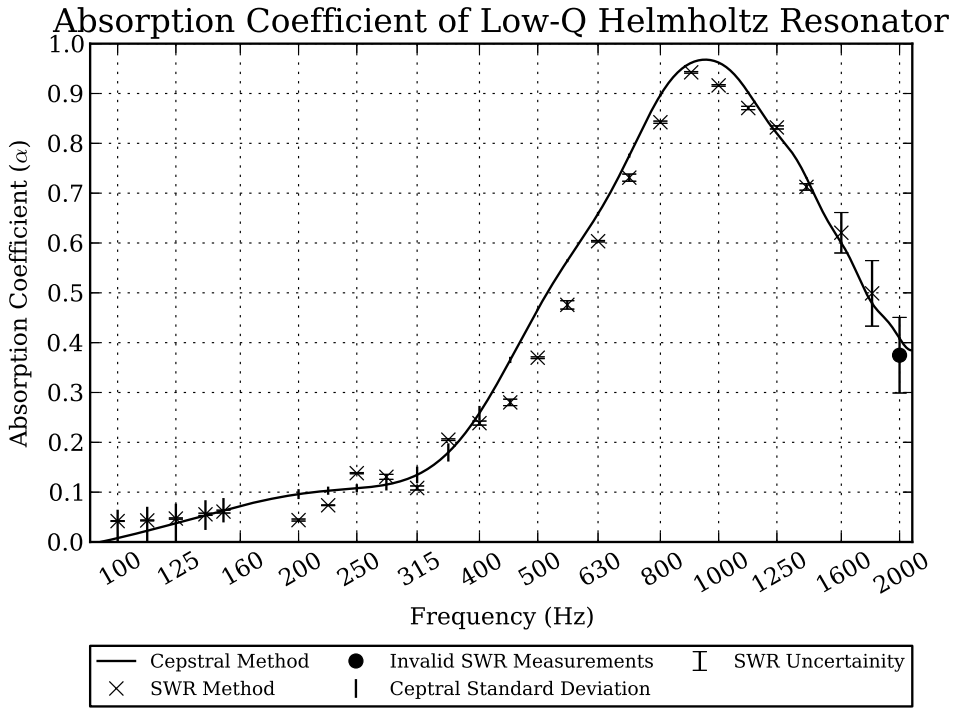

Figure 68: Absorption coefficient of the Helmholtz resonator with a thin glass fibre layer behind the hardboard.

University

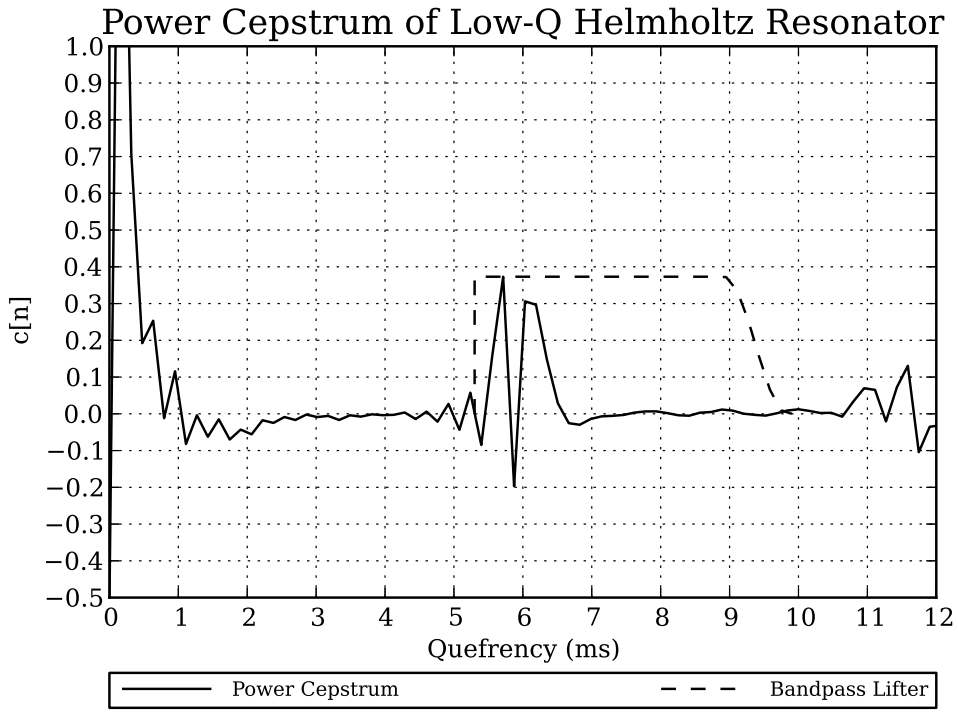

Figure 69: Power cepstrum of the Helmholtz resonator with a thin glass fibre layer behind the hardboard.

9.9 DISCUSSION OF RESULTS

It was shown that a very close correlation between the absorption coefficient measured with the cepstral method and the standing wave ratio method between the frequency range of 200 Hz and 2000 Hz. Below 200 Hz, the standard deviation of the cepstral method monotonically increased with decreasing frequency.

The low frequency roll off of the measurement system and the non-linearities in the loudspeaker introduced a small DC offset in the cepstrum. This offset superimposes a ripple into the measurement results. The effect of the low frequency roll off is discussed in Section 5.2.1. Section 5.2.3 illustrates the effect that the non-linearities in the loudspeaker has on the cepstrum. This offset can be seen in all the presented power cepstrum.

The reflective sample highlighted the errors in both the cepstral technique and the impedance tube technique. A superimposed ripple is noted in the absorption coefficient obtained with the cepstral technique, this is due to the band pass *lifterer* and the apparent acausal effects due to the nature of the DFT.

The power cepstrum for all the measurements present a small offset. This small offset reduced the accuracy of the measurements, which caused undulations in the absorption coefficient graphs.

University of Cape Town

Despite these disadvantages, the close correlation with the cepstral tube results and the impedance tube results show that the IRS is a suitable excitation signal to use with the cepstral technique.

University of Cape Town

10 CONCLUSIONS

Jongens [27] investigated the feasibility of applying cepstral techniques to determine the plane wave sound power absorption coefficient of materials using an adaptation of the impedance tube. A good correlation between Jongen's cepstral tube method and the standard wave ratio method was obtained for a wide variety of materials. The measurements were performed using the low pass swept sine signal.

This thesis continued the work of Jongens, with the focus of creating an automated apparatus to determine the plane wave sound power absorption coefficient. The factors of the measurement system which influence the accuracy of the results were highlighted and examined. Possible methods that could be employed to reduce the influence of these factors were discussed. Software was developed which allowed the measurement of the absorption coefficient to be performed by clicking a single button. It was shown that the IRS is a suitable excitation signal to use with the cepstral technique, offering noise immunity over the frequency range of 200 Hz to 2000 Hz. However, the low pass swept sine showed higher noise immunity over the range 315 Hz to 2000 Hz.

The objectives of this thesis were to:

DETERMINE THE FACTORS THAT INFLUENCE THE ACCURACY OF THE CEPSTRAL MEASUREMENTS: The influences of each of the links in the measurement chain were discussed. Methods that may be employed to reduce these effects were presented.

MEASURE THE ABSORPTION COEFFICIENT OF MATERIALS WITH THE VALUES DIFFERING BY NO MORE THAN 0.05: The results obtained using the cepstral technique correlated within 0.05 in the frequency range 200 Hz to 2000 Hz for a wide variety of samples. There were some measurement points that differed by more than 0.05, but could be explained by limitations in the measurement apparatus.

THE MEASUREMENT SHOULD BE PERFORMED BY A NON-SKILLED OPERATOR: The software developed for this thesis allowed the user to measure the absorption coefficient by clicking a single button. It did require that the sound level be adjusted first, before performing the measurements. The adjustment process may be relaxed with the use of a high quality loudspeaker and sound card.

University of Cape Town

THE MEASUREMENT SHOULD BE CARRIED OUT IN A NOISY ENVIRONMENT: The IRS signal used in this thesis offered high noise immunity and would be suitable for *in-situ* measurements.

10.1 FUTURE WORK

It was found that better correlation can be achieved by adjusting the sound level. The reason for this was due to the low quality loudspeaker and sound card being used for measurements. Using the IRS signal it is important to reduce the non-linearities in the system, as they appear as spikes in the system impulse response, which in turn corrupt the cepstrum. Research should be undertaken to select a more suitable loudspeaker. The loudspeaker should have a smooth frequency response, low total harmonic distortion, as well as a short transient response.

The non-linearities and the low frequency roll off of the loudspeaker results in an offset in the cepstrum. This offset is convolved with the frequency response of the *band pass lifterer*, which corrupts the results. There are two approaches that could be explored in obtaining a more linear - or less non-linear - loudspeaker. The first is developing such a loudspeaker. Merit [30] found that by removing the iron from the loudspeaker, the Eddy currents and reluctant effects are also removed. This improves the linearity of the loudspeaker. The second approach to be explored is using signal processing techniques to linearise the loudspeaker. Gao [15] used adaptive nonlinear filters to significantly reduce the nonlinear distortions in the loudspeaker.

One of the main attractions of using the cepstral technique, is that it allows one to improve the frequency resolution of the measurement. The theory of improving the frequency resolution is given in [6], and discussed in Subsection 3.3.5. Attempts were, unsuccessfully, made to implement the method. It was found that the incident wave corrupts the reflected wave to such a degree that cepstral deconvolution was not possible. This is mainly due to the impulse response of the loudspeaker. The improvement in frequency resolution should be researched with the use of a high quality loudspeaker and sound card.

Finally, an important characteristic of a material, is its impedance. The impedance of the sample can also be determined by its impulse response. This thesis was focused only on determining the sound power absorption coefficient. Therefore the phase of the impulse response was ignored. Work should be undertaken to preserve the phase of the impulse response, using the complex cepstrum - instead of the power cepstrum. There are two factors that complicate the process. First, misidentifying the start of the impulse introduces undulations into the phase. Bolton [4] recommends first up-sampling the *liftered* impulse response so that the onset of the impulse can accurately be determined. The delay can then

University of Cape Town

be subtracted, and reduce the distortion. Second, it was found necessary to subtract the sound generating and acquisition cepstrum from the microphone's cepstrum. This subtraction is going to distort the phase, and should be taken into account when determining the impedance.

University of Cape Town

APPENDIX

University of Cape Town

A

RAW DATA

This appendix tabulates the sound power absorption coefficient obtained automatically using the cepstral technique, compared to the coefficient obtained using the impedance tube. It also tabulates the pressure maximum and minimum recorded in the impedance tube measurements.

A.1 REFLECTIVE SAMPLE

Table 6: Table showing the absorption coefficient determined using the cepstral technique, compared to the coefficient obtained with the impedance tube for the reflective sample.

Frequency	α_{Cepstral}	$\alpha_{\text{Impedance}}$	Difference	Std Dev	ρ_{max}	ρ_{min}	$\alpha_{\text{Impedance}}$ Error
100	0.01	0.02	0.01	0.03	77.95	0.41	0
112	0	0.02	0.01	0.02	75.01	0.37	0
125	0	0.02	0.02	0.02	75.28	0.36	0
140	0	0.03	0.03	0.02	28.32	0.19	0
150	0	0.02	0.02	0.02	27.67	0.13	0
160	**0**	**0.23**	**0.23**	**0.02**	**22.79**	**1.5**	**0**
170	**0**	**0.21**	**0.21**	**0.02**	**21.1**	**1.23**	**0**
180	**0**	**0.25**	**0.24**	**0.02**	**10.33**	**0.73**	**0.01**
200	0.01	0.03	0.01	0.02	31.55	0.2	0
224	0.02	0.01	0.02	0.02	72.19	0.12	0
250	0.04	0.04	0.01	0.01	79.07	0.82	0
280	**0.04**	**0.15**	**0.11**	**0.02**	**15.03**	**0.6**	**0**
300	0.04	0.05	0.01	0.02	14.22	0.2	0.01
315	0.04	0.05	0.01	0.02	14.61	0.2	0.01
330	0.04	0.01	0.02	0.02	43.44	0.15	0

University of Cape Town

Frequency	α_{Cepstral}	$\alpha_{\text{Impedance}}$	Difference	Std Dev	ρ_{max}	ρ_{min}	$\alpha_{\text{Impedance}}$ Error
355	0.03	0.02	0.01	0.02	49.19	0.2	0
400	**0.01**	**0.08**	**0.07**	**0.01**	**40.66**	**0.8**	**0**
450	0	0.03	0.03	0.01	17.79	0.13	0
500	0	0.01	0.01	0	86.32	0.18	0
560	**-0.01**	**0.21**	**0.22**	**0.01**	**15.36**	**0.88**	**0**
630	-0.02	0.03	0.05	0.01	26.35	0.17	0
710	0	0.04	0.04	0.01	9.5	0.1	0.01
800	0.05	0.02	0.03	0.01	76.26	0.37	0
900	0.05	0.03	0.03	0.01	19.8	0.13	0
1000	0.05	0.06	0	0.01	11.09	0.16	0.01
1120	**0.08**	**0.02**	**0.06**	**0.01**	**39.92**	**0.19**	**0**
1250	0.07	0.05	0.02	0.01	17.44	0.22	0
1400	0.08	0.04	0.04	0.01	9.14	0.1	0.01
1600	0.07	0.03	0.05	0	9.28	0.06	0.01
1800	0.07	0.1	0.03	0.01	1.99	0.05	0.04
2000	0.09	0.12	0.03	0.02	1.9	0.06	0.04

University of Cape Town

A.2 7-4 TWINLAY ASPHALT SAMPLE

Table 7: Table showing the absorption coefficient determined using the cepstral technique, compared to the coefficient obtained with the impedance tube for the 7-4 TWINLay asphalt sample.

Frequency	α_{Cepstral}	$\alpha_{\text{Impedance}}$	Difference	Std Dev	ρ_{max}	ρ_{min}	$\alpha_{\text{Impedance}}$ Error
100	0.05	0.02	0.02	0.05	82.63	0.52	0
112	0.04	0.02	0.02	0.04	68.13	0.43	0
125	0.04	0.02	0.02	0.03	70.05	0.42	0
140	0.04	0.03	0.01	0.02	27.56	0.2	0
150	0.04	0.06	0.02	0.01	27.1	0.42	0
200	0.07	0.03	0.04	0.01	33.31	0.29	0
224	**0.09**	**0.02**	**0.07**	**0.01**	**72.33**	**0.41**	**0**
250	0.11	0.06	0.05	0.01	70.4	1.11	0
300	0.12	0.15	0.03	0.02	14.25	0.58	0.01
315	0.11	0.06	0.05	0.02	15.31	0.23	0.01
330	0.11	0.06	0.04	0.02	22.2	0.36	0
355	0.1	0.13	0.03	0.02	51.4	1.8	0
400	0.14	0.15	0.02	0.01	17.71	0.73	0
450	0.27	0.29	0.02	0.01	6.42	0.55	0.01
500	0.49	0.46	0.03	0	46.92	7.21	0
630	0.76	0.79	0.04	0.01	17.83	6.66	0
710	0.52	0.54	0.02	0	4.67	0.9	0.01
800	0.3	0.34	0.04	0.01	33.8	3.5	0
900	0.24	0.22	0.02	0.01	5.71	0.35	0.01
1000	0.19	0.19	0	0	11.61	0.61	0.01
1120	0.18	0.14	0.04	0	36.22	1.37	0
1250	0.18	0.15	0.03	0	17.26	0.71	0

University of Cape Town

Frequency	α_{Cepstral}	$\alpha_{\text{Impedance}}$	Difference	Std Dev	ρ_{max}	ρ_{min}	$\alpha_{\text{Impedance}}$ Error
1400	0.2	0.15	0.04	0	9.28	0.39	0.01
1600	**0.27**	**0.21**	**0.06**	**0**	**2.73**	**0.16**	**0.02**
1800	0.46	0.44	0.02	0	0.97	0.14	0.06
2000	0.73	0.73	0.01	0	1.59	0.5	0.02

University of Cape Town

A.3 60 mm glass fibre

Table 8: Table showing the absorption coefficient determined using the cepstral technique, compared to the coefficient obtained with the impedance tube for the 60 mm glass fibre sample.

Frequency	α_{Cepstral}	$\alpha_{\text{Impedance}}$	Difference	Std Dev	ρ_{max}	ρ_{min}	$\alpha_{\text{Impedance}}$ Error
100	0.15	0.1	0.05	0.03	77.89	2.01	0
112	0.14	0.12	0.02	0.03	40.65	1.35	0
125	0.14	0.15	0.01	0.02	47.56	1.98	0
140	0.15	0.17	0.02	0.02	21.64	1.01	0
150	0.16	0.18	0.02	0.02	23.28	1.12	0
200	0.24	0.22	0.02	0.01	41.54	2.57	0
224	0.3	0.33	0.03	0.01	40.3	4.06	0
250	**0.38**	**0.43**	**0.06**	**0.01**	**49.53**	**7.01**	**0**
300	0.53	0.58	0.05	0.01	14.75	3.18	0
315	0.57	0.56	0.01	0.01	17.05	3.44	0
330	0.61	0.59	0.01	0.01	24.69	5.48	0
355	0.66	0.65	0.01	0.01	23.41	6.02	0
400	0.73	0.7	0.03	0.01	14.62	4.26	0
450	0.77	0.74	0.03	0	6.62	2.14	0
500	0.79	0.79	0	0	24.7	9.27	0
630	0.86	0.89	0.03	0	19.57	9.89	0
710	0.89	0.91	0.02	0	3.82	2.09	0
800	0.91	0.93	0.02	0	13.2	7.63	0
900	0.93	0.93	0	0	5.93	3.51	0
1000	0.93	0.94	0.01	0	8.21	5.03	0
1120	0.94	0.94	0	0	7.37	4.45	0
1250	0.94	0.94	0.01	0	10.26	6.28	0

University of Cape Town

Frequency	α_{Cepstral}	$\alpha_{\text{Impedance}}$	Difference	Std Dev	ρ_{max}	ρ_{min}	$\alpha_{\text{Impedance}}$ Error
1400	0.93	0.93	0	0	6.02	3.56	0
1600	0.93	0.92	0.01	0	0.87	0.48	0.02
1800	0.93	0.93	0	0	0.38	0.22	0.04
2000	0.93	0.91	0.02	0	0.65	0.35	0.03

University of Cape Town

A.4 FOAM SAMPLE #1

Table 9: Table showing the absorption coefficient determined using the cepstral technique, compared to the coefficient obtained with the impedance tube for the foam sample #1 sample.

Frequency	α_{Cepstral}	$\alpha_{\text{Impedance}}$	Difference	Std Dev	ρ_{max}	ρ_{min}	$\alpha_{\text{Impedance}}$ Error
100	0.07	0.06	0.01	0.08	81.81	1.26	0
112	0.08	0.07	0	0.07	57.53	1.1	0
125	0.09	0.08	0.01	0.05	62.92	1.24	0
140	0.1	0.09	0.01	0.03	25.02	0.62	0
150	0.11	0.1	0.01	0.03	25.08	0.69	0
200	0.16	0.12	0.04	0.01	34.09	1.09	0
224	0.18	0.18	0.01	0	57.3	2.8	0
250	0.22	0.25	0.04	0.01	60.9	4.41	0
300	**0.3**	**0.39**	**0.09**	**0.02**	**14.01**	**1.73**	**0**
315	0.34	0.33	0.01	0.02	15.09	1.49	0
330	0.37	0.37	0	0.03	21.65	2.49	0
355	0.44	0.45	0.01	0.02	34.46	5.04	0
400	0.55	0.59	0.04	0.01	15.96	3.52	0
450	0.64	0.65	0	0.01	5.72	1.45	0.01
500	**0.67**	**0.59**	**0.08**	**0.01**	**40.58**	**8.81**	**0**
630	0.62	0.63	0.01	0.01	22.86	5.51	0
710	0.66	0.68	0.02	0.01	4.1	1.13	0.01
800	0.71	0.65	0.06	0.01	25.83	6.58	0
900	**0.64**	**0.57**	**0.07**	**0.01**	**5.62**	**1.16**	**0.01**
1000	0.57	0.56	0.01	0	10.34	2.1	0
1120	0.58	0.6	0.01	0.01	16.1	3.58	0
1250	0.58	0.62	0.04	0.01	14.21	3.37	0

University of Cape Town

Frequency	α_{Cepstral}	$\alpha_{\text{Impedance}}$	Difference	Std Dev	ρ_{max}	ρ_{min}	$\alpha_{\text{Impedance}}$ Error
1400	0.62	0.63	0.01	0.01	7.56	1.82	0.01
1600	0.68	0.66	0.02	0	1.46	0.38	0.03
1800	0.7	0.71	0.01	0.01	0.94	0.28	0.04
2000	0.7	0.69	0.01	0.01	0.71	0.2	0.05

University of Cape Town

A.5 WOOD FIBREBOARD SAMPLE

Table 10: Table showing the absorption coefficient determined using the cepstral technique, compared to the coefficient obtained with the impedance tube for the *Haraklith* sample.

Frequency	α_{Cepstral}	$\alpha_{\text{Impedance}}$	Difference	Std Dev	ρ_{max}	ρ_{min}	$\alpha_{\text{Impedance}}$ Error
100	0.06	0.04	0.02	0.03	85.06	0.81	0
112	0.06	0.04	0.02	0.02	65.46	0.62	0
125	0.06	0.04	0.02	0.02	69.28	0.68	0
140	0.06	0.05	0	0.01	26.33	0.36	0
150	0.06	0.04	0.01	0.01	26.95	0.3	0
200	0.08	0.02	0.05	0	34.02	0.18	0
224	0.09	0.04	0.05	0	70.51	0.68	0
250	0.1	0.09	0.01	0	70.92	1.73	0
300	**0.11**	**0.18**	**0.07**	**0.01**	**14.85**	**0.75**	**0**
315	0.11	0.07	0.04	0.01	15.73	0.28	0
330	0.11	0.06	0.05	0.01	23.23	0.39	0
355	0.11	0.11	0.01	0.01	56.31	1.57	0
400	0.12	0.1	0.02	0.01	18.37	0.49	0
450	0.14	0.14	0.01	0	6.67	0.26	0.01
500	0.16	0.15	0.01	0	75.68	3.14	0
630	0.19	0.24	0.05	0.01	43.06	2.91	0
710	**0.24**	**0.3**	**0.07**	**0**	**4.24**	**0.38**	**0.01**
800	0.35	0.35	0	0	33.72	3.67	0
900	0.46	0.44	0.02	0	7.57	1.1	0.01
1000	0.55	0.56	0	0	8.96	1.8	0.01
1120	0.67	0.65	0.03	0	9.88	2.51	0
1250	0.78	0.76	0.01	0	15.5	5.37	0

University of Cape Town

Frequency	α_{Cepstral}	$\alpha_{\text{Impedance}}$	Difference	Std Dev	ρ_{max}	ρ_{min}	$\alpha_{\text{Impedance}}$ Error
1400	0.86	0.86	0.01	0	7.96	3.58	0
1600	0.92	0.9	0.02	0	0.9	0.47	0.02
1800	0.94	0.94	0	0	0.41	0.25	0.03
2000	0.95	0.96	0.01	0	0.61	0.41	0.02
2000	0.91	0.94	0.02	0	0.64	0.38	0.02

University of Cape Town

A.6 HELMHOLTZ RESONATOR

Table 11: Table showing the absorption coefficient determined using the cepstral technique, compared to the coefficient obtained with the impedance tube for the Helmholtz resonator.

Frequency	α_{Cepstral}	$\alpha_{\text{Impedance}}$	Difference	Std Dev	ρ_{max}	ρ_{min}	$\alpha_{\text{Impedance}}$ Error
100	0.05	0.03	0.02	0.05	202	1.59	0
125	0.05	0.03	0.02	0.03	135.4	1.15	0
150	0.06	0.04	0.02	0.02	53.5	0.55	0
160	**0.06**	**0.14**	**0.08**	**0.01**	**46**	**1.75**	**0**
200	0.08	0.05	0.03	0	79.5	1.02	0
250	**0.12**	**0.06**	**0.06**	**0**	**123.4**	**1.81**	**0**
300	**0.14**	**0.06**	**0.08**	**0.01**	**30.8**	**0.46**	**0**
315	**0.14**	**0.02**	**0.12**	**0.02**	**35.8**	**0.15**	**0.01**
400	**0.14**	**0.05**	**0.09**	**0.02**	**32.4**	**0.42**	**0**
500	0.12	0.07	0.05	0	78.2	1.32	0.01
630	**0.04**	**0.12**	**0.08**	**0**	**97.6**	**3.14**	**0**
800	0.21	0.19	0.02	0.01	22.7	1.18	0.01
850	**0.32**	**0.24**	**0.08**	**0.01**	**13.47**	**0.92**	**0.01**
900	**0.4**	**0.51**	**0.11**	**0**	**40.8**	**7.19**	**0**
920	**0.42**	**0.55**	**0.13**	**0**	**34.6**	**6.76**	**0**
930	**0.42**	**0.6**	**0.18**	**0**	**26.9**	**6.08**	**0**
940	**0.42**	**0.61**	**0.19**	**0**	**21.4**	**4.91**	**0**
950	**0.42**	**0.57**	**0.15**	**0**	**17.78**	**3.7**	**0**
960	**0.42**	**0.53**	**0.11**	**0**	**15.61**	**2.88**	**0.01**
970	0.42	0.47	0.05	0	14.61	2.27	0.01
1000	0.4	0.35	0.05	0	20.5	2.21	0
1250	0.25	0.26	0.01	0	15.1	1.15	0

University of Cape Town

Frequency	α_{Cepstral}	$\alpha_{\text{Impedance}}$	Difference	Std Dev	ρ_{max}	ρ_{min}	$\alpha_{\text{Impedance}}$ Error
1600	0.2	0.21	0.01	0	1.88	0.11	0.04
2000	0.15	0.15	0	0	1.44	0.06	0.05

University of Cape Town

A.7 HELMHOLTZ RESONATOR WITH GLASS FIBRE

Table 12: Table showing the absorption coefficient determined using the cepstral technique, compared to the coefficient obtained with the impedance tube for the Helmholtz resonator with thin glass fibre layer.

Frequency	α_{Cepstral}	$\alpha_{\text{Impedance}}$	Difference	Std Dev	ρ_{max}	ρ_{min}	$\alpha_{\text{Impedance}}$ Error
100	0.01	0.04	0.03	0.06	89.4	0.96	0
112	0.02	0.04	0.02	0.05	93.2	1.03	0
125	0.04	0.05	0.01	0.04	63.1	0.76	0
140	0.05	0.06	0	0.03	34.3	0.49	0
150	0.06	0.06	0	0.02	26.7	0.42	0
200	0.1	0.04	0.05	0.01	38.2	0.43	0
224	0.1	0.07	0.03	0.01	115.5	2.21	0
250	0.11	0.14	0.03	0.01	61.9	2.3	0
280	0.12	0.13	0.02	0.01	14.57	0.51	0.01
315	0.13	0.11	0.03	0.02	18.14	0.52	0
355	0.18	0.21	0.03	0.02	42	2.41	0
400	0.26	0.24	0.02	0.01	16.46	1.12	0
450	**0.37**	**0.28**	**0.09**	**0.01**	**9.88**	**0.81**	**0.01**
500	**0.47**	**0.37**	**0.1**	**0**	**34.9**	**4.01**	**0**
560	**0.56**	**0.48**	**0.09**	**0**	**6.06**	**0.97**	**0.01**
630	0.66	0.6	0.05	0	31.5	7.16	0
710	0.78	0.73	0.04	0	4.51	1.43	0.01
800	0.9	0.84	0.05	0	10.68	4.61	0
900	0.96	0.94	0.02	0	7.78	4.77	0
1000	0.96	0.92	0.05	0	9.98	5.5	0
1120	0.9	0.87	0.03	0	6.11	2.88	0
1250	0.82	0.83	0.01	0	7.79	3.26	0

University of Cape Town

Frequency	α_{Cepstral}	$\alpha_{\text{Impedance}}$	Difference	Std Dev	ρ_{max}	ρ_{min}	$\alpha_{\text{Impedance}}$ Error
1400	0.73	0.71	0.02	0	5.2	1.57	0.01
1600	0.6	0.62	0.02	0	1.01	0.24	0.04
1800	0.48	0.5	0.02	0	0.76	0.13	0.07
2000	0.41	0.37	0.03	0	0.77	0.09	0.08

University of Cape Town

EQUIPMENT SPECIFICATIONS

B.1 TASCAM US-122MKII SOUND CARD

9 – Specifications

Input/output ratings

Analog audio input/outupt

MIC IN (Balanced) terminal

Connector: XLR-3-31 equivalent

Nominal input level:
–58 dBu (When **INPUT** konb is set to **MIC**)
–14 dBu (When **INPUT** knob is set to **LINE**)

Maximum input level:
+2 dBu (When **INPUT** knob is set to **LINE**)

Input impedance: 2.2 kΩ

LINE IN (Balanced) terminal

Connector: TRS Standard phone jack

L channel, and R channel with **MIC/LINE-GUTAR** set to **MIC/LINE**

Nominal input level:
–40 dBu (When **INPUT** konb is set to **MIC**)
+4 dBu (When **INPUT** knob is set to **LINE**)

Maximum input level:
+20 dBu (When **INPUT** knob is set to **LINE**)

Input impedance: 15 kΩ

R channel with **MIC/LINE-GUTAR** set to **GUITAR**

Nominal input level:
–51 dBV (When **INPUT** konb is set to **MIC**)
–7 dBV (When **INPUT** knob is set to **LINE**)

Maximum input level:
+9 dBV (When **INPUT** knob is set to **LINE**)

Input impedance: 1 MΩ

LINE OUT (Unbalanced) terminal

Connector: RCA pin jack

Nominal output level: –10 dBV

Maximum output level: +6 dBV

Output impedance: 200Ω

PHONES terminal:

Connector:Standard stereo phone jack

Maximum output level: 18 mW + 18 mW or more (THD+N less than 0.1%, 32Ω load)

Control input/output

MIDI IN terminal

Connector: DIN 5 pin

Format: Standard MIDI format

MIDI OUT terminal

Connector: DIN 5 pin

Format: Standard MIDI format

USB terminal

Connector: USB B type 4 pin

Format:

USB 2.0 High speed (480 MHz)

USB 2.0 Full speed
(12 MHz USB 1.1 equivalent)

B.2 AGILENT 34410A MULTIMETER

Accuracy Specifications ± (% of reading + % of range)[1]

Function	Range[3]	Frequency, Test Current or Burden Voltage	24 Hour[2] Tcal ± 1 °C	90 Day Tcal ± 5 °C	1 Year Tcal ± 5 °C	Temperature Coefficient/°C 0 °C to (Tcal -5 °C) (Tcal +5 °C) to 55 °C
DC Voltage	100.0000 mV		0.0030 + 0.0030	0.0040 + 0.0035	0.0050 + 0.0035	0.0005 + 0.0005
	1.000000 V		0.0020 + 0.0006	0.0030 + 0.0007	0.0035 + 0.0007	0.0005 + 0.0001
	10.00000 V		**0.0015 + 0.0004**	**0.0020 + 0.0005**	**0.0030 + 0.0005**	**0.0005 + 0.0001**
	100.0000 V		0.0020 + 0.0006	0.0035 + 0.0006	0.0040 + 0.0006	0.0005 + 0.0001
	1000.000 V[4]		0.0020 + 0.0006	0.0035 + 0.0006	0.0040 + 0.0006	0.0005 + 0.0001
True RMS AC Voltage[5]	100.0000 mV to 750.000 V	3 Hz – 5 Hz	0.50 + 0.02	0.50 + 0.03	0.50 + 0.03	0.010 + 0.003
		5 Hz – 10 Hz	0.10 + 0.02	0.10 + 0.03	0.10 + 0.03	0.008 + 0.003
		10 Hz – 20 kHz	**0.02 + 0.02**	**0.05 + 0.03**	**0.06 + 0.03**	**0.005 + 0.003**
		20 kHz – 50 kHz	0.05 + 0.04	0.09 + 0.05	0.10 + 0.05	0.010 + 0.005
		50 kHz – 100 kHz	0.20 + 0.08	0.30 + 0.08	0.40 + 0.08	0.020 + 0.008
		100 kHz – 300 kHz	1.00 + 0.50	1.20 + 0.50	1.20 + 0.50	0.120 + 0.020
Resistance[6]	100.0000 Ω	1 mA	0.0030 + 0.0030	0.008 + 0.004	0.010 + 0.004	0.0006 + 0.0005
	1.000000 kΩ	1 mA	0.0020 + 0.0005	0.007 + 0.001	0.010 + 0.001	0.0006 + 0.0001
	10.00000 kΩ	**100 µA**	**0.0020 + 0.0005**	**0.007 + 0.001**	**0.010 + 0.001**	**0.0006 + 0.0001**
	100.0000 kΩ	10 µA	0.0020 + 0.0005	0.007 + 0.001	0.010 + 0.001	0.0006 + 0.0001
	1.000000 MΩ	5 µA	0.0020 + 0.0010	0.010 + 0.001	0.012 + 0.001	0.0010 + 0.0002
	10.00000 MΩ	500 nA	0.0100 + 0.0010	0.030 + 0.001	0.040 + 0.001	0.0030 + 0.0004
	100.0000 MΩ	500 nA || 10 MΩ	0.200 + 0.001	0.600 + 0.001	0.800 + 0.001	0.1000 + 0.0001
	1.000000 GΩ	500 nA || 10 MΩ	2.000 + 0.001	6.000 + 0.001	8.000 + 0.001	1.0000 + 0.0001
DC Current	100.0000 µA	< 0.03 V	0.010 + 0.020	0.040 + 0.025	0.050 + 0.025	0.0020 + 0.0030
	1.000000 mA	**< 0.3 V**	**0.007 + 0.006**	**0.030 + 0.006**	**0.050 + 0.006**	**0.0020 + 0.0005**
	10.00000 mA	< 0.03 V	0.007 + 0.020	0.030 + 0.020	0.050 + 0.020	0.0020 + 0.0020
	100.0000 mA	< 0.3 V	0.010 + 0.004	0.030 + 0.005	0.050 + 0.005	0.0020 + 0.0005
	1.000000 A	< 0.8 V	0.050 + 0.006	0.080 + 0.010	0.100 + 0.010	0.0050 + 0.0010
	3.000000 A	< 2.0 V	0.100 + 0.020	0.120 + 0.020	0.150 + 0.020	0.0050 + 0.0020
True RMS AC Current[7]	100.0000 µA to 3.00000 A	**3 Hz – 5 kHz**	**0.10 + 0.04**	**0.10 + 0.04**	**0.10 + 0.04**	**0.015 + 0.006**
		5 kHz – 10 kHz	0.20 + 0.04	0.20 + 0.04	0.20 + 0.04	0.030 + 0.006
Frequency or Period	100 mV to 750 V	3 Hz – 5 Hz	0.070 + 0.000	0.070 + 0.000	0.070 + 0.000	0.005 + 0.000
		5 Hz – 10 Hz	0.040 + 0.000	0.040 + 0.000	0.040 + 0.000	0.005 + 0.000
		10 Hz – 40 Hz	0.020 + 0.000	0.020 + 0.000	0.020 + 0.000	0.001 + 0.000
		40 Hz – 300 kHz	**0.005 + 0.000**	**0.006 + 0.000**	**0.007 + 0.000**	**0.001 + 0.000**
Capacitance[8]	1.0000 nF	500 nA	0.50 + 0.50	0.50 + 0.50	0.50 + 0.50	0.05 + 0.05
	10.000 nF	1 µA	0.40 + 0.10	0.40 + 0.10	0.40 + 0.10	0.05 + 0.01
	100.00 nF	10 µA	0.40 + 0.10	0.40 + 0.10	0.40 + 0.10	0.01 + 0.01
	1.0000 µF	10 µA	0.40 + 0.10	0.40 + 0.10	0.40 + 0.10	0.01 + 0.01
	10.000 µF	100 µA	0.40 + 0.10	0.40 + 0.10	0.40 + 0.10	0.01 + 0.01
Temperature[9]						
RTD	-200 °C to 600 °C		0.06 °C	0.06 °C	0.06 °C	0.003 °C
Thermistor	-80 °C to 150 °C		0.08 °C	0.08 °C	0.08 °C	0.002 °C
Continuity	1000.0 Ω	1 mA	0.002 + 0.010	0.008 + 0.020	0.010 + 0.020	0.0010 + 0.0020
Diode Test[10]	1.0000 V	1 mA	0.002 + 0.010	0.008 + 0.020	0.010 + 0.020	0.0010 + 0.0020

1 Specifications are for 90 minute warm-up and 100 PLC.

2 Relative to calibration standards.

3 20% overrange on all ranges, except DCV 1000 V, ACV 750 V, DCI and ACI 3 A ranges.

4 For each additional volt over ± 500 V add 0.02 mV of error.

5 Specifications are for sinewave input > 0.3% of range and > 1 mV_{rms}. Add 30 µV error for frequencies below 1 kHz. 750 VAC range limited to 8 x 10^7 Volts-Hz. For each additional volt over 300 V_{rms} add 0.7 mV_{rms} of error.

6 Specifications are for 4-wire resistance measurements, or 2-wire using Math Null. Without Math Null, add 0.2 Ω additional error in 2-wire resistance measurements.

7 Specifications are for sinewave input > 1% of range and > 10 µArms. Frequencies > 5 kHz are typical for all ranges. For the 3 A range (all frequencies) add 0.05% of reading + 0.02% of range to listed specifications.

8 Specifications are for 1-hour warm-up using Math Null. Additional errors may occur for non-film capacitors.

9 For total measurement accuracy, add temperature probe error.

10 Accuracy specifications are for the voltage measured at the input terminals only. 1 mA test current is typical. Variation in the current source will create some variation in the voltage drop across a diode junction.

University of Oregon Test

C

MLS DECONVOLUTION

Cohn and *Lempel* [11] give an efficient method of recovering the system's period impulse response, by noting the similarities of M-sequence matrices to Walsh-Hadamard matrices.

It was shown in subsection 4.4.3 that the periodic system impulse response, $h'[n]$ can be recovered by cross-correlating the output of a system, $y'[n]$, that was excited by a MLS, $s'[n]$, with periodicity of L,

$$h'[n] = \frac{1}{L+1} \sum_{k=0}^{L-1} y'[k]\, s'[k-n]\,. \tag{86}$$

For the case of $L = 7$, Equation 86, can be written in matrix form,

$$\begin{bmatrix} h[0] \\ h[1] \\ h[2] \\ h[3] \\ h[4] \\ h[5] \\ h[6] \end{bmatrix} = \frac{1}{8} \begin{bmatrix} s[0] & s[1] & s[2] & s[3] & s[4] & s[5] & s[6] \\ s[1] & s[2] & s[3] & s[4] & s[5] & s[6] & s[0] \\ s[2] & s[3] & s[4] & s[5] & s[6] & s[0] & s[1] \\ s[3] & s[4] & s[5] & s[6] & s[0] & s[1] & s[2] \\ s[4] & s[5] & s[6] & s[0] & s[1] & s[2] & s[3] \\ s[5] & s[6] & s[0] & s[1] & s[2] & s[3] & s[4] \\ s[6] & s[0] & s[1] & s[2] & s[3] & s[4] & s[5] \end{bmatrix} \begin{bmatrix} y[0] \\ y[1] \\ y[2] \\ y[3] \\ y[4] \\ y[5] \\ y[6] \end{bmatrix}. \tag{87}$$

The matrix in Equation 87 containing the circular shifted MLS, $s[n]$, is referred to as the M-sequence matrix, $\mathbf{M}$,

$$\mathbf{M} = \left[m_{i,j}\right]_{P\times P} = s\left[i + j - 2 \bmod P\right]. \tag{88}$$

For the MLS generated with $N = 3$,

$$\mathbf{M} = \begin{bmatrix} 0 & 0 & 1 & 0 & 1 & 1 & 1 \\ 0 & 1 & 0 & 1 & 1 & 1 & 0 \\ 1 & 0 & 1 & 1 & 1 & 0 & 0 \\ 0 & 1 & 1 & 1 & 0 & 0 & 1 \\ 1 & 1 & 1 & 0 & 0 & 1 & 0 \\ 1 & 1 & 0 & 0 & 1 & 0 & 1 \\ 1 & 0 & 0 & 1 & 0 & 1 & 1 \end{bmatrix}. \tag{89}$$

As each row and each column satisfy the recursive relation used to generate the MLS, every row (or column) can be expressed as a linear combination of the first N rows (or columns),

$$\mathbf{M} = \mathbf{LS} = \mathbf{S}'\mathbf{L}', \tag{90}$$

University Of Capetown

where $\mathbf{L}$ is a binary matrix of order $P \times N$, $\mathbf{S}$ is order $N \times P$ formed by the first N rows of $\mathbf{M}$, and $\mathbf{S}'$ and $\mathbf{L}'$ the transpose matrices of $\mathbf{S}$ and $\mathbf{L}$ respectively. Since all rows of $\mathbf{M}$ are distinct, all rows of $\mathbf{L}$ must be distinct and therefore every non-zero binary vector of length N must appear in some row of $\mathbf{L}$. Also, the first N rows of $\mathbf{L}$ form the the identity matrix of order N.

Let σ be a square matrix of order N, formed by the first N columns of $\mathbf{S}$, then

$$\mathbf{L}\sigma = \mathbf{S}'. \tag{91}$$

Since every non-zero binary N-vector appears in both $\mathbf{L}$ and $\mathbf{S}'$, the matrix $\mathbf{œ}$ is necessarily non-singular and therefore $\mathbf{L}$ can be determined by,

$$\mathbf{L} = \mathbf{S}'\sigma^{-1}. \tag{92}$$

Continuing with the MLS of periodicity 7,

$$\mathbf{S} = \begin{bmatrix} 0 & 0 & 1 & 0 & 1 & 1 & 1 \\ 0 & 1 & 0 & 1 & 1 & 1 & 0 \\ 1 & 0 & 1 & 1 & 1 & 0 & 0 \end{bmatrix}, \tag{93}$$

$$\sigma = \begin{bmatrix} 0 & 0 & 1 \\ 0 & 1 & 0 \\ 1 & 0 & 1 \end{bmatrix}, \tag{94}$$

$$\sigma^{-1} = \begin{bmatrix} 1 & 0 & 1 \\ 0 & 1 & 0 \\ 1 & 0 & 0 \end{bmatrix}. \tag{95}$$

Therefore,

$$\mathbf{L} = \begin{bmatrix} 0 & 0 & 1 \\ 0 & 1 & 0 \\ 1 & 0 & 1 \\ 1 & 1 & 0 \\ 1 & 1 & 1 \\ 0 & 1 & 1 \\ 0 & 0 & 1 \end{bmatrix} \begin{bmatrix} 1 & 0 & 1 \\ 0 & 1 & 0 \\ 1 & 0 & 0 \end{bmatrix} = \begin{bmatrix} 1 & 0 & 0 \\ 0 & 1 & 0 \\ 0 & 0 & 1 \\ 1 & 1 & 0 \\ 0 & 1 & 1 \\ 1 & 1 & 1 \\ 1 & 0 & 1 \end{bmatrix}. \tag{96}$$

In order to continue the derivation of using Fast Walsh-Hadamard Transforms to deconvolve the system impulse response from the output of the system, Hadamard Matrices need to be introduced.

Hadamard Matrices are a special class of square matrices defined by the recursive relation,

$$\mathbf{H}_{2^k} = \begin{bmatrix} \mathbf{H}_{2^{k-1}} & \mathbf{H}_{2^{k-1}} \\ \mathbf{H}_{2^{k-1}} & \overline{\mathbf{H}}_{2^{k-1}} \end{bmatrix}, \tag{97}$$

University of Cape Town

the subscript is the order of the Hadamard matrix, and

$$\mathbf{H_1} = [\mathbf{1}], \tag{98}$$

$$\mathbf{H}_2 = \begin{bmatrix} 1 & 1 \\ 1 & 0 \end{bmatrix}. \tag{99}$$

An order 8 Hadamard Matrix, $\mathbf{H}_8$, is therefore,

$$\mathbf{H_8} = \begin{array}{ccc} & & \text{indices} \\ 0 & 0 & 0 \\ 0 & 0 & 1 \\ 0 & 1 & 0 \\ 0 & 1 & 1 \\ 1 & 0 & 0 \\ 1 & 0 & 1 \\ 1 & 1 & 0 \\ 1 & 1 & 1 \end{array} \begin{array}{c} \begin{array}{cccccccc} 0 & 0 & 0 & 0 & 1 & 1 & 1 & 1 \\ 0 & 0 & 1 & 1 & 0 & 0 & 1 & 1 \\ 0 & 1 & 0 & 1 & 0 & 1 & 0 & 1 \end{array} \\ \begin{bmatrix} 0 & 0 & 0 & 0 & 0 & 0 & 0 & 0 \\ 0 & 1 & 0 & 1 & 0 & 1 & 0 & 1 \\ 0 & 0 & 1 & 1 & 0 & 0 & 1 & 1 \\ 0 & 1 & 1 & 0 & 0 & 1 & 1 & 0 \\ 0 & 0 & 0 & 0 & 1 & 1 & 1 & 1 \\ 0 & 1 & 0 & 1 & 1 & 0 & 1 & 0 \\ 0 & 0 & 1 & 1 & 1 & 1 & 0 & 0 \\ 0 & 1 & 1 & 0 & 1 & 0 & 0 & 1 \end{bmatrix} \end{array}. \tag{100}$$

The numbers surrounding the matrix are the binary indices of the rows and columns. Using a similar method used to decompose $\mathbf{M}$ into $\mathbf{L}$ and $\mathbf{S}$, $\mathbf{H_8}$ can be decomposed into $\mathbf{B}$ and $\mathbf{B}'$, where $\mathbf{B}$ is a binary representation of the numbers of 0 to 2^{N-1},

$$\mathbf{B}\mathbf{B}' = \begin{bmatrix} 0 & 0 & 0 \\ 0 & 0 & 1 \\ 0 & 1 & 0 \\ 0 & 1 & 1 \\ 1 & 0 & 0 \\ 1 & 0 & 1 \\ 1 & 1 & 0 \\ 1 & 1 & 1 \end{bmatrix} \begin{bmatrix} 0 & 0 & 0 & 0 & 1 & 1 & 1 & 1 \\ 0 & 0 & 1 & 1 & 0 & 0 & 1 & 1 \\ 0 & 1 & 0 & 1 & 0 & 1 & 0 & 1 \end{bmatrix} = \begin{bmatrix} 0 & 0 & 0 & 0 & 0 & 0 & 0 & 0 \\ 0 & 1 & 0 & 1 & 0 & 1 & 0 & 1 \\ 0 & 0 & 1 & 1 & 0 & 0 & 1 & 1 \\ 0 & 1 & 1 & 0 & 0 & 1 & 1 & 0 \\ 0 & 0 & 0 & 0 & 1 & 1 & 1 & 1 \\ 0 & 1 & 0 & 1 & 1 & 0 & 1 & 0 \\ 0 & 0 & 1 & 1 & 1 & 1 & 0 & 0 \\ 0 & 1 & 1 & 0 & 1 & 0 & 0 & 1 \end{bmatrix} = \mathbf{H_8}. \tag{101}$$

Now, modifying $\mathbf{M}$ to create $\hat{\mathbf{M}}$, and equivalence can be shown between $\mathbf{H}$ and $\hat{\mathbf{M}}$, this will allow for the use of algorithms, such as the Fast Walsh-Hadamard Transform, designed for a Hadamard matrix to be used on $\mathbf{M}$. $\hat{\mathbf{M}}$ is constructed in the following manner, let $\hat{\mathbf{L}}$ be the matrix formed by bordering the top of $\mathbf{L}$ with a row of zeros, and $\hat{\mathbf{S}}$ being the

University of Cape Town

Algorithm C.1 An elegant Fast Walsh-Hadamard Transform algorithm.

Input: A vector x
Output: A vector y, the Hadamard transform of x

1. Construct $N+1$ columns, each with 2^N rows
2. Place x in column the first column
3. In the next column, construct the first half of the column by taking the pairwise, mutually exclusive sum of the previous column. The second half contains the pairwise, mutually exclusive difference of the previous column.
4. Repeat step 3 until all columns have been filled.

The final column contains the vector y, the Hadamard transform of x.

matrix formed by bordering the left of $\mathbf{S}$ by a column of zeros, then $\hat{\mathbf{M}}$ is given as,

$$\hat{\mathbf{M}} = \hat{\mathbf{L}}\hat{\mathbf{S}}. \tag{102}$$

Now the decomposed matrices $\hat{\mathbf{L}}$ and $\mathbf{B}$ contain all the binary N-vectors in their rows, and $\hat{\mathbf{S}}$ and $\mathbf{B}'$ contain all the binary N-vectors in their columns. Therefore, permutation matrices, $\mathbf{P}_L$ and $\mathbf{P}_S$, can be found such that,

$$\hat{\mathbf{L}} = \mathbf{P}_L\mathbf{B}, \tag{103}$$

$$\hat{\mathbf{S}} = \mathbf{B}'\mathbf{P}_S. \tag{104}$$

Therefore,

$$\hat{\mathbf{M}} = \hat{\mathbf{L}}\hat{\mathbf{S}} = \mathbf{P}_L\mathbf{B}\mathbf{B}'\mathbf{P}_S = \mathbf{P}_L\mathbf{H}\mathbf{P}_S. \tag{105}$$

In summary, the process to recover the periodic system impulse response, $h'[n]$, the system is excited with an MLS signal, and the output of the system reordered according to the matrix $\mathbf{P}_S$. Perform the Walsh-Hadamard transform on the resulting sequence. The result of the Walsh-Hadamard transform is then reordered according the matrix $\mathbf{P}_L$ and divide by $P+1$.

To finish the discussion on recovering the periodic system impulse response, an elegant, efficient Fast Walsh-Hadamard Transform algorithm is given in Algorithm C.1, and illustrated in Table 13.

University of Cape Town

Table 13: Illustrating an elegant Fast Walsh-Hadamard Transform for a vector of length 8.

x	a	b	y
$x[0]$	$a[0] = x[0] + x[1]$	$b[0] = a[0] + a[1]$	$y[0] = b[0] + b[1]$
$x[1]$	$a[0] = x[2] + x[3]$	$b[0] = a[2] + a[3]$	$y[0] = b[2] + b[3]$
$x[2]$	$a[0] = x[4] + x[5]$	$b[0] = a[4] + a[5]$	$y[0] = b[4] + b[5]$
$x[3]$	$a[0] = x[6] + x[7]$	$b[0] = a[6] + a[7]$	$y[0] = b[6] + b[7]$
$x[4]$	$a[0] = x[0] - x[1]$	$b[0] = a[0] - a[1]$	$y[0] = b[0] - b[1]$
$x[5]$	$a[0] = x[2] - x[3]$	$b[0] = a[2] - a[3]$	$y[0] = b[2] - b[3]$
$x[6]$	$a[0] = x[4] - x[5]$	$b[0] = a[4] - a[5]$	$y[0] = b[4] - b[5]$
$x[7]$	$a[0] = x[6] - x[7]$	$b[0] = a[6] - a[7]$	$y[0] = b[6] - b[7]$

University of Cape Town

D

WAVE PROPAGATION IN CYLINDRICAL PIPES

Given the $3D$ wave equation in cylindrical coordinates (for a derivation of the wave equation see Kinsler et al. [28]),

$$\nabla^2\phi\left(r,\theta,z,t\right)=\frac{1}{c^2}\frac{\partial^2\phi\left(r,\theta,z,t\right)}{\partial t^t}=0, \tag{106}$$

where $\nabla^2\left(\cdot\right)$ is defined as:

$$\nabla^2(\cdot)=\frac{1}{r}\frac{\partial}{\partial r}\left\{r\frac{\partial(\cdot)}{\partial r}\right\}+\frac{1}{r^2}\frac{\partial\left(\cdot\right)}{\partial\theta^2}+\frac{\partial^2\left(\cdot\right)}{\partial z^2}. \tag{107}$$

The $3D$ wave equation describes the velocity potential of the acoustic wave, it is related to particle velocity, u, as,

$$u\left(r,\theta,z,t\right)=\nabla\phi\left(r,\theta,z,t\right), \tag{108}$$

with $\nabla\left(\cdot\right)$ given as:

$$\nabla\left(\cdot\right)=\frac{\partial\left(\cdot\right)}{\partial r}+\frac{1}{r}\frac{\partial\left(\cdot\right)}{\partial\theta}+\frac{\partial\left(\cdot\right)}{\partial z}. \tag{109}$$

The equation relating acoustic pressure and velocity potential is,

$$p\left(r,\theta,z,t\right)=\rho_0\frac{\partial\phi\left(r,\theta,z,t\right)}{\partial t}. \tag{110}$$

Assuming harmonic motion, Equation 106 reduces to the Helmholtz equation in cylindrical ordinates,

$$\nabla^2\psi\left(r,\theta,z,t\right)+k^2\psi\left(r,\theta,z,t\right)=0, \tag{111}$$

with

$$\phi\left(r,\theta,z,t\right)=\psi\left(r,\theta,z,t\right)e^{j\omega t}, \tag{112}$$

and the wavenumber, $k=\omega/c$, ω the frequency of the wave and c is the speed of sound.

To solve the partial differential equation, assume a separable solution of the form,

$$\psi\left(r,\theta,z,t\right)=F\left(r\right)G\left(\theta\right)H\left(z\right). \tag{113}$$

Substituting this into Equation 111, and separating the variables leaves three ordinary differential equations of the forms,

$$\frac{d^2H\left(z\right)}{dz^2}+k_z^2H\left(z\right)=0, \tag{114}$$

University of Cape Town

$$\frac{d^2G(\theta)}{d\theta^2} + m^2G(\theta) = 0, \tag{115}$$

$$\frac{1}{r}\frac{d}{dr}\left\{r\frac{dF(r)}{dr}\right\} + \left\{\left(k^2 + k_z^2\right) - \frac{m^2}{r^2}\right\}F(r) = 0. \tag{116}$$

No boundary conditions are assumed for the z-direction, therefore the general solution is used,

$$H(z) = A_z e^{-jk_z z} + B_z e^{jk_z z}. \tag{117}$$

There are no boundary conditions for the θ-direction, but periodicity of 2π is assumed, therefore

$$G(\theta = 0) = G(\theta = 2\pi). \tag{118}$$

leading to the solution for the θ direction of,

$$G(\theta) = A_\theta \cos(m\theta) + B_\theta \sin(m\theta). \tag{119}$$

The equation for the r-direction can be re-arranged, resulting in Bessel's equation of order m,

$$r^2\frac{d^2F(r)}{dr^2} + r\frac{F(r)}{dr} + \left(r^2\eta^2 - m^2\right)F(r) = 0, \tag{120}$$

where $\eta = k^2 - k_z^2$. The solution for the Bessel equation is

$$F(r) = A_r J_m(r\eta) + B_r Y_m(r\eta), \tag{121}$$

where $J_m(\cdot)$ is referred to as the Bessel function of the first kind of order m and $Y_m(r\eta)$ is called the Bessel function of the second kind of order m. One boundary condition for the r-direction is that $F(r)$ is bounded at $r = 0$. $Y_m(r)$ is unbounded at $r = 0$, which reduces $F(r)$ to,

$$F(r) = A_r J_m(r\eta). \tag{122}$$

Another condition is that the particle velocity at the wall of the tube is 0, so

$$\frac{dF(a)}{dr} = 0, \tag{123}$$

where a is the radius of the cylinder. This is satisfied when

$$\frac{dJ_m(\beta_{mn})}{dr} = 0, \tag{124}$$

where $\beta_{mn} = a\eta_{mn}$, η_{mn} is the n^{th} zero of the m^{th} order Bessel function. The solution $F(r)$ of the mn mode can then be written as

$$F(r)_{mn} = A_{mn} J_{mn}\left(\beta_{mn}\frac{r}{a}\right). \tag{125}$$

University of Cape Town

The total solution for cross-modes in a circular duct that are propagating in the positive z-direction is obtained by combining Equation 113 and Equations 117, 119 and 125,

$$\phi(r,\theta,z,t) = \sum_{m=0}^{\infty}\sum_{n=0}^{\infty} A_{mn} \begin{matrix}\cos(m\theta)\\ \sin(m\theta)\end{matrix} J_m\left(\beta_{mn}\frac{r}{a}\right) e^{j(\omega t - k_z z)}. \tag{126}$$

The mode function for the mn cross-modes is given by

$$\psi(r,\theta) = \begin{matrix}\cos(m\theta)\\ \sin(m\theta)\end{matrix} J_m\left(\beta_{mn}\frac{r}{a}\right). \tag{127}$$

This function implies that either the sine or cosine term can be used for the mode function.

Finally, to determine the cut-off frequency for a mn cross-mode the following equation is used,

$$k^2 - k_z^2 = \left(\frac{\beta_{mn}}{a}\right)^2, \tag{128}$$

or,

$$k_z = \sqrt{k^2 - \left(\frac{\beta_{mn}}{a}\right)^2}. \tag{129}$$

If k_z is an imaginary number, then 126 will exponentially decay, and therefore will not propagate. This constraint implies that in order for the mn cross-mode to propagate, k_z is real, or

$$k \geq \frac{\beta_{mn}}{a}, \tag{130}$$

and therefore the cut-off frequency for the mn cross-mode, f_{mn} is

$$f_{mn} = \frac{\beta_{mn} c}{2\pi a}. \tag{131}$$

University of Cape Town

E

SELECTING NUMBER OF NOISE SAMPLES AND THRESHOLD MULTIPLIER

Assume that the background noise is normally distributed. From the properties of normal distributions[2], the addition or subtraction of two independent normally distributed variables is also normally distributed. By symmetry, the distribution of the absolute value of a set of normally distributed values is simply the normal distribution folded onto itself along the x-axis. Therefore the envelope of forward difference of the noise floor is half-normally distributed. In order to make the analysis easier, without the loss of generality, assume that the half-normal distribution has a scale factor $\theta = 1$. This implies that mirroring the distribution along the x-axis will give the standard normal distribution with 0 mean and unity standard deviation.

The Extreme Value Distribution[50] can be used to determine the expected maximum value after n samples, with the location and scale parameters, α and β respectively;

$$\begin{aligned} \alpha &= \Phi^{-1}\left(1-\tfrac{1}{n\cdot e}\right) \\ \beta &= \Phi^{-1}\left(1-\tfrac{1}{n}\right), \end{aligned} \tag{132}$$

where $\Phi^{-1}(\cdot)$ is the inverse cumulative distribution function of the standard normal distribution. The Extreme Value Distribution, shown in Figure 70, is given as

$$F(x,\alpha,\beta)=\frac{e^{-e^{\frac{-x+\alpha}{\beta}}+\frac{-x+\alpha}{\beta}}}{\beta}. \tag{133}$$

The expected maximum value after n samples is the simplified mean value, $M(n)$, of the distribution is given as

$$M(n) = \sqrt{(2)}\left((-1+\gamma)\,\mathrm{erfc}^{-1}\left(2-\frac{2}{n}\right)-\gamma\cdot\mathrm{erfc}^{-1}\left(2-\frac{2}{n\cdot e}\right)\right), \tag{134}$$

where γ is the Euler-Mascheroni Constant, $\gamma = \int_1^\infty \left(\frac{1}{\lfloor x\rfloor}-\frac{1}{x}\right)dx \approx 0.57721$, $\lfloor x\rfloor$ is equal to the highest integer less than x, and erfc^{-1} is the inverse error function. $M(n)$ can be seen in Figure 71, after 1000 samples, the expected maximum is approximately 3.2.

The probability,

$$\begin{aligned} \boldsymbol{P}(X > M(n)+\xi) &= 1-\boldsymbol{P}(X < M(n)+\xi) \\ &= \Phi(M(n)+\xi), \end{aligned} \tag{135}$$

University of Cape Town

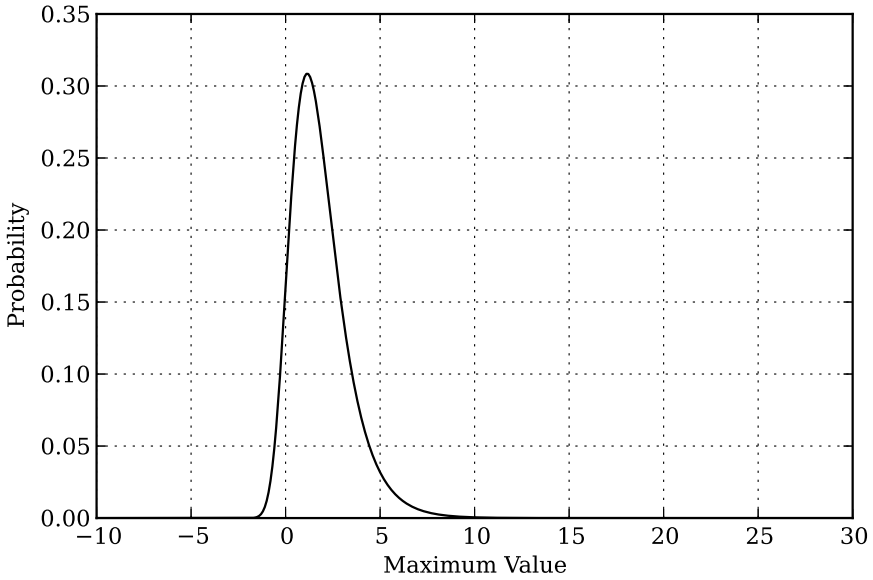

Figure 70: Extreme Value Distribution for 10 samples.

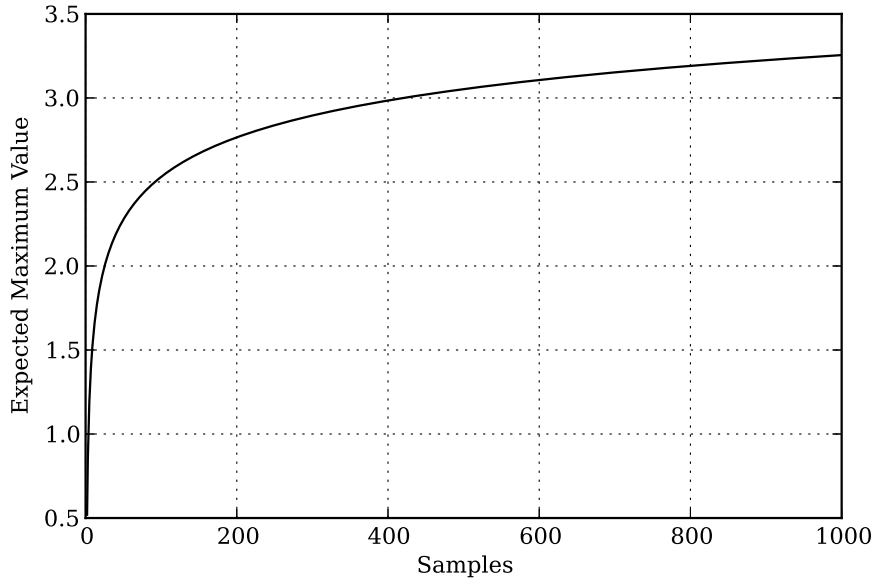

Figure 71: Expected maximum value for a set of n sampled values.

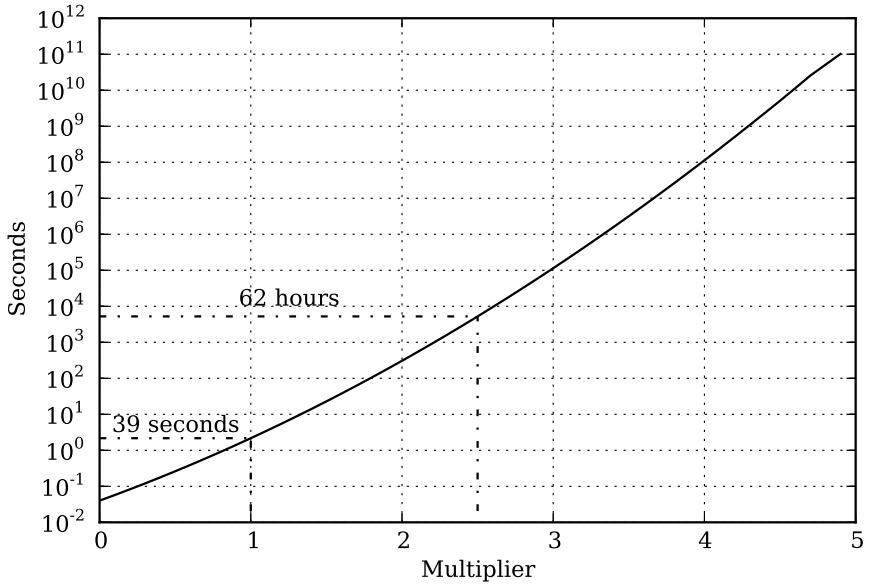

Figure 72: Expected maximum value for a set of n sampled values.

where ξ is the multiplier. If the number of samples is set to 1000, and the sampling frequency is 44100 Hz then the number of seconds before the expected maximum is greater than the threshold $\delta = M(1000) + \xi$ is shown in Figure 72. It can be seen that if ξ is set to 1, it will only take 39 seconds before a random sample is larger than the threshold δ. But if ξ is increased to 2.5, it will take 62 hours of sampling before a random sample is greater than the threshold.

University of Cape Town

F

USER MANUAL FOR RAPID ALPHA

F.1 INTRODUCTION

Rapid Alpha was developed to automatically determine the absorption coefficient of a material sample. The application was designed to perform the measurement without the need for pre-measurement calibration. Measuring the absorption coefficient of a material sample is performed with a click of the button, and can be undertaken by an unspecialised operator.

This user manual gives a list of software that is required to run *Rapid Alpha.* The recommended apparatus setup is then shown. Afterwards, an overview of using the application is given, with a look at the user interface and how to use it, is discussed. Finally, some issues that the user may encounter are given.

University of Cape Town

F.2 SYSTEM REQUIREMENTS

Rapid Alpha was developed using *Python 2.7*[37], an excellent programming language for signal analysis with ample libraries available to assist in analysing and displaying data. The user interface was implemented with *PyQt*, the *Python* bindings for the *QT* GUI framework. *PortAudio,* a cross platform audio library, was used to send and receive audio from the sound card.

If *Rapid Alpha* is being run in a Windows environment, it is recommended that Windows XP, or later, is used. The easiest method to get *RapidAlpha* running in Windows is to obtain *Python(X,Y)* from `http://code.google.com/p/pythonxy/`. *Python(X,Y)* is a software development environment that includes all the Python libraries that are required.

In order to get *Rapid Alpha* running in a *Linux* or *OS X* environment, the following packages are required:

- Python 2.7
- Numpy
- Scipy
- Matplotlib
- PyQt
- PortAudio

These packages can be installed with a package management system, such as *Homebrew* for *OS X*, or *APT* for *Debian* based *Linux* distributions.

The following commands, run from the *Terminal.app* application, will install the required packages on *OS X*, including *Homebrew*:

```
/usr/bin/ruby -e "$(/usr/bin/curl –fsSL https://raw.github.com/mxcl/
    homebrew/master/Library/Contributions/install_homebrew.rb)"
brew install python
brew install portaudio
sudo easy_install numpy
sudo easy_install scipy
sudo easy_install matplotlib
sudo easy_install pyqt
```

A similar process is followed to get the environment set up on a *Debian* based *Linux* distribution,

```
sudo apt-get install python
sudo apt-get install libportaudio2
sudo easy_install numpy
sudo easy_install scipy
sudo easy_install matplotlib
sudo easy_install pyqt
```

The *sudo* command will require the administrative password to be entered, if using *Ubuntu*, this will probably be the normal user password - unless it is a multiuser environment. If it is run on *OS X*, and there is no password administrative password, refer to http://support.apple.com/kb/HT4103.

University of Cape Town

F.3 APPARATUS SETUP

Rapid Alpha assumes that the measurement apparatus conforms to a specific geometry. There is also an assumption that the measurement signal is confined to a tube, and is not free-field measurement - the consequence of this, is that spreading of the signal is ignored. A sketch of the apparatus used to perform the measurements is shown in Figure 73. The figure displays that length of the tube, L, and the length from the microphone to the sample, l. These values for L and l are 2 meters and 1 meter respectively. It also shows that the sound card is connected to the loudspeaker, as well as directly back to itself. It also shows that the microphone is connected to the sound card. The expected connection settings for the loudspeaker are shown in Table 14.

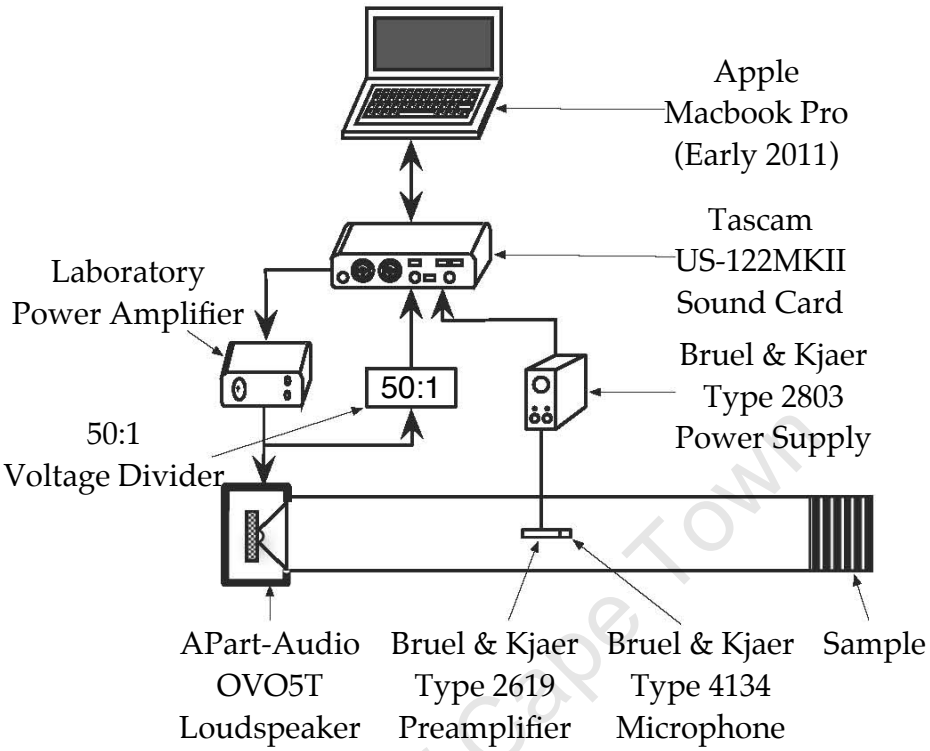

Figure 73: Sketch of apparatus used to determine the absorption coefficient with *Rapid Alpha*.

University of Cape Town

Table 14: The expected connection configuration for the sound card.

Channel	Output	Input
Left	Power Amplifier	Microphone
Right	No Connection	Left Output Channel

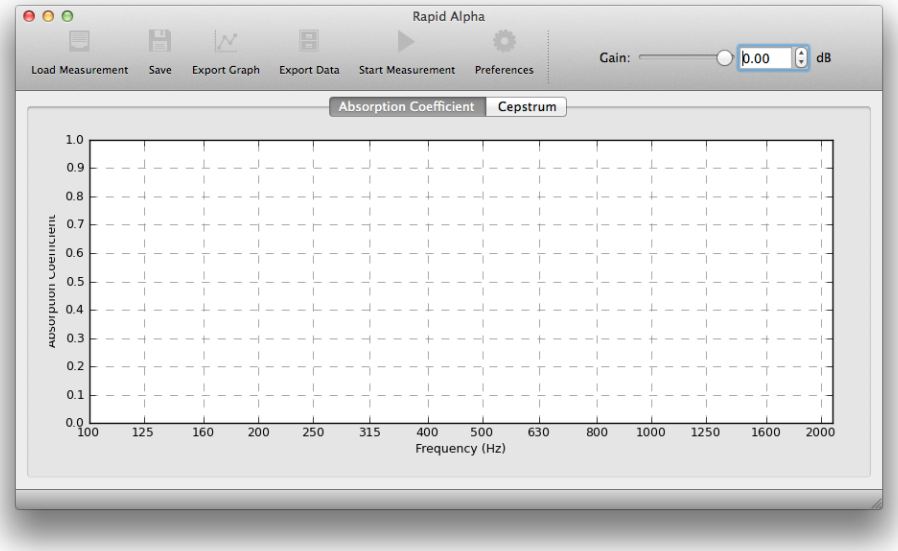

Figure 74: The user interface used to determine the absorption coefficient of a material sample, showing the default absorption coefficient plot area.

University of Cape Town

F.4 THE USER INTERFACE

The user interface of *Rapid Alpha* is shown in Figure 74 as soon as the application has been launched. Here one may start a measurement by clicking on the *Start Measurement* button, or display the measurement preferences by clicking on the *Preferences* button. A previously performed measurement my also be loaded by clicking on the *Load Measurement* button.

Once a measurement has been performed, the absorption coefficient is displayed in the plot area. The cepstra of the microphone and generator as well as the impulse response my be viewed by clicking on the *Cepstrum* tab, above the plot area. A sample of these are shown in Figure 75. The top plot shows the cepstra of the captured microphone signal, as well as the generated signal. Below that, in the middle plot, the power cepstrum is shown. This is simply the result of subtracting the generator's cepstrum from the microphone's cepstrum. The window used to *lift* the impulse response is also shown in the middle plot. Finally, the bottom plot shows the *liftered* impulse response.

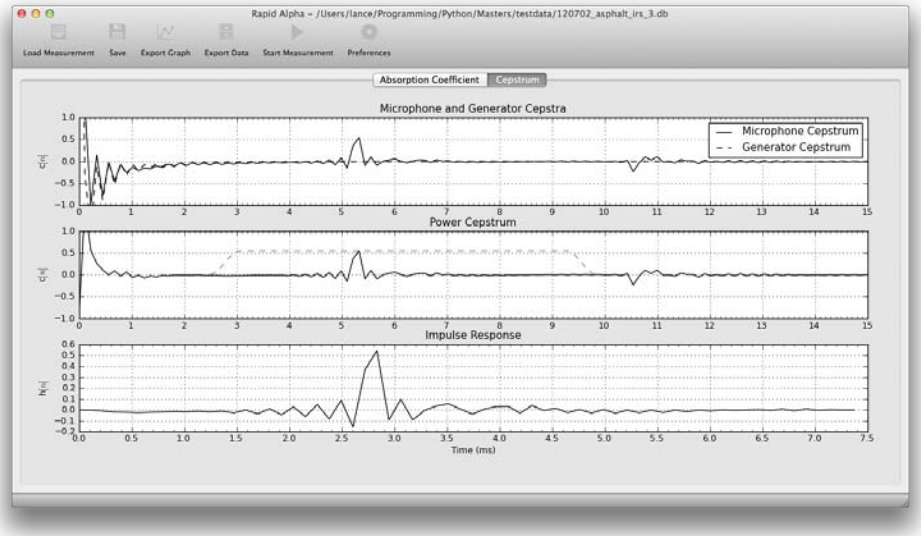

Figure 75: The *Cepstrum* tab shows the microphone, generator and power cepstrum as well as the *liftered* impulse response.

F.5 USING RAPID ALPHA

F.5.1 *Measuring the Absorption Coefficient*

Rapid Alpha was designed to measure the absorption coefficient rapidly and simply. Before starting a measurement, click the *Preferences* button to ensure that the correct input and output device are selected. If the wrong devices are shown, refer to subsection F.5.3 in order to change the settings and save them as default settings.

Clicking the *Start Measurement* button will begin the measurement. There will be a slight delay, in the order of 10 to 20 seconds depending on the computer, before the sound signal is propagated from the loudspeaker. The measurement itself will take approximately 30 seconds to complete, after which a dialog will be presented so that the measurement can be saved. If the dialog is shown, but no sound was heard, or the signal sounded *choppy* refer to the troubleshooting section, Section F.6.

Saving the measurement will take approximately 10 to 20 seconds, afterwards the measurement will be analysed and graphed. The absorption coefficient, by default, is displayed. The captured cepstra may also be viewed by clicking on the *Cepstrum* tab, above the graph.

F.5.2 *Exporting the Measurement*

The graph of the absorption may be exported, so that it may be used in a report. Clicking on the *Export Graph* button on the application's toolbar

University of Cape Town

will present a save dialog. Here the desired filename can be entered, as well as the output format.

The 1/3 octave data may also be exported in *Comma Separated Values* (CSV) format. Here the absorption coefficient at the centre value of the 1/3 octave frequency band is exported between 200 Hz and 2000 Hz. These values are; 200 Hz, 250 Hz, 315 Hz, 400 Hz, 500 Hz, 630 Hz, 800 Hz, 1000 Hz, 1250 Hz, 1600 Hz and 2000 Hz.

F.5.3 *Modifying Measurement Settings*

It may be necessary to modify the measurement settings, for instance if the correct input and output device need to be selected. It may also be that the measurement settings need to be changed or calibrated, this should be undertaken by a skilled operator. The effects on the results due to modification of the measurement settings are beyond the scope of this user manual, instead the reader is referred to Jenkin's thesis.

Clicking on the *Preferences* button on the *Rapid Alpha* interface will bring up the dialog shown in Figure76. Here the input and output devices can be selected, these should be set to the sound card used for measurements. The gain is used to scale the signal before it is sent to the sound card. The gain should be set at 0.8 to avoid clipping. The buffer size is the number of bytes sent and received by the sound card, if the sound is choppy this value may need to be increased.

The *Measurement Settings* tab contains settings pertaining to the excitation signal and analysis of the signal. Switching to this tab, will show the settings for the excitation signal, shown in Figure 77. The excitation signal can be selected in the *Signal* drop down box. The number of repetitions of the signal can be entered in the *Signal Repetition* spin box. A simple rule of thumb is that the *Signal-to-Noise Ratio* SNR, increasing with the root of the number of measurements,

$$SNR_f = SNR_0\sqrt{N}, \tag{136}$$

where SNR_0 is the initial signal to noise ratio, N is the number of signal repetitions and SNR_f is the improved signal to noise ratio.

For *Inverse Repeat Sequences* (IRS) and *Maximum Length Sequences* (MLS), the number of taps used to generate the signal and the number of bursts of the signal can be set. The number of samples in an MLS signal is equal to $2^N - 1$, where N is the number of taps. The number of samples in an IRS signal is twice that of the MLS signal. The number of MLS repetitions specifies how many times the MLS signal repeats itself with no gap - as opposed to signal repetitions where there is a gap between MLS bursts. The first burst is ignored, as it is used to get the system into a steady state, and the remaining bursts of the MLS signal are averaged

University of Cape Town

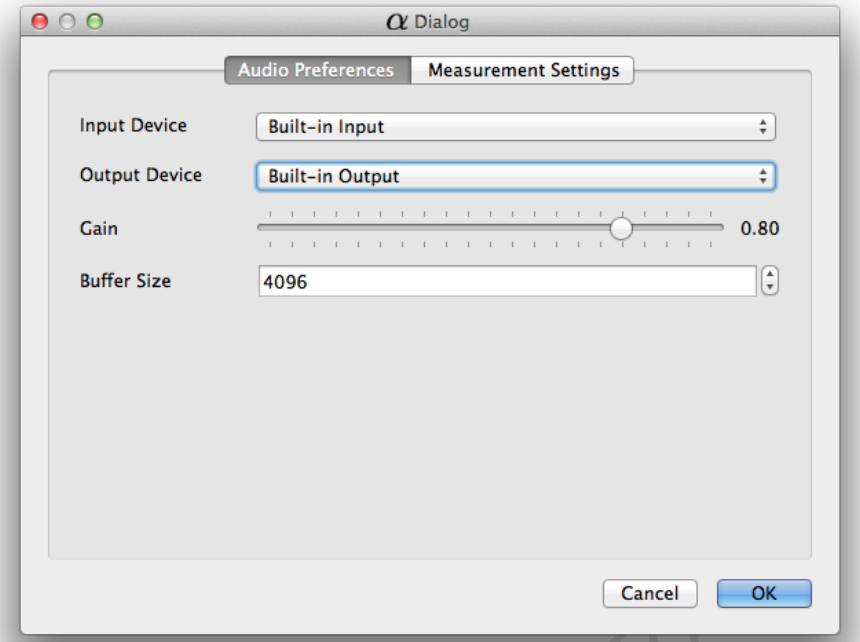

Figure 76: Preferences window, used to modify settings related to the audio device. The settings that can be changed are the input and output devices, the gain, and the buffer size.

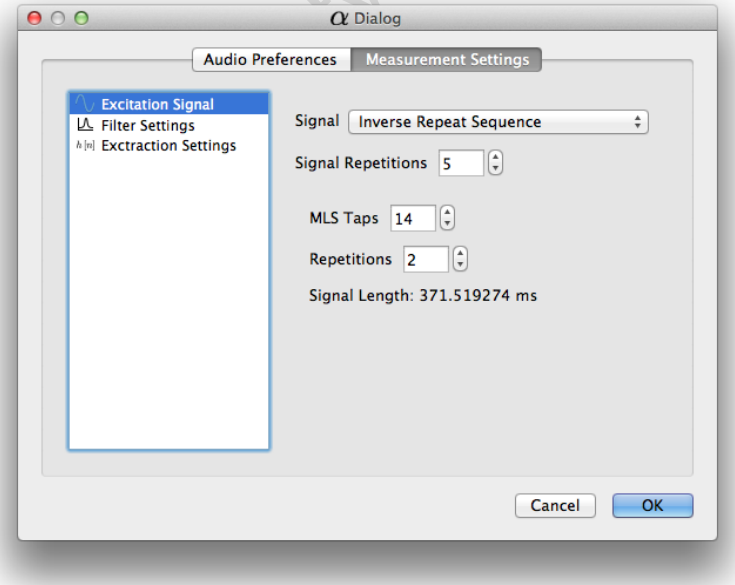

Figure 77: The preference window showing the settings for the excitation signal, the Inverse Repeat Sequence is shown here.

together. These average bursts are then again averaged with the number of signal repetitions.

Swept Sine and *Low Pass Swept Sine* excitation signals can have the upper and lower frequency ranges specified. For the Swept Sine signal, a sine wave is swept up in frequency from the lower frequency up to the upper frequency in the time length specified. For the Low Pass Swept Sine, a sine wave is swept up in frequency from the lower frequency up to the *Nyquist* frequency - half the sampling rate of the sound card - in the time length specified. It is then inverse filtered, to produce a flat spectrum, and low pass filtered down to the upper frequency. The signal therefore is shortened to $2f_u/f_s$ of the signal length. The variables f_u and f_s are the upper frequency and sampling frequency of the sound card respectively.

The excitation signal is digitally filtered before being sent to the sound card, the low pass filter is used to reduce energy above the frequency of interest. The effects of the high order propagation modes in the tube are also reduced. The low pass filter is used to equalise the effect of the impedance loading the tube has on the loudspeaker, as well as the fibre glass plug in-front of the loudspeaker. These settings can be set by clicking on the *Filter Settings* in the list on the left side.

The *Extraction Settings* allow the user to specify the window used to *lift* the impulse response from the cepstrum, as well as the decimation factor used. The signal is decimated so that the impulse response is not hidden in *cepstral noise.*

Again, it is important to note that these *Measurement Settings* should only be modified by a skilled operator as they can adversely effect the measurement.

F.6 TROUBLESHOOTING

F.6.1 *No Sound Signal is Produced*

If, after pressing the *Start Measurement* button on the *Rapid Alpha* interface, the *Save File* dialog is displayed with no sound having been produced then either the sound card has not been correctly connected, or the incorrect sound card has been selected.

To ensure that the sound card has been correctly connected, refer to Section F.3 above.

The selected sound card can be seen by clicking the *Preferences* button on the the *Rapid Alpha* interface. Confirm that the correct input and output devices are selected in the drop down boxes displayed in the *Audio Preferences* tab.

University of Cape Town

F.6.2 *The Sound is Choppy*

If the sound sounds *choppy* or *broken up* from the loudspeaker, the computer may be too slow or the buffer size may be too small. Try increasing the size of the buffer to 8192 samples. If two sound cards are being used, the buffer size may have to be reduced to 1024 samples.

University of Cape Town

G

SOURCE CODE

The source code for the software developed is available on the accompanying CD. The source code is also available at https://github.com/lancejenkinuct/RapidAlpha.

University of Cape Town

REFERENCES

[1] Leo Beranek. *Acoustics*. Acoustical Society of America, 1986. (Cited on page 49.)

[2] Dimitri P. Bertsekas and John N. Tsitsiklis. *Introduction to Probability*. Athena Scientific, 2002. (Cited on page 130.)

[3] BP Bogert, MJR Healy, and JW Tukey. The quefrency alanysis of time series for echoes: Cepstrum, pseudo-autocovariance, cross-cepstrum and saphe cracking. *Symposium on Time Series Analysis*, 1963. (Cited on page 15.)

[4] J Bolton. The application of cepstral techniques to the measurement of transfer functions and acoustical reflection coefficients. *Journal of Sound and Vibration*, 93(2):217–233, March 1984. ISSN 0022460X. doi: 10.1016/0022-460X(84)90309-2. URL http://linkinghub.elsevier.com/retrieve/pii/0022460X84903092. (Cited on pages 16, 19, 21, 22, and 103.)

[5] J Bolton and E Gold. The determination of acoustic reflection coefficients by using cepstral techniques, II: Extensions of the technique and considerations of accuracy. *Journal of Sound and Vibration*, 110(2):203–222, October 1986. ISSN 0022460X. doi: 10.1016/S0022-460X(86)80205-X. URL http://linkinghub.elsevier.com/retrieve/pii/S0022460X8680205X. (Cited on page 16.)

[6] John Stuart Bolton. *Cepstral Techniques in the Measurement of Acoustic Reflection Coefficients, with Applications to the Determination of Acoustic Properties of Elastic Porous Materials*. Phd thesis, University of Southampton, 1984. (Cited on pages 1, 16, 28, 59, 77, and 103.)

[7] JS Bolton and E Gold. The determination of acoustic reflection coefficients by using cepstral techniques, I: Experimental procedures and measurements of polyurethane foam. *Journal of sound and vibration*, 110(2):179–202, October 1986. ISSN 0022460X. doi: 10.1016/S0022-460X(86)80204-8. URL http://linkinghub.elsevier.com/retrieve/pii/S0022460X86802048. (Cited on page 16.)

[8] Bruel & Kjaer. Bruel and Kjaer Instructions and Applications: Standing Wave Apparatus Type 4002. 1970. (Cited on page 8.)

[9] K. G. Budden. *The Wave-Guide Mode Theory of Wave Propagation*. Logos Press, 1961. (Cited on pages 50, 53, and 54.)

University of Cape Town

[10] W. T. Chu. Transfer function technique for impedance and absorption measurements in an impedance tube using a single microphone. *Journal of the Acoustical Society of America*, 80(August 1986): 555–560, 1986. (Cited on page 11.)

[11] Martin Cohn and Abraham Lempel. On Fast M-Sequence Transforms. *IEEE Transactions on Information Theory*, pages 135–137, 1972. (Cited on page 122.)

[12] A. Cummings. Impedance tube measurements on porous media: The effects of air-gaps around the sample. *Journal of Sound and Vibration*, 151(1):63–75, November 1991. ISSN 0022460X. doi: 10.1016/0022-460X(91)90652-Z. URL http://linkinghub.elsevier.com/retrieve/pii/0022460X9190652Z. (Cited on page 69.)

[13] Chris Dunn and Malcolm Hawksford. Distortion Immunity of MLS-Derived Impulse Response Measurements. *Journal of the Audio Engineering Society*, 41(5):314–335, 1993. (Cited on pages 36 and 37.)

[14] F.J.M Frankort. *Vibration and Sound Radiation of Loudspeaker Cones*. Phd thesis, Delft University of Technology, 1975. (Cited on pages 42 and 43.)

[15] FXY Gao. Adaptive linearization of a loudspeaker. *Acoustics, Speech, and Signal*, pages 3589–3592, 1992. URL http://ieeexplore.ieee.org/xpls/abs_all.jsp?arnumber=150251. (Cited on page 103.)

[16] M Garai. Measurement of the sound-absorption coefficient in situ: The reflection method using periodic pseudo-random sequences of maximum length. *Applied Acoustics*, 39:119–139, 1993. URL http://www.sciencedirect.com/science/article/pii/0003682X93900322. (Cited on page 37.)

[17] Geller Labs. Making Low Level AC Voltage Measurements below 1-5 mV with the Agilent 34401A and 34410A Digital Multimeters, 2012. URL http://www.gellerlabs.com/34401AACzero.htm. (Cited on pages 69 and 79.)

[18] ER Green, PM Tathavadekar, and D Poliquin. Measurement System for Acoustic Absorption Using the Cepstrum Technique. In *The 2002 International Congress and Exposition on Noise Control Engineering*, 2002. URL http://www.roush.com/Portals/1/Downloads/Articles/EdsInternoise02Paper8.pdf. (Cited on pages 21 and 37.)

[19] Neil Groll. *Application of Cepstral Signal Processing Techniques*. Msc thesis, University of Cape Town, 1996. (Cited on page 21.)

University of Cape Town

[20] F.J. Harris. On the use of windows for harmonic analysis with the discrete Fourier transform. *Proceedings of the IEEE*, 66(1): 51–83, 1978. ISSN 0018-9219. doi: 10.1109/PROC.1978.10837. URL http://ieeexplore.ieee.org/lpdocs/epic03/wrapper.htm?arnumber=1455106. (Cited on pages 58, 60, 61, and 62.)

[21] Jens Hee. Impulse response measurements using MLS. Technical Report August, 2003. (Cited on pages 31 and 33.)

[22] International Organization for Standardization. ISO 10534-1:1996 Acoustics - Determination of sound absorption coefficient and impedance in impedance tubes - Part 1: Method using standing wave ratio, 1996. (Cited on page 8.)

[23] International Organization for Standardization. ISO 266:1997 Acoustics - Preferred frequencies, 1997. (Cited on page 7.)

[24] International Organization for Standardization. ISO 10534-2:1998, Acoustics - Determination of sound absorption coefficient and impedance in impedance tubes - Part 2: Transfer-function method, 1998. (Cited on page 9.)

[25] International Organization for Standardization. ISO 13472-1:2002, Measurement of sound absorption properties of road surfaces in situ - Part 1: Extended surface method, 2002. (Cited on page 12.)

[26] International Organization for Standardization. ISO 13472-2:2010, Measurement of sound absorption properties of road surfaces in situ - Part 2: Spot method for reflective surfaces, 2010. (Cited on page 11.)

[27] A.W.D Jongens. *Application of Cepstrum Techniques to in-situ Sound Absorption Measurements*. Msc thesis, University of Cape Town, 1993. (Cited on pages iv, 1, 2, 16, 20, 40, and 102.)

[28] Lawrence E. Kinsler, Austin R. Frey, Alan B. Coppens, and James V. Sanders. *Fundamentals of Acoustics*. Wiley, 1999. (Cited on pages 47, 49, 73, and 127.)

[29] Paul Lesso and Anthony Magrath. An ultra high performance DAC with controlled time domain response. In *Audio Engineering Society*, 2005. (Cited on page 73.)

[30] B Merit. In pursuit of increasingly linear loudspeaker motors. ..., *IEEE Transactions on*, 45(6):2867–2870, 2009. URL http://ieeexplore.ieee.org/xpls/abs_all.jsp?arnumber=4957682. (Cited on page 103.)

University of Cape Town

[31] P Morgan. A novel approach to the acoustic characterisation of porous road surfaces, December 2003. ISSN 0003682X. URL http://linkinghub.elsevier.com/retrieve/pii/S0003682X03000859. (Cited on page 69.)

[32] National Instruments. Zero Padding Does Not Buy Spectral Resolution. Technical report, 2006. (Cited on pages 19 and 62.)

[33] Alan V Oppenheim and Ronald W Schafer. From Frequency to Quefrency: A History of the Cepstrum. *IEEE Signal Processing Magazine*, pages 95–100. (Cited on pages 15 and 16.)

[34] Alan V Oppenheim and Ronald W Schafer. *Discrete-Time Signal Processing*. Prentice Hall, 1999. (Cited on page 59.)

[35] PortAudio. Audio Latency, 2002. URL http://www.portaudio.com/docs/latency.html. (Cited on page 73.)

[36] PortAudio. PortAudio, 2012. URL http://www.portaudio.com/. (Cited on page 73.)

[37] Python. Python Programming Language - Official Website, 2012. (Cited on pages 71 and 133.)

[38] D.D. Rife and John Vanderkooy. Transfer-function measurement with maximum-length sequences. *J. Audio Eng. Soc*, 37(6):419–444, 1989. URL http://www.aes.org/e-lib/browse.cfm?elib=6086. (Cited on page 36.)

[39] Mario Rossi. *Acoustics and Electroacoustics*. Artech House, 1988. (Cited on page 44.)

[40] J. Schoukens, R. Pintelon, E. van der Ouderaa, and J. Renneboog. Survey of excitation signals for FFT based signal analyzers. *IEEE Transactions on Instrumentation and Measurement*, 37(3):342–352, 1988. ISSN 00189456. doi: 10.1109/19.7453. URL http://ieeexplore.ieee.org/lpdocs/epic03/wrapper.htm?arnumber=7453. (Cited on page 27.)

[41] Scipy. Scipy Decimation, 2012. URL http://docs.scipy.org/doc/scipy/reference/generated/scipy.signal.decimate.html. (Cited on page 77.)

[42] A F Seybert. Experimental determination of acoustic properties using a two-microphone random-excitation technique *. *America*, 61(5):1362–1370, 1977. (Cited on page 9.)

University of Cape Town

[43] AF Seybert and B Soenarko. Error analysis of spectral estimates with application to the measurement of acoustic parameters using random sound fields in ducts. *The Journal of the Acoustical Society of*, 69(April), 1981. URL http://link.aip.org/link/?JASMAN/69/1190/1. (Cited on page 11.)

[44] WW Smith. Handbook of Real-Time Fast Fourier Transforms. 1995. URL http://ieeexplore.ieee.org/iel1/28/11488/x0054396.pdf. (Cited on page 18.)

[45] G.B. Stan, J.J. Embrechts, and D. Archambeau. Comparison of different impulse response measurement techniques. *Journal of the Audio Engineering Society*, 50(4), 2002. URL http://orbi.ulg.ac.be/handle/2268/34825. (Cited on page 37.)

[46] University of Sydney. Manuals for the Equipment, 2009. URL http://web.arch.usyd.edu.au/~stewa_k/Manuals.html. (Cited on pages xii and 67.)

[47] John Vanderkooy. Aspects of MLS Measuring Systems. *Journal of the Audio Engineering Society*, 42(4):219–231, 1994. (Cited on page 56.)

[48] A von Meier, G.J van Blockland, and G.G van Bochove. Hoofdrapport: Vermindering verkeersgeluid door wegdekontwerp en afstemming band-wegdek. Technical report, 1991. (Cited on page 85.)

[49] P Welch. The use of fast Fourier transform for the estimation of power spectra: A method based on time averaging over short, modified periodograms. *Audio and Electroacoustics, IEEE Transactions on*, pages 1–84, 1967. URL http://helio.estec.esa.int/SP/LISAPATHFINDER/docs/Data_Analysis/GH_FFT.pdfhttp://ieeexplore.ieee.org/xpls/abs_all.jsp?arnumber=1161901. (Cited on page 44.)

[50] Wolfram. Extreme Value Distribution, 2012. URL http://reference.wolfram.com/mathematica/ref/ExtremeValueDistribution.html. (Cited on page 130.)

[51] World Health Organization. Burden of disease from environmental noise: Quantification of healthy life years lost in Europe. Technical report, 2011. (Cited on page 1.)

University of Cape Town